Ab initio theory for ultrafast electron dynamics in metallic nanoparticles

Dissertation

zur Erlangung des akademischen Grades
doctor rerum naturalium (Dr. rer. nat.)

vorgelegt der
Mathematisch-Naturwissenschaftlich-Technischen Fakultät
(mathematisch-naturwissenschaftlicher Bereich)
der Martin-Luther-Universität Halle-Wittenberg

von Herrn Yaroslav Pavlyukh
geb. am 26.02.1976 in Drogobych

Gutachter:

1.

2.

3.

Halle (Saale),

Contents

0.1 Abbreviations

BBGKY	Bogolyubov, Born, Green, Kirkwood, Yvon (hierarchy)
CI	configuration interaction (method)
DFT	density functional theory
DMFT	dynamical mean-field theory
ECP	effective core potential
ERI	electron repulsion integral
FFT	fast Fourier transform
GW	approximation for the self-energy $\Sigma(12) = iG(12)W(1^+2)$
G^0W^0	simplified GW approximation, G and W are computed from the LDA or HF calculations.
GW^0	simplified GW approximation, G is involved in self-consistency loop, while W is computed from the LDA or HF calculations.
HF	Hartree-Fock approximation
HOMO	highest occupied molecular orbital
HRR	horizontal recurrence relation
lanl2dz	Los Alamos National Laboratories double zeta (basis set)
LCAO	linear combination of atomic orbitals
LDA	local density approximation
LTH	linearized time-dependent Hartree (approximation)
LUMO	lowest unoccupied molecular orbital
MBPT	many-body perturbation theory
ODE	ordinary differential equation
ph	particle-hole (excitation)
RPA	random phase approximation
RHF	restricted Hartree-Fock (method, approximation)
RHS	right-hand side
RWA	rotating wave approximation
SCF	self-consistent field
SHG	second harmonic generation
TBRIM	two-body random interaction model
TDDFT	time-dependent density functional theory
TDHF	time-dependent Hartree-Fock (approximation)
TDLDA	time-dependent local density approximation
TR-2PPE	time-resolved two photon photoemission
VRR	vertical recurrence relation

0.2 Units

In this thesis we adopted the following conventions:

- Formulae for the observables are shown in SI units in order to make them comparable with experimental results.

- For the abstract quantities that cannot be measured in experiments like operators, Green's functions, Hamiltonians etc. we use a system of units in which they look most naturally. In the case of cluster physics this is *atomic units*.

- Interatomic distances in clusters are shown in Å (1 Å=$1 \cdot 10^{-10}$ m).

- Energy levels, photon energies are shown in eV. (1 eV= $1.602188 \cdot 10^{-19}$ J).

Throughout the text we use *atomic units* of length, energy, time etc. The atomic unit of length is the so-called Bohr radius

$$1 \ a_{\mathrm{B}} = \hbar^2/me^2 = 0.529 \cdot 10^{-10} \ \mathrm{m} = 0.529 \ \text{Å}.$$

The atomic unit of energy (so called Hartree) is

$$1 \ \mathrm{Hr} = me^4/\hbar^2 = 27.21 \ \mathrm{eV}.$$

Chapter 1

Introduction

The success of physics as a science can be explained to a large extend by its refusal to build a complete picture of the whole world and by its general method to reduce complicated phenomena to simple models. The most representative example closest to our discussion of this is, probably, scattering theory. We have initially a target (elementary particle, atom or cluster in our case) and a particle interacting with this target (another elementary particle, electron or photon). Based on the initial information about the position and velocity of the particles the scattering theory predicts the final state of the system after the interaction process has been completed. The processes, that happened during the interaction normally are not considered to be important and are assumed to be instantaneous. In the application to the interaction of an atom with light, normally, one uses the terminology that the atom absorbs the photon and goes to the excited state. The energy of the final excited state, as well as a ground state can be computed on different levels of theory, for example configuration interaction (CI), that takes into account the internal properties of the system such as the number of electrons, spin-multiplicity etc., but does not care about the excitation process itself.

Although the many-body problem of the electrons in an atom, molecule, or cluster is not solvable in general, many approximate methods have been developed to treat these systems approximately. The oldest, but still in many cases reliable Hartree-Fock approximation, treats electrons on the mean-field level. Attempts to go beyond that, in the many-particle theory terminology, to take account of the *correlations* — the part of the electron energy, not taken into account in the mean-field approach – have lead to the development of density functional theory (DFT). This approach owes its origin to the Hohenberg-Kohn theorem, published in 1964, which demonstrates the existence of a unique functional which determines the ground state energy and density exactly. The theorem does not provide the form of this functional, however. One has to use some approximation to derive it for simple systems such as the homogeneous electron gas, and then to transfer this dependence on the real systems. The diagram technique of many-body perturbation theory provides necessary tools for that.

There is, however, one question, that has only recently gained sufficient attention, namely, what happens to the system between the initial and final state. The answer requires the extension of the model, that is exhausted by describing only static properties.

The word *transition* must now acquire a deeper meaning, revealed in life-times of the states, typical switching speeds, no longer being something, that happens instantly and traceless. There are two cases that can be described relatively easy in the framework of perturbation theory: the limit of instantaneous disturbance and the limit of slowly varying perturbation. The intermediate situation, when the time scale of the excitation is comparable with the speed of internal processes in the system, is the most interesting, but at the same time, the most difficult one.

The systems under investigation in this work are metallic clusters. Our interest in metallic clusters is raised by the recent advances in nanotechnology, fabrication and investigation of quantum dots, improvement of quantum chemical *ab initio* methods as well as of computational facilities, which enable the modelling of hundreds of atoms. On the other hands progress in technology with its steady tendency to the miniaturization is constantly demanding for novel materials. Clusters, that may be considered to form a new phase of materials lying between macroscopic solids and microscopic particles such as atoms and molecules, possess a large number of physical properties making them so attractive for future applications. Among them stands out a large flexibility in changing their qualities by varying their geometry and size. Addition of even a single atom may change the electronic structure of the cluster drastically. Clusters with certain numbers of atoms (magic numbers) are very stable due to completion of atomic-like electronic shells. Increasing the number of atoms by one then leads to the formation of a new incomplete shell, lowering the stability. Metallic clusters inhere the high density of electronic states from their bulk material counterparts combining it with seemingly contradictory large band-gap peculiar to insulators and semi-conductors.

To better realize the typical time scales in this kind of systems let us consider as an example a Na_N cluster interacting with a laser field. Sodium is a material that is often used for comparison of the theoretical results with experiments because of its relatively simple electronic structure, which makes it an almost perfect realization of the free electron gas model. There are several relaxation mechanisms, that take place during and after the excitation: electron-electron and electron-plasmon scattering, generation of phonons. They can be described by the relaxation times τ_{el}, τ_p, τ_{ph} respectively.

To estimate the typical time of electron-electron interaction we can use perturbation theory, which in the limit of a small electron density parameter r_s (so called Wigner-Seitz radius[1]) and a small quasiparticle energy E with respect to the Fermi energy E_F is reduced to the simple expression [1]:

$$\tau_{el} = \frac{263}{r_s^{5/2}(E - E_F)^2} \ \text{fs} \tag{1.1}$$

As a measure of the time scale for the second process it is convenient to take the period of one collective electron oscillation — elementary excitation plasmon, whose properties can be derived already on the classical level of the theory. In terms of the Wigner-Seitz

---

[1] For the homogeneous infinite electron gas r_s is the only parameter that determines its properties. It is defined as $\frac{4}{3}\pi r_s^3 = \frac{N}{V}$, where N is the number of electrons, contained in the volume V.

radius r_s the plasma frequency for bulk materials can be written as:

$$\hbar\omega_p = 13.6\sqrt{\frac{12}{r_s^3}} \ \text{eV} \qquad (1.2)$$

For the clusters, surface effects reduce this value by a factor of $\frac{1}{\sqrt{3}}$. Thus, for Na$_N$ with electron density of $r_s = 3.96 \ a_B$ we obtain a plasmon energy of $\hbar\omega = 3.45$ eV (this is close to the experimental values of $\hbar\omega = 2.7 - 3.2$ eV depending on geometry). This corresponds to the duration of one period of oscillation of $\tau_p = 1.2$ fs. For the measure of $E - E_F$ in Eq. (1.1) one can use the energy distance between the highest occupied molecular orbital (HOMO) of the cluster and its lowest unoccupied molecular orbital (LUMO). For the small sodium clusters, the HOMO-LUMO gap lies around $\Delta E = 3.5$ eV yielding an extremely short quasiparticle life-time of $\tau_{el} = 0.69$ fs.

To include the role of electron-phonon interaction (generation of phonons), we can use the result of Migdal [2], who determined that electron spectra are affected by electron-phonon interaction, when the excitation energies are of the order of ω_D (the Debye frequency). Thus

$$\tau_{ph} = \frac{E - E_F}{\hbar\omega_D}\tau_{el}. \qquad (1.3)$$

Using the experimental value of the Debye temperature for sodium $T_D = 158$ K [3] we obtain characteristic time of the electron-phonon relaxation $\tau_{pn} = 177$ fs.

From that we can conclude that *typical electronic processes are much faster than the electron-phonon relaxation.* The former take place on the femtosecond time scale, while the latter ones occurs on sub-picosecond time intervals. Thus, if a sufficient time resolution is provided one can not only ascertain a fact that a system under the influence of some perturbation has been switched from one quantum state to another, but also follow the electron dynamics during that process.

Lasers provide a unique excitation source for these purposes supplying pulses of an extraordinary wide range of frequencies and intensities. Currently optical pulses as short as 10 fs or even less are available yielding a time resolution of about 1 fs. Typically experiments comprise the excitation of the system by a strong pump-pulse and the subsequent detection of the time evolution by monitoring its response to a second weaker pulse (probe) impinging after a variable time delay (so called pump-probe experiments).

Investigation of the ultrafast electron dynamics is not only a question of purely fundamental interest. It has a wide range of possibilities for technological applications first of all in quantum state manipulation with further perspectives on quantum computing. There are several aspects that have made this area of science recently so attractive. First, the typical speed of the quantum processes is very high compared to conventional ones, used in the silicon devices. The second stems from the superposition principle of quantum mechanics and in turn from the simple fact, that *Hilbert space is a big place.* Heavy parallelization lies in the nature of the quantum computing. Besides that, one can take advantage of quantum operations (quantum gates) to build more effective algorithms for solving a variety of computational problems, that are difficult to solve by conventional,

classical bit operations: quantum Fourier transform, factorization of numbers, quantum cryptography.

The problem of the ultrafast electron dynamics in small metallic clusters on the *ab initio* level has several aspects. Here the word *small* is used in order to emphasize the fact that a real first principles investigation is only possible for systems, that contain a limited number of atoms. In contrast to bulk materials, where translational invariance helps to overcome the problem of an infinite (or very large) number of particles, in the case of molecules or clusters the symmetry group is normally much smaller. The number of atoms in the cluster is the critical parameter, that determines the level of the theory. Let us consider several examples.

The simplest approach is to treat electrons in the system on the one-electron level. It means that the many-body Hamiltonian in this case is reduced to an effective one-particle Hamiltonian. In both cases, viz. the Hartree-Fock and local density approximations, it depends self-consistently on the one-particle density. In contrast to bulk materials, where one has to deal with delocalized eigenstates that can be approximated by plane-waves, the wave-functions in finite systems can be better represented as linear combination of atomic-like orbitals. Thus the number of basis functions is approximately proportional to the number of atoms in the cluster. In we denote the number of basis functions by N_{bf} then both the Hamiltonian and the electronic density can be represented as matrices $N_{bf} \times N_{bf}$. The self-consistent computation of the Hamiltonian from the density matrix would then require, without any simplifying approximation, N_{bf}^4 operations. It means, that even systems containing hundreds of atoms or thousands of basis functions are accessible on this level of the theory. In the time-dependent case the numerical efforts will increase considerably. Each time step will require at least one evaluation of the Hamiltonian matrix. The number of time steps should be at least larger than the ratio of the largest and smallest energy scales in the system, which determine the length of the integration step and the total observation time respectively. For small clusters our experience shows that typically $10^5 - 10^6$ time steps are needed.

Considering an opposite example, when the system is treated without any simplifying approximation with respect to electron-electron interaction (correlations are fully taken into account) by means of the full configuration interaction method one can see the extreme increase of the computational efforts with system size. The method amounts to the diagonalization of the full many-body Hamiltonian. Its size is proportional to the number of ways one can distribute all electrons in the system over the states. The number of such configurations (this gave the name to the method) grows factorially with the system size. Without any further approximations only molecules or clusters with very few atoms are accessible to the method.

From these two examples one can see that there are two extreme approaches to our problem. Either one treats the electronic correlations on a low level, or even neglects them, and then is able to follow the electron dynamics for a long time interval, or one treats the electron-electron interaction without any approximations, but then is limited to a very small system without any chance to address its dynamics. Many-body perturbation theory (MBPT) provides an intermediate approach, giving the possibility to stop at any desired

level of the theory. At the same time it also contains any other approximations derived by various other methods as a partial case. For example, the Hartree-Fock approximation, initially derived from a variational principle, from the point of view of MBPT simply comprises the first two lowest order terms in the perturbation expansion.

MBPT is based on the Green's function technique. The Green functions used in the many-body problems are extremely useful generalizations of the original Green function, well known from the theory of ordinary differential and integral equations. They form basic elements in the field theoretical approach to the many-body problem and provide a direct way to calculate physical properties. They have also an obvious physical interpretation: the one-particle Green function describes the propagation of the electron or hole in the many-body system. The Green function of the next order describes the propagation of two particles in the field of other particles and so on. They are connected by an infinite chain of equations, where the equation of motion for the nth order Green function depends on Green's function of order $n+1$. Ironically, these equations are named differently, according to Dyson for the first order and to Bethe and Salpeter for the second. Breaking this chain at a certain level leads to an approximate treatment of the electron-electron interactions. From the numerical point of view the number of calculations needed for the computation according to such a scheme increases rapidly, with the increase of the order of the Green function explicitly taken into account. For real systems such calculations became possible only recently. Both computations that involve one-particle Green's functions, used to describe the ground state electronic structure, and two-particle Green's functions, aiming on excited-state properties, are currently *state of the art.*

In addition to the eigenstate energies and wave-functions, containing information about the static properties of the system, that can be obtained from the Green's function technique, one can also gain information on the system dynamics such as the life-times of the quasiparticle states and collective excitations. The former manifest themselves as an imaginary part of the eigenstate energies and have a simple physical meaning: decay of the quasiparticle state because of interaction with other particles. The latter is visible as a broadening of the plasmon peak in the inverse dielectric function. However, both of them are effects of a higher order than the phenomena they pertain to. For instance to obtain a non-zero imaginary correction to the eigenstate energies one needs to go beyond the mean-field approach and consider diagrams of at least second-order in the Coulombic interaction.

In the present work two approaches are used to study the electron dynamics in metallic clusters:

- the solution of the time-dependent Hatree-Fock equation in order to monitor the time evolution of the system upon ultrashort laser pulse excitation and

- a Green's function technique, namely the GW method to compute the correction to the eigenstates energies and to obtain decay constants for the plasmon excitations and quasiparticles.

The work is organized as follows. Chapter 2 is devoted to the presentation of the main concepts of MBPT and its application to real systems. Starting from the many-body

Hamiltonian and second quantization we introduce key quantities such as the Green function, the dielectric function, or the polarization operator that describe quasiparticle states and collective excitations in the clusters. This is, however, only one side of the problem. Although we can get insight in the electron dynamics of clusters by going further in the treatment of correlations and interpreting the imaginary part of the eigenstate energy as an inverse life-time of the state, we would like to have also a method, that is able to treat the electron dynamics explicitly, by propagating the wave-functions in time. This is necessary when one wants to reveal what happens in experiment, during the interaction of the electromagnetic field or any other perturbation with a cluster and on the subsequent – relaxation period. Next we describe different approaches for the treatment of the electron dynamics in clusters, starting from the simplest single-particle picture, the adiabatic approximation to the time-dependent mean-field equation, and compare them to the anticipated evolution from the exact solution of the time-dependent Schrödinger equation. In Chapter 3 we concentrate on the two complementary *ab initio* methods: TDHF equation and GW approximation. Special attention is paid to the accurate reformulation of the theory for the numerical implementation. In the first part, the properties of the TDHF equation are discussed and compared with other existing methods. We show the application of this method to different systems including a model system, alkali clusters, and transition-metal clusters in Chapter 4. Considering the GW approximation, several aspects have to be addressed: conservation of the particle number, effect of self-consistency, comparison with other existing numerical implementations. In Chapter 5 numerical results for a variety of systems are presented. Finally, the conclusions of our investigation are drawn. Appendix A is devoted to the analytical evaluation of the 3D integrals over gaussian basis functions. The latter ones are described in Appendix B. Appendix C makes our work self-contained by highlighting the derivation of the system of GW equations.

Chapter 2

Concepts of Many-Particle Theory

As mentioned in the introduction the electron-electron interaction processes are most important for the investigation of the electron dynamics on the femtosecond time scale. Here we neglect other slower relaxation mechanisms, like generation of phonons, that take place on the picosecond time scale. Thus, in what follows we assume the Born-Oppengeimer approximation, neglecting the motion of atomic nuclei.

The results of this chapter are valid for the electrons in clusters, molecules, bulk materials, as well as for the model system – the 3D homogeneous electron gas – eventually for systems for which perturbational theory converges and that can be mimicked by the Fermi liquid. The dimension of the space is important here, because only for the 3D electron gas and three dimensional systems[1] one can introduce the concept of the quasiparticle states, which are absent in lower dimensions, where the Tomonaga-Luttinger liquid model becomes adequate, substituting the Fermi liquid concept.

In this chapter we consider different theoretical approaches to study the electron gas in clusters and in particular their relation to quantum chemical methods. We promote the idea of the representation of localized wave-functions by linear combinations of atomic orbitals, show how the shell model explains the high stability of magic clusters, give an illustrative example of the quasiparticle description, thus, elucidating it from the point of view of an Green's functions approach and show the origin of the plasmon excitation from the equation of motion for the density matrix. In the last section we focus on the dynamics in many-body systems and compare the mean-field evolution of electronic states with other approaches.

2.1   Electronic states in different systems

Depending on the choice of the system the wave-functions of the electrons can have different spatial and momentum configuration. Let us forget for the moment about the many-body nature of the problem and consider just one electron in the electric field of rigid nuclei. In the case of single atoms the electron wave-functions are strongly localized and similar to

---

[1] We refer to spatial degrees of freedom in the Hamiltonian, but not to the geometric structure. From this point of view clusters are considered to be 3D objects.

that of the H atom. In this case, the solution of the Schrödinger equation yields the mean spatial extent of the wave-functions:

$$\bar{r} = \frac{1}{2}[3n^2 - l(l+1)]\,a_{\mathrm{B}}, \tag{2.1}$$

where n and l are the main and orbital quantum numbers. Thus for the 1s wave function $\bar{r} = 1.5\ a_{\mathrm{B}}$, for 2p $\bar{r} = 5.0\ a_{\mathrm{B}}$, and for 3d $\bar{r} = 10.5\ a_{\mathrm{B}}$. On the larger distance from the nuclei the wave-functions decay exponentially. This behavior is completely different from bulk metals, where the wave-functions of the conduction electrons are delocalized and to first approximation can be considered as plane waves.

For the numerical calculations one has two options how to describe the wave-functions or the electronic density as a set of numbers. First one can work in the real space representation introducing an appropriate mesh. To each point of the mesh a number is assigned and stored in the memory. Another option would be to expand wave-functions over a certain basis set and store the coefficients of this expansion, the so-called linear combination of atomic orbitals method (LCAO). The advantage of the second approach is the smaller number of parameters that describe the wave-functions. As basis functions it is convenient to take functions from one of three classes:
Gaussian functions

$$\phi(\boldsymbol{r}, \zeta, \boldsymbol{n}, \boldsymbol{R}) = (x - R_x)^{n_x}(y - R_y)^{n_y}(z - R_z)^{n_z}e^{-\zeta(\boldsymbol{r} - \boldsymbol{R})^2}, \tag{2.2}$$

Bessel functions[2]

$$B(\boldsymbol{r}, \zeta, \boldsymbol{n}, \boldsymbol{R}) = (x - R_x)^{n_x}(y - R_y)^{n_y}(z - R_z)^{n_z}k_{n-1/2}(\zeta|\boldsymbol{r} - \boldsymbol{R}|) \tag{2.3}$$

or Slater functions

$$\chi(\boldsymbol{r}, \zeta, \boldsymbol{n}, \boldsymbol{R}) = (x - R_x)^{n_x}(y - R_y)^{n_y}(z - R_z)^{n_z}r^{n-1}e^{-\zeta|\boldsymbol{r} - \boldsymbol{R}|}. \tag{2.4}$$

Here $\boldsymbol{R}$ denotes the position of the atom on which the functions are centered, the vector $\boldsymbol{n} = (n_x, n_y, n_z)$ shows the spherical symmetry of the functions. We use Cartesian spherical harmonics, that consist of an one-component s function, 3-component p functions, 6-component d functions, etc.

Gaussian basis functions are most commonly used for localized systems because of the simplicity of performing 3D integrations where they are involved. In order to further reduce the number of functions for better performance one uses contracted Gaussian functions

$$g(\boldsymbol{r}, \boldsymbol{n}, \boldsymbol{R}) = \sum_i c_i \phi(\boldsymbol{r}, \zeta_i, \boldsymbol{n}, \boldsymbol{R}) \tag{2.5}$$

that better represent atomic orbitals. Coefficients c_i and ζ_i are specific for each kind of atoms. They are optimized in order to represent the wave-functions in the atoms very

---

[2] in this formula $k_{n-1/2}(x) = x^{n-1/2}K_{n-1/2}(x)$, where $K_\gamma(x)$ is the Mcdonald function or the modified Bessel function of the second kind.

accurately, and can be used by various of *ab initio* programs. Increasing the number of basis functions leads to a more precise representation of the electronic density in the cluster and to a higher accuracy of calculations. The basis functions, however, are designed to represent the wave-functions of the occupied states. Unoccupied states normally are never required for ground-state calculations. For the investigation of the excited states as well as for some Green's function methods it is also important to have the information about unoccupied or virtual states. As their energy increases they become more and more extended, until, finally, they form a continuous spectrum. The wave-functions are then delocalized and very similar to plane-waves. As an example let us consider the density of states for the Na_9^+ cluster, obtained with different basis sets (Fig. 2.1).

On the first step we use the standard `lanl2dz` basis set together with effective core potential (ECP) for the core electrons. This consists of 2 s-type and 2 p-type basis functions for each of the atoms. In order to better represent virtual states close to the Fermi level we extended this basis set with diffusive functions, adding one function of s symmetry and one function of p symmetry in the second step, and 4 s and 1 p on the third step. One sees (Fig. 2.1) that states below the Fermi energy (their spectral function is positive) are not affected by the addition of the new function: the position of the peaks remains almost the same in the three cases. The number of virtual states close to Fermi level, however, in-

Fig. 2.1: *Density of states for a Na_9^+ cluster computed within the Hartree-Fock approximation.*

creases drastically, indicating initially their poor representation. We would like to mention, that unbound states cannot be represented by a linear combination of the localized functions. Thus it looks like they cannot be taken into account for further Green's function calculations[3].
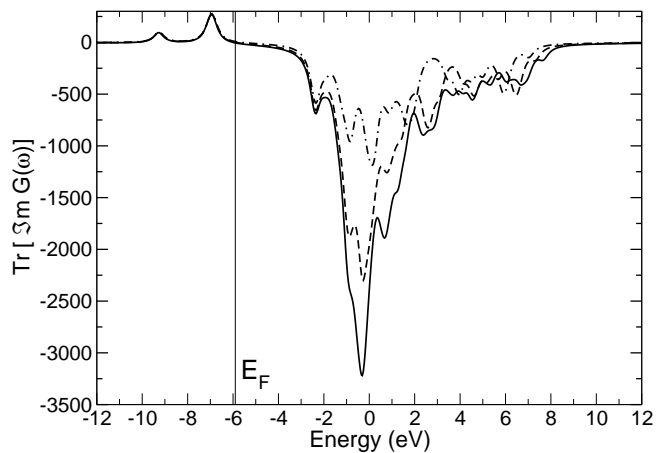
The electronic structure in small cluster exhibits another interesting feature – a high stability of clusters with a certain number of atoms. It was first revealed by observing anomalies of the mass spectrum (Fig. 2.2) of a Na cluster beam at specific sizes, called *magic numbers*. Then it was experimentally confirmed that the magic numbers come from the shell structure of the valence electrons. The stability and magic behavior of these clusters have been understood using a simple model of particles in a potential well or a jellium model in which the atomic structure of the cluster is ignored and the ionic

---

[3] Virtual states can be accounted by using the Dalgarno-Lewis scheme [4] that employs the closure relation in order to eliminate the need of an explicit knowledge of the empty states. This was applied to calculate the dynamical response and plasmon dispersion in metals (A. A. Quong, Phys. Rev. Lett. **70** (1993), 3955.) as well as for the supercell GW calculation of the sodium tetramer [5].
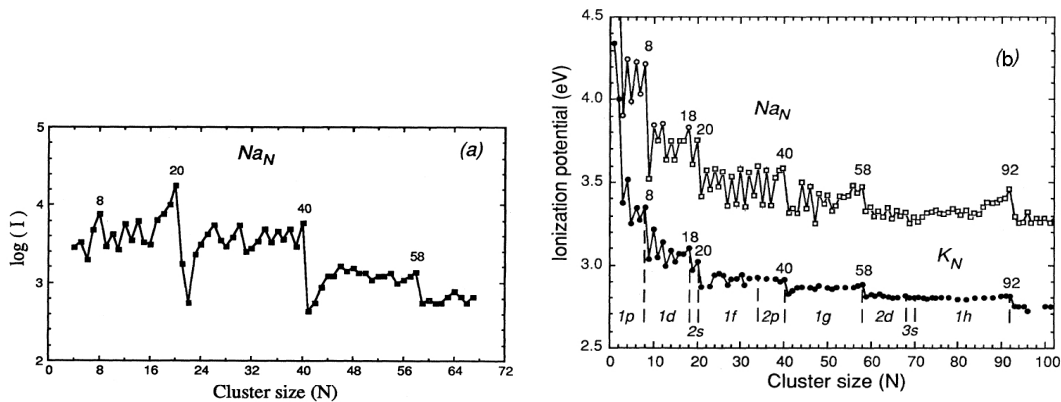
Fig. 2.2: *Abundance spectrum (a) and ionization potential (b) of sodium clusters (Ref. [7]).*

charge is smeared into a uniform positive spherical background[4]. The solution of the one-electron Schrödinger equation in such potentials leads to $1s$, $1p$, $1d$, $2s$, $1f$, $2p$, $1g$ $2d$, ..., electronic shells similar to the shell model of nuclei. Shell closure occurs for clusters having 8, 18, 20, 40, 58, 70, 92, ... valence electrons, which explains the strong stability of such clusters[5]. This was further confirmed by LDA calculations within the spherical jellium model [6]. Because of the high stability of magic-number clusters a variety of experimental investigations is possible. That is why we use some of these clusters (Na_9^+, two isomers of Na_{21}^+) for our theoretical investigation.

2.2 Electronic excitations in clusters

2.2.1 Many-body Hamiltonian

If one neglects relativistic effects, such as the spin-orbit interaction, the behavior of electrons in the clusters can be explained by the Schrödinger equation. The Hamiltonian describes the interaction of electrons with ions, electron-electron interactions and, possibly, the interaction with an external perturbation, like the electromagnetic field of the laser. In the system of N electrons one has:

$$\hat{H} = -\frac{1}{2}\sum_{i=1}^{N}\Delta_i + \sum_{i>j}^{N}\frac{1}{|\boldsymbol{r}_i - \boldsymbol{r}_j|} + \sum_{i=1}^{N} v(\boldsymbol{r}_i), \qquad (2.6)$$

where the first term on the right-hand side represents the electron kinetic energy, the second term is the electron-electron interaction and the third one, $v(\boldsymbol{r}_i)$, denotes the Coulomb

---

[4] This explanation is valid only for the clusters composed of the open shell atoms which possess valence electrons (alkali metals). In the case of rare-gas clusters the magic numbers were also observed, but they results from packing of atoms into a specific geometric structure. For instance, for xenon clusters the magic numbers 13, 19, 25, 55, 71, 87, 147 result from the completion of the icosahedral structure.

[5] The ordering of the shells at high principal quantum number, in principle, depends on the specific form of the potential. For example, the $3s$ and $1h$ energy levels are interchanged in the square potential well compared to the spherical one.

potential caused by the nuclei.

Each electron has a spin coordinate equal to either $+1/2$ (spinup) or $-1/2$ (spindown). In the nonrelativistic case, since the Hamiltonian does not depend on the spin coordinate, spins are good quantum numbers, i.e. the spin state of each electron is either upwards or downwards.

To get insight into the physics of such a many-body system let us first consider the simpler case, when the electrons do not interact one with each other (the second term in the Hamiltonian is absent). In this case the Hamiltonian breaks into N independent commuting parts that describe the motion of each electron.

$$\hat{H} = \hat{H}_1 + \hat{H}_2 + \cdots + \hat{H}_N$$

In this case the whole many-body wave-function can be factorized as an antisymmetrized product of the N one-particle wave-functions, satisfying the eigenvalue equation:

$$\hat{H}_i \psi_j(i) = \varepsilon_j \psi_j(i). \tag{2.7}$$

Here the subscript i labels the electrons, and j labels the eigenstates. The antisymmetrization can be expressed as an determinant of the matrix built from the N lowest energy one-particle eigenfunctions and is called Slater determinant:

$$\Psi = \frac{1}{N!} \begin{vmatrix} \psi_1(1) & \psi_2(1) & \cdots & \psi_N(1) \\ \psi_1(2) & \psi_2(2) & \cdots & \psi_N(2) \\ \vdots & \vdots & & \vdots \\ \psi_1(N) & \psi_2(N) & \cdots & \psi_N(N) \end{vmatrix} \tag{2.8}$$

This is the many-body wave-function of the ground state of the system. The wave-functions of the excited states can be expressed in the same way, by taking different combinations of the one-particle wave-functions as a basis for the Slater determinant. This can conveniently be represented in the second quantized form by introducing creation ($a_i^\dagger$) and annihilation (a_i) operators. This approach is fully equivalent to the usual representation of quantum mechanics and allows to deal with systems of variable particle number. If we denote the state without any electrons as $|0\rangle$ then the ground state can be expressed as:

$$|1, 2, \cdots, N\rangle = a_1^\dagger a_2^\dagger \cdots a_N^\dagger |0\rangle$$

and any excited state as:

$$|k_1, k_2, \cdots, k_N\rangle = a_{k_1}^\dagger a_{k_2}^\dagger \cdots a_{k_N}^\dagger |0\rangle$$

From the second quantized representation of the interacting Hamiltonian (Eq. 2.6):

$$\hat{H} = \sum_i \varepsilon_i a_i^\dagger a_i + \frac{1}{2} \sum_{i_1, i_2, i_3, i_4} \langle i_1 i_2 | \frac{1}{|\boldsymbol{r} - \boldsymbol{r'}|} | i_3 i_4 \rangle a_{i_1}^\dagger a_{i_2}^\dagger a_{i_4} a_{i_3} \tag{2.9}$$

one sees that the electron-electron interaction mixes Slater determinants corresponding to different configurations. Thus one can build the many-body Hamiltonian in a basis of Slater determinants corresponding to different configurations. This is exactly the Configuration Interaction (CI) approach used in quantum chemistry.

2.2.2   Quasiparticles

To better understand, what happens to the system, when we switch on electron-electron interaction it is useful to introduce the exact definition of the one-particle Green function:

$$G(\boldsymbol{r}t, \boldsymbol{r}'t') = -i\langle N|T[\hat{\psi}(\boldsymbol{r}, t)\hat{\psi}^\dagger(\boldsymbol{r}', t')]|N\rangle, \tag{2.10}$$

Here $|N\rangle$ denotes the ground state of the N particle system, and $\hat{\psi}^\dagger(\boldsymbol{r}, t)$ and $\hat{\psi}(\boldsymbol{r}, t)$ are creation and annihilation field operators, defined as:

$$\hat{\psi}(\boldsymbol{r}, t) = \sum_j \hat{a}_j(t)\psi_j(\boldsymbol{r}),$$
$$\hat{\psi}^\dagger(\boldsymbol{r}, t) = \sum_j \hat{a}_j^\dagger(t)\psi_j^*(\boldsymbol{r})$$

For $t > t'$, Green's function describes the propagation of an additional electron injected at time t' in the system, whereas for $t < t'$ it describes the propagation of a hole (removal of an electron). The corresponding ordering of operators is given by T – the time ordering operator.

From the definition it is clear that Green's function in the equal time limit (i.e. $t' = t^+$) denotes the density matrix of the system:

$$\rho(\boldsymbol{r}, \boldsymbol{r}') = \langle N|\hat{\psi}^\dagger(\boldsymbol{r}')\hat{\psi}(\boldsymbol{r})|N\rangle = -iG(\boldsymbol{r}t, \boldsymbol{r}'t^+) \tag{2.11}$$

In what follows we will assume that the Green function can be represented in a more general basis[6], not just a real space $(\boldsymbol{r}, \boldsymbol{r}')$. We will denote it as (r, r') without loss of generality. In the absence of time-dependent interactions the Green function depends only on the difference of t and t'. Introducing $\tau = t - t'$ we can obtain an expression for Green's function:

$$G(r, r', \tau) = -i\sum_k f_k(r)f_k^*(r')e^{-i\epsilon_k\tau}\left\{\theta(\tau)\theta(\epsilon_k - \epsilon_F) - \theta(-\tau)\theta(\epsilon_F - \epsilon_k)\right\} \tag{2.12}$$

with

$$f_k(r) = \langle N|\psi(r)|N+1, k\rangle, \quad \epsilon_k = E_{N+1,k} - E_N \quad \text{for} \quad \epsilon_k \geq \epsilon_F$$
$$f_k(r) = \langle N-1, k|\psi(r)|N\rangle, \quad \epsilon_k = E_N - E_{N-1,k} \quad \text{for} \quad \epsilon_k < \epsilon_F.$$

The different states of the $N+1$ and $N-1$ particle Hamiltonian are distinguished by the index k, $|N\rangle$ is the ground state of the N particle Hamiltonian. The above expression is valid for both interacting and non-interacting cases. It is useful to make a Fourier transform of the above equation to get Green's function in the ω representation:

$$G(r, r', \omega) = \sum_k \frac{f_k(r)f_k^*(r')}{\omega - \epsilon_k} \tag{2.13}$$

Here we redefined the ϵ_k, adding infinitesimally small imaginary parts to the energies coming from the Fourier transform of the Θ functions:

$$\epsilon_k \rightarrow \epsilon_k + i\delta \quad \text{for} \quad \epsilon_k < \epsilon_F, \quad \delta > 0$$
$$\epsilon_k \rightarrow \epsilon_k - i\delta \quad \text{for} \quad \epsilon_k > \epsilon_F, \quad \delta > 0. \tag{2.14}$$

---

[6] One can have additional indices for spin coordinates, expansion within a certain basis set, etc.

The computation of the Green function according to this definition is never used in practice because it requires the knowledge of not only the ground state properties of the N particle system, but as well of the excited states of the $N + 1$ and $N - 1$ particle systems.

In the non-interacting case the expression can be further simplified:

$$G(r, r', \omega) = \sum_j \frac{\psi_j(r)\psi_j^*(r')}{\omega - \varepsilon_j}. \qquad (2.15)$$

Here ε_j is the energy of the single-particle state, determined from Eq. (2.7), and should not be mixed with ϵ_k that denotes the energy difference between states with different particles number.

It is useful to introduce the spectral representation of the Green function.

$$G(r, r', \omega) = \int_C \frac{A(r, r', \omega')}{\omega - \omega'} d\omega' \qquad (2.16)$$

where the integration is performed along the path C in Fig. 2.3. The spectral function is closely related to the imaginary part of the Green function:

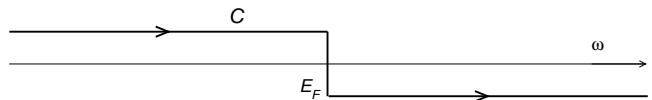$$A(r, r', \omega) = \frac{1}{\pi} |\Im G(r, r', \omega)|$$

From the definition of the spectral function Eq. (2.16) and the expression for non-interacting Green's function

Fig. 2.3: *Integration path in the definition of the $G(r, r', \omega)$.*

Eq. (2.15) one can easily see that the spectral function in this case is just a set of δ-functions. They are positioned at the eigenenergies ε_i of the non-interacting Hamiltonian. Switching on the interaction one can expect several scenarios, according to which the spectral function can be modified. First the position of the peaks may shift. Due to the electron-electron interaction the peaks can also split in many one-particle states that were originally degenerate. At small splittings this will lead just to a broadening of the peaks, and can be described by Lorentzians with some finite peak width instead of δ functions. If the interaction strength will increase further the splitting might become comparable with the distance between the states of the non-interacting Hamiltonian. Additional satellite peaks will appear. When going even further the spectral function $A(\omega)$ cannot be described in some regular way[7].

To better understand the behavior of the spectral function upon an increase of the interaction strength we performed model calculations on the *random-interaction* system.

---

[7] At this point we would like to mention one of the most beautiful ideas of modern theoretical physics, related to this discussion. It goes back to the work of G. t'Hooft, Nucl. Phys. B**72**, 461 (1974) and shows the possibility of mapping the graph problem in a certain configurational space to a surprisingly new problem. For example the generating functional of diagrams in the large N limit of QCD or random triangulations of space in 2D quantum gravity can be related to the random matrix model. Similarly, the problem of quasiparticle decay can be mapped onto the Anderson localization problem in configurational space due to B. L. Altshuler et al., Phys. Rev. Lett., **78**, 2803 (1997). In this new language one considers quasiparticles as localized states and their broadening as a delocalization in Fock space.
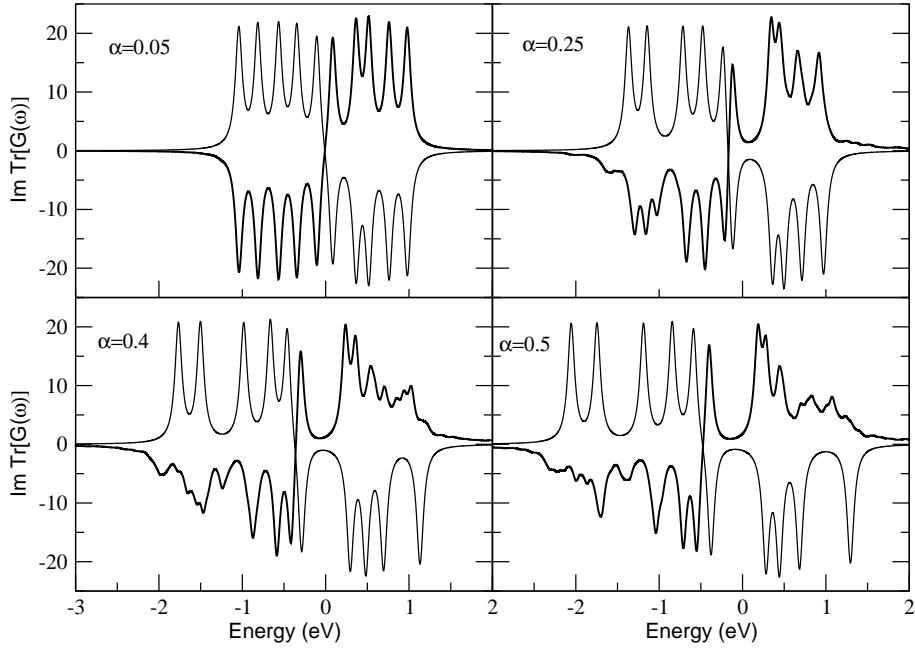
Fig. 2.4: *Imaginary part of the Green function for the model system with $n = 10$ and $m = 5$ for different interaction strength. The thick line denotes the exact Green function computed according to the definition Eq. (2.13), the thin line shows the Hartree-Fock Green function. In order to improve the readability the exact Green function is multiplied by -1.*

We will use this model also further, that is why we consider it in more detail. The system consists of n states among which m spinless electrons can be distributed. In the second quantized form the Hamiltonian can be written as:

$$\hat{H} = \sum_{i=1}^{n} \varepsilon_i a_i^\dagger a_i + \alpha \sum_{i,j,k,l=1}^{n} V_{ij,kl} a_i^\dagger a_j^\dagger a_k a_l \tag{2.17}$$

The ε_i are distributed on the energy interval $[-1, 1]$ eV. The matrix elements of the electron-electron interaction $V_{ij,kl}$ are random numbers distributed according to a Gaussian law with standard deviation $\sigma = 1$. The parameter α controls the interaction strength.

We consider the case $n = 10$ and $m = 5$, and perform exact diagonalization of the Hamiltonian in order to build the Green function according to the definition Eq. (2.13) for different interaction strengths. For comparison we computed the Green function from the approximate calculations on the Hartree-Fock level (Fig. 2.4). In order to represent the δ-functions graphically we applied an artificial broadening $\delta = 0.05$ eV to each of the states.

One can see that for low interaction strength ($\alpha = 0.05$) both exact and approximate methods give almost identical results. The spectral function consists of 10 peaks, shifted slightly from the eigenvalues of non-interacting Hamiltonian. The peaks are well pronounced. They manifest the existence of *quasiparticle* states in the system – states, that result from the introduction of an additional particle or hole ($a|N\rangle$, $a^\dagger|N\rangle$) in the

system. Due to the presence of electron-electron interaction they are no longer eigenstates of the $(N-1)$ or $(N+1)$-particle Hamiltonian, but are very close to the true eigenstates. Consequently they have an admixture of some other states. Increasing the strength of interaction more and more states get admixed to the quasiparticle state. As a result the width of the quasiparticle peak gets larger, additional satellite peaks appear. At $\alpha = 0.5$ only two states around the Fermi level can be called quasiparticles. The other ones are smeared out over the large energy interval and cannot be described in the quasiparticle approximation. The Hartree-Fock method, which operates with quasiparticles fails in this case. At an intermediate strength of the interaction $\alpha = 0.25$ it is clear that with a small exception of satellite states the quasiparticle approach is adequate in this case. However, the Hartree-Fock approach is not sufficient in this case. Without taking into account correlations one cannot describe the broadening of the states. Also the position of the peaks is not the same as in the exact result.

Thus from the above consideration we see that there is a need to go for a higher-order treatment of the correlations. This will improve the energy of the quasiparticle states and give information about their broadening. The second point is important for the dynamics. The inverse of the imaginary part of the energy gives the life-time of the excitation.

2.2.3 Collective excitations

Besides quasiparticle excitations that have properties very similar to usual particles – electrons or holes – in the electron gas there is another kind of excitations – plasmons. In the classical picture they are defined as a collective motion of the electrons. The frequency of the plasmon oscillations depends on the density of the electron gas. For real materials it lies in the energy interval ranging from $\omega_{pl} = 2.82$ eV for cesium with density $r_s = 5.62\ a_{\mathrm{B}}$ to $\omega_{pl} = 18.9$ eV for beryllium with density $r_s = 1.87\ a_{\mathrm{B}}$ (Tab. 2.1). The classical result for the plasma frequency can also be confirmed from quantum theory in a variety of ways: by the random phase approximation (RPA) of the diagram technique, the equation-of-motion method for the density matrix or by introducing collective coordinates. However, the classical picture only gives the value of the plasmon energy in the limit of $q = 0$. To get the dependence of w_{pl} on the q vector – plasmon dispersion, classical theory is not sufficient.

Metal	Electron density, r_s (a_{B})	ω_{pl} (eV)	
		Calculated	Experimental
Li	3.25	8.04	6.64
Na	3.93	6.05	5.4-5.94
K	4.86	4.40	3.79-4.15
Rb	5.19	3.98	3.45
Cs	5.62	3.54	2.82
Al	2.07	15.8	12.2-14.7
Cu	2.67	10.8	8.0
Ag	3.02	8.98	3.83
Pt	2.90	9.55	6.0

Tab. 2.1: *Bulk plasmon frequency for different metals. Calculations are done by the classical formula Eq. (1.2), experimental values are deduced from Ref. [8], by looking for the zeroes of the dielectric function.*

Here we will use the equation of motion method for the density matrix, described in

Ref. [9] in order to get the plasmon dispersion. Assuming that the system is subject to the time-dependent external electric field $\phi(\boldsymbol{r}, t)$, one can obtain the equation for the density matrix in first order perturbation theory as:

$$\rho_{kk'}(\omega) = \frac{n_k - n_{k'}}{\varepsilon_k - \varepsilon_{k'} - \omega - i\delta} \delta V_{kk'}(\omega) \tag{2.18}$$

Here δV is the variation of the average potential that acts on the electrons of the system (it is different from ϕ because the external potential, besides affecting the electronic density directly, also causes the change of the potential, created by the electrons themselves). To obtain expression Eq. (2.18) the following has been done:

- The quasiparticle picture is assumed to be valid here. It means that the many-body system can be described effectively by the single-particle Hamiltonian.

- We denote the eigenenergies of this Hamiltonian as ε_k. k labels the eigenstates.

- The unperturbed density matrix is diagonal in the eigenstate representation. In real space it is given as a sum of over the occupied states:

$$\rho(\boldsymbol{r}, \boldsymbol{r}') = \sum_{k \in \text{occ}} \psi_k^*(\boldsymbol{r}')\psi_k(\boldsymbol{r}) \tag{2.19}$$

It is useful to introduce the *dielectric function*[8] $\epsilon(\boldsymbol{r}, \boldsymbol{r}', t)$ that builds a connection between the external time-dependent potential $\phi(\boldsymbol{r}', t')$ and the effective potential $\delta V(\boldsymbol{r}, t)$:

$$\delta V(\boldsymbol{r}, t) = \int \varepsilon^{-1}(\boldsymbol{r}, \boldsymbol{r}'; t - t')\phi(\boldsymbol{r}', t')d\boldsymbol{r}'dt' \tag{2.20}$$

In what follows we will use matrix notations and make a Fourier transform of the time-dependent quantities. If we denote

$$P_{kk'}(\omega) = \frac{n_k - n_{k'}}{\varepsilon_k - \varepsilon_{k'} - \omega - i\delta} \tag{2.21}$$

we can relate the dielectric function to the response function $P_{kk'}(\omega)$ through the following set of equations:

$$\begin{aligned} \delta\rho &= P\delta V = P(v\delta\rho + \phi) \\ \delta\rho &= (1 - Pv)^{-1}P\phi \\ \delta V &= \left[1 + v(1 - Pv)^{-1}P\right]\phi. \end{aligned} \tag{2.22}$$

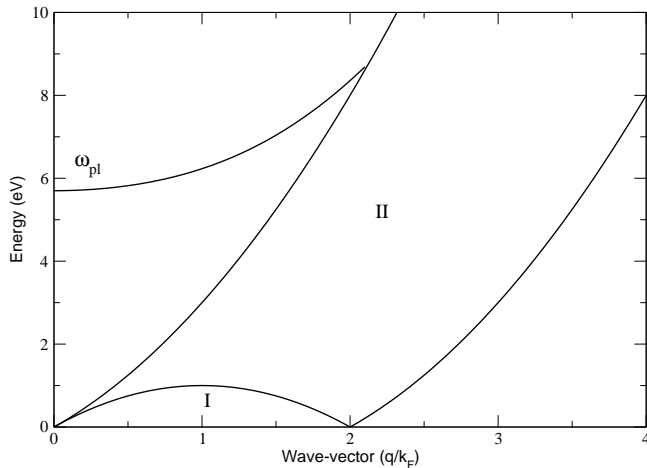

Fig. 2.5: *Plasmon dispersion according to the Lindhard dielectric function. Labels I and II show areas in the q − ω plane, where the imaginary part of the dielectric function is non-zero.*

---

[8] The dielectric function defined here has the same meaning as in electrodynamics, but is more general in a sense that it describes non-local effects (two space coordinates) in contrast to the well known rank-two tensor dielectric function for the translationally invariant media.

Here v is the matrix of the Coulomb interaction between the electrons. Comparing the last equation with the definition of the dielectric function one finds:

$$\varepsilon(\omega) = 1 - vP(\omega) \tag{2.23}$$

If the condition $\varepsilon(\omega) = 0$ is fulfilled, then according to Eq. (2.20) we can have a charge oscillation in the system even in the absence of the external field.

In the case of an homogeneous electron gas it is possible to obtain the expression for the response function $P(\omega)$ in the q representation. This gives the famous Lindhard [10] formula for the dielectric function.

The dielectric function is complex, and it has a nonzero imaginary part in the so-called particle-hole continuum (Fig. 2.5, areas I and II).

$$\Im m\, \varepsilon(q, \omega) = \frac{(4/9\pi)^{1/3} r_s}{q^3} \begin{cases} \omega & \text{region I} \\ 1 - \frac{1}{4}\left[q - (\omega/q)\right]^2 & \text{region II} \end{cases}$$

As a consequence the plasmon frequency, determined as a root of the dielectric function has a non-zero imaginary part in these regions. This indicates the decay of the plasmon, when the wave-vector reaches a certain value. From a physical point of view it means that the plasmon is long-range oscillation.

In the small metallic clusters surface effects become important. Confinement of the system leads to a red shift of the plasmon resonance. One can analyze this situation from the classical point of view (the so-called Mie theory) as well and estimate the plasmon frequency in the limit of vanishing radius of a spherical particle to be $1/\sqrt{3}\omega_{pl}$. In the literature it is often called *surface plasmon* of the cluster.

2.3 Dynamics in many-body systems

Time-dependent problems in quantum mechanics are in general much more complicated than stationary ones. Analytical solutions are known only in few cases: periodically driven free particle, harmonic oscillator, as well as some spin systems. Even the one-electron two-level system under the influence of a periodic perturbation can be solved only approximately[9] (so called Rabi solution [11]).

In relation to many-body systems several theoretical methods have been developed to describe the electron dynamics:

- Hierarchy of equations for the reduced classical density matrices (BBGKY) and its generalization to quantum systems.

- Method of Nonequilibrium Green's functions.

- Molecular dynamics simulations.

---

[9] An analytic solution in the form of an infinite series is known for arbitrary time-dependent perturbation due to X.-G. Zhao, Phys. Rev. B **49**, 16753 (1994).

- Monte Carlo methods.

Closest to our target is the first approach with its concept of the hierarchy of the relaxation times. Although all scattering mechanisms differ greatly with respect to the intensity, effective length scale and number of particles involved it is possible to classify them according to the relaxation time peculiar to each of the processes. Then at a given time stage one can pick up the dominating relaxation mechanism, neglecting other more slowly varying phenomena and build a correct approximation to the theory. In contrast to the single-particle picture, where changes of the quantum state can only be due to the interaction with an environment, the many-body nature of the electron gas also provides an internal clock mechanism. There exists a hierarchy of relaxation times corresponding to the equilibration of the one-, two-, three-particle distribution, etc. For each of the periods it is possible to build a quantum-kinetic theory [12, 13] that takes into account the necessary number of correlation functions while neglecting correlation functions of higher order. The simplest approximation is to treat the electron dynamics on the Hartree-Fock level, i.e. to neglect two-particle correlations.

In this section we compare the time-dependent mean-field approach and simpler methods like the adiabatic solution or the evolution of the matrix Hamiltonian with the exact solution of the dynamical problem.

2.3.1   Four approaches

The time-dependent Hartree-Fock equation will be considered in details in the next chapter. Here we are interested only in its general properties following from the functional dependence of the Hamiltonian on the electronic density. As a result we can write the following general form of the mean-field evolution:

$$
\begin{cases}
i\frac{\partial \psi_i(\boldsymbol{r},t)}{\partial t} &= [\hat{H}_{\mathrm{HF}}(\rho) + \hat{V}(t)]\psi_i(\boldsymbol{r},t) \\
\rho(\boldsymbol{r},\boldsymbol{r}',t) &= \sum_{i=\mathrm{occ}} \psi_i^*(\boldsymbol{r},t)\psi_i(\boldsymbol{r}',t)
\end{cases}
\tag{2.24}
$$

Here $\psi_i(\boldsymbol{r},t)$ is the time-dependent single particle wave-function, $\rho(\boldsymbol{r},\boldsymbol{r}',t)$ is the density matrix, $\hat{V}(t)$ is perturbation operator that describes the interaction of the system with the electric field of the laser. The Hartree-Fock Hamiltonian $\hat{H}_{\mathrm{HF}}$ describes an electron that moves in the electric field of the nuclei and the field created by the other electrons. In the TDHF scheme, shortly after the system has been excited it exhibits oscillations with the plasmon frequency Fig. 2.6(c), which is the zero of the longitudinal dielectric function on the RPA level. But, as scattering processes are not very accurately described in the mean-field approximation, the plasmon oscillation will last considerably longer in time, compared to the higher level treatment of electronic correlations Fig. 2.6(d).

In the regime of a slowly varying external field we can expect the adiabatic approximation to give a reasonable result. In that way, instead of solving Eq. (2.24), we perform a self-consistent solution of the eigenvalue problem:

$$
\left[\hat{H}_{\mathrm{HF}}(\rho) + \hat{V}(t)\right]\psi_i(\boldsymbol{r},t) = \varepsilon_i(t)\psi_i(\boldsymbol{r},t)
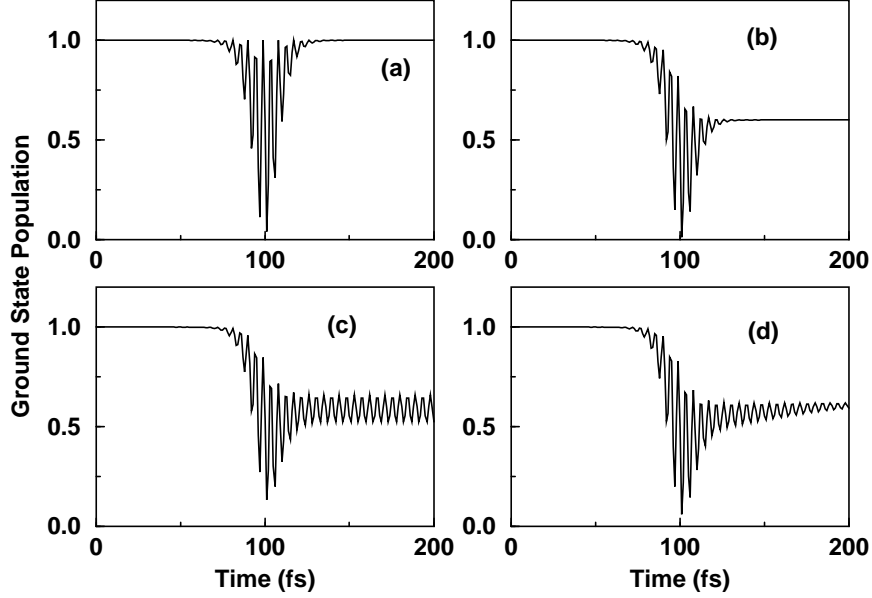\tag{2.25}
$$

Fig. 2.6: *Typical time evolution of the electron population within different approaches. (a) Adiabatic solution of Hartree-Fock equation. (b) Evolution of matrix Hamiltonian, Rabi oscillations. (c) Solution of the TDHF equation. (d) Full quantum kinetic solution.*

with the eigenvalues $\varepsilon_i(t)$, dependent on time. The main feature of this approach is that it is fully reversible, and, after switching off the perturbation, the systems returns to its initial state Fig. 2.6(a).

Another approach to study the time evolution would be to find the excitation levels of the system, which in the many-body picture do not coincide with the quasiparticle states of the Hamiltonian and should be determined on a higher-level approximation, e.g. as the poles of two-particle Green's function. Then we can follow the electron dynamics of the system in the basis of ground and excited states. The Hamiltonian in this case could be represented in a matrix form, with excited state energies on the diagonal, and off-diagonal perturbation operators:

$$\begin{pmatrix} \varepsilon_0 & V_{01} & \cdots & V_{0n} \\ V_{10} & \varepsilon_1 & \cdots & V_{1n} \\ & & \ddots & \\ V_{n0} & V_{n1} & \cdots & \varepsilon_n \end{pmatrix} \begin{pmatrix} \psi_0(\mathbf{r},t) \\ \psi_1(\mathbf{r},t) \\ \vdots \\ \psi_n(\mathbf{r},t) \end{pmatrix} = i\frac{\partial}{\partial t} \begin{pmatrix} \psi_0(\mathbf{r},t) \\ \psi_1(\mathbf{r},t) \\ \vdots \\ \psi_n(\mathbf{r},t) \end{pmatrix}. \tag{2.26}$$

Here the matrix elements of the perturbation operator correspond to the transitions between different states:

$$V_{i,j}(t) = \langle \psi_i(\mathbf{r})|V(\mathbf{r},t)|\psi_j(\mathbf{r})\rangle$$

The evolution of such a system has widely been studied in the literature [14], but even in the simplest case of a two level system this equation has no analytical solution. In the rotating wave approximation (RWA) we have so called Rabi oscillations [11] between levels, which accompany transitions from one state to another one. After the external perturbation stops the system displays no more oscillation, but, in contrast to the adiabatic approximation, it remains in the last state it achieved. This state could be different from the initial state, and, if no further perturbation takes place, the system will remain in that state forever Fig. 2.6(b).

From these considerations we can see, that the time-dependent Hartree-Fock equation is capable of explaining the gross features of the quantum evolution of the system, such as reversibility vs. irreversibily, transitions between states, plasmon oscillations, which cannot be achieved in the simpler theories.

As a conclusion we discussed in this chapter:

- the description of the electron wave-functions in the clusters by means of linear combination of atomic orbitals.

- the stability of the clusters

- two different electronic states in the electron gas:

  - quasiparticles

  - plasmons

  We saw that the properties of the first are very similar to that of the usual particles. They can be analyzed considering the one-particle Green function. The plasmon oscillation is a collective effect, that is most easily studied using the dielectric function.

- three approximate approaches to study the electron dynamics in many-body systems and to compare them with the exact solution of the Schrödinger equation.

Chapter 3

Methods

In this chapter we explain the implementation of the TDHF and GW methods from a unified point of view. As a starting point we consider diagrammatic expansions of the MBPT. Based on that we rewrite the equations in the form suitable for the numerical calculations. This is achieved by expanding all operators and functions in a certain basis set (Gaussian in our case, although the formulae are valid in general). The third section is devoted to the calculation of non-linear properties of the system, in particular, second harmonic generation and Kleinman symmetry of its tensor.

In order to achieve high numerical performance every operation should be rewritten in matrix form. Because of this the form of some equations differs from the usual notations. That is why we spend additional efforts to clarify relations between different representations of the main results.

Although both approximations are known for a long time (TDHF was established by Dirac [15] in the early 1930s and GWA originates from the work of Hedin [16] published in 1965) their numerical implementation became possible only with the development of modern computers. On the first stages a lot of additional approximations were used to facilitate computations. Thus we consider our implementations in the light of previous works.

3.1 TDHF equation

3.1.1 Theory

In a similar way as the stationary HF equation the TDHF equation can be obtained from the variational principle:

$$\left\langle \delta\Psi(t) \left| \left\{ H_{HF} - i\hbar\frac{\partial}{\partial t} \right\} \right| \Psi(t) \right\rangle = 0.$$

The many-body (MB) problem is then reduced to an effective one-body one imposing a particular form of the MB wave-function $\Psi(t)$, namely so that it can be represented as a single Slater determinant Eq. (2.8) based on the one-body wave-functions that yet have

to be determined. The time-dependent HF equation Eq. (2.24) then describes the time evolution of the electron wave-functions in the effective field created by the other electrons in the presence of an external perturbation. The Hamiltonian $\hat{H}_{\mathrm{HF}}$ can be written as:

$$\hat{H}_{\mathrm{HF}} = -\frac{1}{2}\Delta + \sum_{i=1}^{N}\frac{Z_i}{|\boldsymbol{r}-\boldsymbol{R}_i|} + \hat{H}_d(\rho) + \hat{H}_{ex}(\rho) \tag{3.1}$$

Note that the fundamental physical constants drop out with the use of atomic units. The first term describes the kinetic energy of the electron, the second represents the electric field of the nuclei of charge Z_i at position $\boldsymbol{R}_i$. The interaction with the other electrons is taken into account through the direct ($\hat{H}_d$) and exchange ($\hat{H}_{ex}$) energy functionals:

$$
\begin{aligned}
\hat{H}_d(\rho)\psi(\boldsymbol{r},t) &= \int d^3 r' \frac{\rho(\boldsymbol{r}',\boldsymbol{r}',t)}{|\boldsymbol{r}-\boldsymbol{r}'|}\psi(\boldsymbol{r},t) \\[2mm]
\hat{H}_{ex}(\rho)\psi(\boldsymbol{r},t) &= -\int d^3 r' \frac{\rho(\boldsymbol{r},\boldsymbol{r}',t)}{|\boldsymbol{r}-\boldsymbol{r}'|}\psi(\boldsymbol{r}',t)
\end{aligned} \tag{3.2}
$$

They depend self-consistently on the electron density:

$$\rho(\boldsymbol{r},\boldsymbol{r}',t) = \sum_{i=occ} \psi_i^*(\boldsymbol{r},t)\psi_i(\boldsymbol{r}',t). \tag{3.3}$$

From the point of view of diagrammatic perturbation theory the stationary HF equation is equivalent to the self-consistent solution of the following Dyson equation (Fig. 3.1) for the one-particle Green's function.
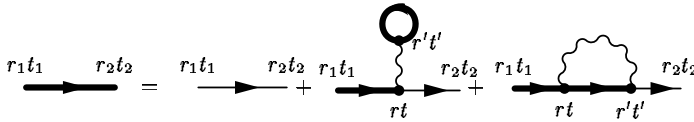

Fig. 3.1: *Dyson's equation for the one-particle Green function on the HF level. The diagrams are shown in the real space, real time representation. To each vertex the time coordinate t and space coordinate r is assigned. Integration over the coordinates of internal vertices is assumed. Wavy lines denote Coulomb interaction, straight lines are electron propagators (Green's functions). The thin line is the Green function of the system without electron-electron interaction.*

From this form of the representation one can easily see how Green's function $G(\boldsymbol{r}_1, t_1; \boldsymbol{r}_2, t_2)$ (denoted on the diagrams as a thick line) is determined iteratively: one starts with the zeroth approximation $G^0(\boldsymbol{r}_1, t_1; \boldsymbol{r}_2, t_2)$ (denoted as a thin line) that represents the non-interacting Green function (first term of RHS) and proceeds by putting the LHS solution in the RHS until convergence is achieved. The second and the third terms in the RHS represent the direct and exchange functionals [Eq. (3.2)] respectively. Up to now we have considered the HF equation in the absence of spin. Upon inclusion of the spin the equations will be modified slightly. Most easily this can be seen from the diagrammatic method (Fig. 3.1). In the presence of spin each fermion line will acquire an additional index that labels the spin. According to the diagrammatic technique the summation over the spin labels of the closed internal lines should be performed. In the

case of equal numbers of electrons with spin-up and spin-down this gives a factor of 2 for the second term in the RHS – direct interaction.

Let us now represent the HF Hamiltonian in the matrix form suitable for the numerical calculations. We will consider here only the case of equal numbers of spin up and spin down electrons (the so call restricted Hartree-Fock (RHF)). Denoting the basis functions as $\phi_\alpha(\boldsymbol{r})$ we can express the wave-functions as a set of time-dependent coefficients:

$$\psi_i(\boldsymbol{r}, t) = \sum_{\alpha=1}^{N_{\rm bf}} c_{i\alpha}(t)\phi_\alpha(\boldsymbol{r}). \tag{3.4}$$

The density matrix then reads:

$$\rho_{\alpha\beta}(t) = 2 \sum_{i=occ} c_{i\alpha}^*(t) c_{i\beta}(t). \tag{3.5}$$

To compute the direct and exchange functionals Eq. (3.2) we introduce matrix elements of the Coulomb interaction – the *electron repulsion integrals* (ERIs):

$$\langle \alpha\beta|\gamma\delta \rangle = \int d^3r d^3r' \frac{\phi_\alpha(\boldsymbol{r})\phi_\beta(\boldsymbol{r})\phi_\gamma(\boldsymbol{r}')\phi_\delta(\boldsymbol{r}')}{|\boldsymbol{r}-\boldsymbol{r}'|} \\ \alpha, \beta, \gamma, \delta = 1, \cdots, N_{\rm bf}. \tag{3.6}$$

Then:

$$\begin{aligned} \left[\hat{H}_d(\rho)\psi_i(\boldsymbol{r}, t)\right]_\alpha &= \sum_{\beta\gamma\delta} \langle \alpha\beta|\gamma\delta \rangle \rho_{\gamma\delta} c_{i\beta} \\ \left[\hat{H}_{ex}(\rho)\psi(\boldsymbol{r}, t)\right]_\alpha &= -\tfrac{1}{2} \sum_{\beta\gamma\delta} \langle \alpha\beta|\gamma\delta \rangle \rho_{\beta\delta} c_{i\gamma} \end{aligned}. \tag{3.7}$$

The first term gains a factor of 2 in the spin case. Introducing matrix elements of the non-interacting part of the Hamiltonian

$$H_{\alpha\beta}^0 = \int d^3r \phi_\alpha^*(\boldsymbol{r}) \left[-\frac{1}{2}\Delta + \sum_{i=1}^N \frac{Z_i}{|\boldsymbol{r}-\boldsymbol{R}_i|} \right] \phi_\beta(\boldsymbol{r})$$

the matrix elements of the total HF Hamiltonian Eq. (3.1) are computed as:

$$H_{\alpha\beta}^{HF} = H_{\alpha\beta}^0 + \sum_{\gamma\delta} \left(\langle \alpha\beta|\gamma\delta \rangle - 1/2\langle \alpha\gamma|\beta\delta \rangle \right) \rho_{\gamma\delta}. \tag{3.8}$$

This form is already suitable for the numerical implementation. However, the symmetry properties of the ERI's

$$\begin{aligned} \langle \alpha\beta|\gamma\delta \rangle &= \langle \beta\alpha|\gamma\delta \rangle \\ \langle \alpha\beta|\gamma\delta \rangle &= \langle \alpha\beta|\delta\gamma \rangle \\ \langle \alpha\beta|\gamma\delta \rangle &= \langle \gamma\delta|\alpha\beta \rangle \end{aligned} \tag{3.9}$$

give the possibility to further reduce the requirements for the memory and number of operations needed to compute HF Hamiltonian.

In general, the ERIs are four-index quantities. Thus, even for the small basis set they form a huge amount of data, that has to be stored in the computer memory[1]. For example

---

[1] Alternatively they can be computed on the fly in the course of the self-consistent loop, when the HF Hamiltonian has to be evaluated. Here we consider the situation, where ERIs are precomputed and stored in the memory.

to properly describe the wave-functions of the Na atom one needs 8 basis functions. The calculations for a cluster, that contains 15 Na atoms will require 120 basis function. This amounts to keeping 120^4 real numbers or 1.5 GB in the memory. According to the definition (Eq. (3.5)) the density matrix is Hermitian:

$$\rho_{\alpha\beta} = \rho^*_{\beta\alpha},$$

or separating the real part $\Re e\, \rho_{\alpha\beta} = \rho'_{\alpha\beta}$ and the imaginary $\Im m\, \rho_{\alpha\beta} = \rho''_{\alpha\beta}$:

$$\begin{array}{rcl} \rho'_{\alpha\beta} & = & \rho'_{\beta\alpha} \\ \rho''_{\alpha\beta} & = & -\rho''_{\beta\alpha} \end{array}.$$

Using that and the symmetry properties of the ERIs Eq. (3.9) we can rewrite the direct and exchange part of the HF Hamiltonian as:

$$\sum_{\gamma\delta} \left(\langle\alpha\beta|\gamma\delta\rangle - 1/2\langle\alpha\gamma|\beta\delta\rangle \right) \rho_{\gamma\delta}$$

$$= \sum_{\gamma\leq\delta} \left(\langle\alpha\beta|\gamma\delta\rangle - 1/2\langle\alpha\gamma|\beta\delta\rangle \right) \left(\rho'_{\gamma\delta} + i\rho''_{\gamma\delta} \right) + \sum_{\gamma\geq\delta} \left(\langle\alpha\beta|\gamma\delta\rangle - 1/2\langle\alpha\gamma|\beta\delta\rangle \right) \left(\rho'_{\gamma\delta} + i\rho''_{\gamma\delta} \right)$$

$$= \sum_{\gamma\leq\delta} \left(\langle\alpha\beta|\gamma\delta\rangle - 1/2\langle\alpha\gamma|\beta\delta\rangle \right) \left(\rho'_{\gamma\delta} + i\rho''_{\gamma\delta} \right) + \sum_{\gamma\leq\delta} \left(\langle\alpha\beta|\gamma\delta\rangle - 1/2\langle\alpha\delta|\beta\gamma\rangle \right) \left(\rho'_{\gamma\delta} - i\rho''_{\gamma\delta} \right)$$

$$= \sum_{\gamma\leq\delta} \left(\langle\alpha\beta|\gamma\delta\rangle - 1/2\langle\alpha\gamma|\beta\delta\rangle - 1/2\langle\alpha\gamma|\beta\delta\rangle \right) \rho'_{\gamma\delta} + i \sum_{\gamma\leq\delta} \left(-1/2\langle\alpha\gamma|\beta\delta\rangle + 1/2\langle\alpha\gamma|\beta\delta\rangle \right) \rho''_{\gamma\delta}$$

Separating real and imaginary parts we can write

$$\Re e\, H^{d-ex}_{\alpha\beta} = \sum_{\gamma\leq\delta} I_{\alpha\beta,\gamma\delta} \rho'_{\gamma\delta} \tag{3.10}$$

$$\Im m\, H^{d-ex}_{\alpha\beta} = \sum_{\gamma\leq\delta} J_{\alpha\beta,\gamma\delta} \rho''_{\gamma\delta}, \tag{3.11}$$

where we introduce the notations:

$$\begin{array}{rcl} I_{\alpha\beta,\gamma\delta} & = & 2\langle\alpha\beta|\gamma\delta\rangle - 0.5(\langle\alpha\gamma|\beta\delta\rangle + \langle\alpha\delta|\beta\gamma\rangle) \\ J_{\alpha\beta,\gamma\delta} & = & -0.5(\langle\alpha\gamma|\beta\delta\rangle - \langle\alpha\delta|\beta\gamma\rangle) \end{array}. \tag{3.12}$$

It seems that after all we achieved more complex expressions than originally. However, a careful inspection shows the advantages of such an approach:

- The HF Hamiltonian is Hermitian, thus $I_{\alpha\beta,\gamma\delta}$ and $J_{\alpha\beta,\gamma\delta}$ should be stored only for $\alpha \leq \beta$ and $\gamma \leq \delta$. Only half of $\langle\alpha\beta|\gamma\delta\rangle$ is required.

- Representing I and J as matrices of size $N_{bf} \cdot (N_{bf} + 1)/2$ and the density matrix as a vector of this size computation of the direct and exchange Hamiltonian can efficiently done by matrix-vector multiplications.

- Because the real and imaginary parts are computed separately the number of floating point operations is further reduced.

3.1.2 Details of the numerical implementation

The general scheme for solving Eq. (2.24) is as follows: initially, we perform a stationary self-consistent field (SCF) calculation in order to obtain the wave-function of the ground state. Then we use this as the initial condition for the system of ordinary differential equations to which Eq. (2.24) reduces after expanding all operators and functions in a given basis set. The size of the basis set can be reduced on the second step by transforming from the Gaussian basis $(\alpha, \beta, ...)$ to the eigenfunction basis $(i, j, ...)$. This is very useful, because it gives the possibility to exclude deeply lying states, that are always populated and highly excited states, that are never occupied. The major computational problem on this stage is the transformation of the ERIs (I and J) to the new basis. This is done in 4 stages:

$$I_{\alpha\beta,\gamma\delta} \to I_{i\beta,\gamma\delta} = \sum_{\alpha} I_{\alpha\beta,\gamma\delta} c_{i\alpha} \to I_{ij,\gamma\delta} = \sum_{\beta} I_{i\beta,\gamma\delta} c_{j\beta} \to I_{ij,k\delta} = \sum_{\gamma} I_{ij,\gamma\delta} c_{k\gamma} \to I_{ij,kl} = \sum_{\delta} I_{ij,k\delta} c_{l\delta}.$$

In a similar way the J integrals are transformed. Here the indices $i, j, k...$ label the eigenstates of the HF Hamiltonian. They can be selected in the desired way to include a certain number of initially occupied and virtual states in the consideration.

We propagate the solution in time by an adaptive Runge-Kutta or Bulirsch-Stoer method [17]. The major computational problem on this stage is the evaluation of the matrix elements of the direct and exchange Hamiltonian according to Eqs. (3.10,3.11). If we denote the number of time-steps by N_t, the numerical cost of the method scales as[2]:

$$N_{\mathrm{op}} = 2 \cdot N_t \cdot (N_{\mathrm{bf}} \cdot (N_{\mathrm{bf}} + 1)/2)$$

From the numerical point of view it is better to propagate only the wave-functions of the initially occupied states, rather than the full density matrix. Thus, at each moment of time the system is characterized by the set of N_{e} vectors of size N_{bf}, where N_{e} is the number of electrons under consideration. They contain all information about the system and give the possibility to compute different observables.

3.1.3 Observables

The system in our approach is described by a set of N_{e} time-dependent one-particle wave-functions (Eq. (3.4)) or $N_{\mathrm{e}} \cdot N_{\mathrm{bf}}$ coefficients. From that we can compute populations of the molecular orbitals as a function of time

$$n_i(t) = \sum_{j=1}^{N_{\mathrm{e}}} \langle \psi_i(\boldsymbol{r}, t = 0) | \psi_j(\boldsymbol{r}, t) \rangle = \sum_{j=1}^{N_{\mathrm{e}}} \sum_{\alpha=1}^{N_{\mathrm{bf}}} c_{i\alpha}^*(0) c_{j\alpha}(t) \tag{3.13}$$

---

[2] N_{bf}^4 scaling in fact can further be lowered. For example, static HF calculations with N_{bf}^2 scaling are possible when neglecting a large part of vanishing ERIs by so called integral prescreening. Using some tricks, which are valid only for non-metallic systems (sparsity of the density matrix) one can even lower the scaling to N_{bf}^1. The ERIs are then computed on the fly at each evaluation of the Hamiltonian matrix. However the gain in speed of the computation of the ERIs has a drawback in the complicated program logics, that on the small and medium size systems is overwhelming.

and consequently the time-dependent density of states

$$\rho(\epsilon, t) = \sum_i n_i(t)\delta(\epsilon - \varepsilon_i). \qquad (3.14)$$

Here the ε_i are the eigenvalues of the unperturbed HF Hamiltonian. A certain broadening should be applied to the δ-function in order to represent the results graphically.

The TDHF method conserves the total energy of the system. Under the influence of the laser pulse the system undergoes a transition from the ground to some excited state. One can follow that by observing the total energy. It can be computed as:

$$
\begin{aligned}
E(t) \quad = \quad & \frac{1}{2}\sum_{i=1}^{N_e}\left[\varepsilon_i(t) + \langle\psi_i(\boldsymbol{r},t)|\hat{H}^0 + \hat{V}(t)|\psi_i(\boldsymbol{r},t)\rangle\right] = \\
& \frac{1}{2}\sum_{i=1}^{N_e}\left[\varepsilon_i(t) + \sum_{\alpha,\beta=1}^{N_{bf}}\left[H^0_{\alpha\beta} + V_{\alpha\beta}(t)\right]c_{i\alpha}(t)^*c_{i\beta}(t)\right].
\end{aligned}
\qquad (3.15)
$$

In this equation $\varepsilon_i(t)$ are the instantaneous eigenvalues of the Hamiltonian. Note, the seemingly contradictory result that the total energy of the system is not just equal to the sum of eigenstate energies. However it has a clear interpretation. Each eigenstate ε_i contains the interactions with all other occupied orbitals. For example, ε_1 contains the interaction with particle 2, particle 3 and so on, up to particle N_e; ε_2 contains once again the energy of the interaction between particle 2 and 1, and so on. Thus, all interaction energies will be counted twice in the sum over ε_i. This double counting is then compensated by adding the average over the noninteracting Hamiltonian and taking half of the sum.

The optical response of the system to the external perturbation can be analyzed by computing the expectation value of the dipole or higher order multipole operators:

$$d_i(t) = \int d^3r\, r^L Y_{L,i}(\frac{\boldsymbol{r}}{r})\rho(\boldsymbol{r}, t).$$

We will consider only the dipole response, thus $L = 1$ – the orbital quantum number for the spherical harmonics $Y_{L,i}(\frac{\boldsymbol{r}}{r})$. The $\rho(\boldsymbol{r}, t)$ are diagonal elements of the density matrix Eq. (3.5) ($\boldsymbol{r}' = \boldsymbol{r}$). The computations are performed as

$$d(t) = \sum_{i=1}^{N_e}\sum_{\alpha\beta=1}^{N_{bf}} d^i_{\alpha\beta}c_{i\alpha}(t)^*c_{i\beta}(t),$$

where the $d_{\alpha\beta}$ are matrix elements of the corresponding dipole operator. The signal $d(t)$ is then transformed to the frequency domain, finally yielding the power spectrum:

$$P(\omega) = \int dt\, e^{i\omega t}d(t). \qquad (3.16)$$

The properties of the power spectrum are considered in detail in a review paper [18].

3.1.4 Alternative implementations

Mean-field methods now are established as a very powerful approach in theoretical physics. They have a very broad range of applications from mathematics, statistical physics to quantum-field theory and many-body systems. Results obtained within this approach serve as a good initial guess for further corrections. The advantage of these methods are their simplicity, and the possibility to derive it without using a complicated diagram technique (for instance from the variational principle).

In relation to many-body physics mean-field theory received its widest attention. Hartree-Fock equations were applied to various systems: atoms, molecules, solids, surfaces, etc. Now it became a standard tool for all *ab initio* programs in quantum chemistry. Some of its disadvantages, such as the non-linearity of HF equations, difficulties in predicting properties of the unoccupied states, or the overestimation of the band (HOMO-LUMO) gap have a trade-off by their simplicity.

The time-dependent HF equation was discovered shortly after its stationary counterpart [15]. At first sight it accounts for electron-electron interaction on the same level as the stationary equation, and, thus, contains no additional information about electronic correlations. This is, however, not the case. One can consider the regime of *linear response* assuming a small temporal deviation of the wave-function from the stationary HF solution. Neglecting the exchange term and transforming to the frequency domain one can obtain eigenvalue equations that describe small oscillations in the systems around the time-independent solution:

$$
\begin{pmatrix} A & B \\ B^* & A^* \end{pmatrix} \begin{pmatrix} X^k \\ Y^k \end{pmatrix} = \omega_k \begin{pmatrix} X^k \\ -Y^k \end{pmatrix}.
\tag{3.17}
$$

The matrix A contains matrix elements of the interaction between particle-hole excitations, whereas matrix B is composed of matrix elements of the interaction between the ground and two-particle two-hole excitations:

$$
\begin{aligned}
A_{ma,nb} &= (\varepsilon_m - \varepsilon_a)\delta_{ab}\delta_{mn} + \langle mb|V|an\rangle \\
B_{ma,nb} &= \langle mn|V|ab\rangle.
\end{aligned}
\tag{3.18}
$$

The indices a, b (m, n) refer to the hole (particle) states. The positive eigenvalues ω_k of Eq. (3.17) are the excitation energies of the system. We will call it linearized time-dependent Hartree (LTH) approximation. Although the extension of the HF self-consistent field method to the time domain looks physically very natural it describes a number of important phenomena, not accessible within the original HF approach. The LTH approximation is equivalent to a sequence of approximations like equation of motion, summation of a certain class of Feynman diagrams, etc. For the uniform electron gas it gives a dielectric function first derived by Lindhard [10]. On the other hand it is equivalent to the random phase approximation of the diagram technique Fig. (3.2), where the effective interaction between electrons accounts for dynamical screening [19].
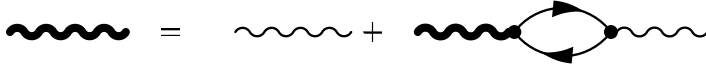
Fig. 3.2: *Dyson's equation for the screened potential on the RPA level. Thick wavy lines denote frequency dependent screened photon propagators, thin wavy lines represent the Coulomb interaction. The bubble is formed by electron propagators (one-particle Green's functions).*

When one uses this result to compute the total energy of the uniform electron gas one obtains results identical to that derived by Gell-Mann and Brueckner in the high-density limit (small r_s) summing up ring diagrams. Thus we see that allowing wavefunctions to change in time leads to the inclusion of some correlations.

Besides the fundamental interest in TDHF and its relation to other methods, this approach was also widely used in nuclear physics to study collective excitations in atomic nuclei.

Density functional theory now is the most popular way to include electronic correlations beyond HF. The formal basis of the theory was laid by Hohenberg and Kohn [20] in their famous theorem. It states that the exact ground-state energy of a correlated electron system is a functional of the density $\rho(\boldsymbol{r})$ alone and that this functional has its variational minimum when evaluated for the exact ground-state density. In principle, the theory maps the full many-body problem onto a simple mean-field equation. However, the exact form of the functional is not known. Many approaches have been used to treat the exchange-correlational functional approximately. To build it one performs more or less sophisticated many-body calculations for hypothetical infinite systems of electrons with constant density ρ. The resulting expression is used to extract the corresponding exchange-correlation part $e_{xc}(\rho)$, which is a function of the variable ρ. One can then proceed further to use the local density approximation (LDA) to express the functional dependence as:

$$E_{xc}^{\mathrm{LDA}}[\rho(\boldsymbol{r})] = \int \rho(\boldsymbol{r}) e_{xc}(\rho(\boldsymbol{r})) \, d^3r.$$

This approach was applied with great success to a large variety of systems often giving considerable improvement over the HF calculations.

As in the case of TDHF it is natural to extend LDA to account for the time dependence. The theory of this type was developed by Gross [21] and has been used for both purposes: to observe the evolution of the system in real time, and to study the system in the limit of linear response, reducing the equations to an eigenvalue problem. Early attempts to compute the atomic polarizabilities [22, 23] in the framework of the second approach showed the practicability of this method. Like TDHF this approach uses an RPA-like set of equations (Eq. (3.17)) to compute the excitation spectra of the system. The only difference between the HF and LDA is in the definition of the matrix elements of the interaction between excited states. In the case of HF it contains besides the direct term the exchange interaction

$$\langle ij|V|kl\rangle = \langle ij|\frac{1}{|\boldsymbol{r}-\boldsymbol{r}'|}|kl\rangle - \langle ij|\frac{1}{|\boldsymbol{r}-\boldsymbol{r}'|}|lk\rangle$$

while in the LDA case it contains the exchange-correlational functional:

$$\langle ij|V|kl\rangle = \langle ij|\frac{1}{|\boldsymbol{r}-\boldsymbol{r}'|}|kl\rangle - \langle ij|\frac{\delta V_{xc}}{\delta\rho}|kl\rangle.$$

The first application of this method to a large system like metallic clusters has been performed by Ekardt [6] employing the jellium model. However, one should be aware of possible pitfalls of the direct transfer of the exchange-correlational functional to the case of time-dependent electronic density [24]:

- the Hohenberg-Kohn theorem and the density-functional theory built upon it are strictly limited to the static ground state. In general, the exchange-correlation functional should be frequency dependent [25], and this cannot be reduced to the indirect dependence through the time-dependent electronic density $\rho(\boldsymbol{r},t)$.

- unlike the time-dependent HF scheme, where the LTH limit is known, there is a risk of double counting of some correlations in the TDLDA approach.

For the thorough comparison of a different type of TDLDA linear response calculations we refer reader to the works of van Gisbergen et al. [26] and Madjet et al. [27]. To the end of this section we concentrate on the first approach – time propagation of the electronic density.

The works in that direction have been initiated almost simultaneously by two groups of investigators [28, 29] soon after the development of the formal basis for TDDFT. In a series of papers [30, 31] Yabana and Bertsch gave a strong argumentation that for the large number of particles in a three dimensional configuration it is a more efficient way than to use the matrix formulation of the linear response. With the growth of the system size the diagonalization of a large matrix (Eq. (3.17)) soon becomes less efficient[3] than the solution of the time-dependent problem, which amounts to a matrix-vector multiplication[4] only.

Both approaches are quite similar. The electronic density is represented on a mesh in the 3D or 2D space exploiting the symmetry of the problem. The Laplace operator entering the Hamiltonian is evaluated by means of a finite-difference scheme, and the propagation in time is done by solving the set of ordinary differential equations by appropriate methods. To eliminate core electrons, that do not affect much the static and dynamic properties of the clusters, the jellium model or pseudopotentials of different kinds are used. Despite general belief, that for the time-dependent calculations one needs to use a frequency-dependent exchange-correlational potential, the standard functionals available from the static DFT are in wide use. This comes from the proven fact that, in the adiabatic limit, both types of functionals should give identical results.

---

[3] The size of the matrix is proportional to the number of particle-hole excitation, that scales as N_{e}^2, where N_{e} is the number of electrons in the system. The diagonalization of the matrix would require N_{e}^6 operations.

[4] In the real-time method the object of interest is the set of N_{e} wave-function vectors, each of the size of the basis N_{bf}. The time evolution is carried out by applying the Hamilton operator to the wave-functions, which require at most N_{bf}^3 operations for each wave-function, or $N_{\mathrm{e}} \cdot N_{\mathrm{bf}}^3$ in total.

The TDLDA method has been applied so far to different systems ranging from organic molecules and fullerenes to metallic clusters. The theory [28] is able to predict the gross features of the excitation spectrum of the C_{60} molecule, such as the position of the plasmon resonance, and its broadening due to Landau damping. For the organic chain molecules TDLDA gives the possibility to check the dependence of the frequency of the collective excitations on the length of the chain [30, 31]. The results are close to those of CI calculations for a small number of atoms and confirm the theoretical prediction $\omega_{pl} \sim \sqrt{\ln N}/N$ in the limit of a large number (N) of atoms. The calculations on alkali-metal clusters show that at large numbers of atoms the response function is not very sensitive to the ionic structure [28]. Thus, calculations can be facilitated by using the jellium model. However, in the case of smaller clusters or systems with localized d-electrons this approach is not permissible. The structure of the excitation spectrum depends very much on the cluster geometry. Extensive calculations [32] were done on sodium clusters from Na_2 to Na_{59}^+. They clearly show the dependence of the optical properties of the clusters on the geometry. In particular, because of the absence of spherical symmetry, the plasmon peaks are composed of several lines. They can be observed in photoabsorption experiments, and results of the TDLDA calculations show very good agreement with the measured spectra.

But not only the photoabsorption spectrum can be obtained from the results of the TDLDA calculations. One can vary parameters of the excitations such as the excitation energy, to observe the non-linear plasmon response [29, 33] or second and higher harmonic generation [34].

3.2   GW approximation

The single-particle Green function contains a great deal of information about the properties of the system under consideration. With its help we can calculate the ground-state expectation value of any single-particle operator as well as the ground-state energy of the system, etc. In principle, it contains more information about the system than the wave-functions and energies in the quasiparticle approximation. The latter is a very strong restriction. It says that the many-body wave-function of the system can be represented in the form of a single Slater determinant based on some one-particle wave-functions that describe quasi-particle states. To understand it better let us consider a simple example. According to a definition of Green's function for the system containing m electrons distributed over n states the Green function has $\frac{n!}{(m+1)!(n-m-1)!} + \frac{n!}{(m-1)!(n-m+1)!}$ poles as a function of energy. They result from the transitions between the ground state of the m particle and the excited states of the $m + 1$ and $m - 1$ particle systems. In the assumption of quasiparticles this is approximated by a function having only n poles. As we saw before this does not always work. The Hartree-Fock Green function, although quite well predicting the position of the major peaks in the spectral functions is not able to describe their broadening. Moreover it fails to describe their satellites simply because of the insufficient number of states it is built on. To remedy that one must go beyond the quasiparticle picture. But even in the framework of this approximation one can improve the description by allowing the energy of the quasiparticle to be complex, and, thus, taking into account its broadening or decay:

$\varepsilon_\alpha = \varepsilon_\alpha^0 + \langle \alpha | \Sigma(\varepsilon_\alpha) | \alpha \rangle$. The real part of the self-energy $\Sigma(\omega)$ also improves the energy of the eigenstates and corrects the gap between occupied and virtual states, which is too high in the Hartree-Fock picture and too low in the local density approximation. In this section we describe how the MBPT can contribute corrections to the Hartree-Fock or LDA eigenstates ε_α^0. Two main functions have to be considered: the single-particle Green function G and the self-energy Σ. They are connected by a complicated set of equations, through which the self-energy has to be determined self-consistently from the screened potential W and Green's function G as a product $\Sigma = -iGW$. This gave the name to the method.

3.2.1 Theory

The equations of the many-body perturbation theory do not form a closed set, rather an infinite chain. The equation of motion for the single-particle Green function contains a two-particle Green function. The equation of motion for two-particle Green's function depends on the Green function for three-particles, and so on. Instead of terminating such a chain at a certain level by an appropriate decoupling scheme we can proceed in different way by imposing a particular form of equation that the single particle Green function fulfills. Introducing the energy dependent self-energy operator $\Sigma(\boldsymbol{r}, \boldsymbol{r}', \omega)$, we can write the equation for Green's function without loss of generality as

$$\left[\omega - \hat{H}^0(\boldsymbol{r}) \right] G(\boldsymbol{r}, \boldsymbol{r}'; \omega) - \int d^3 r'' \Sigma(\boldsymbol{r}, \boldsymbol{r}''; \omega) G(\boldsymbol{r}'', \boldsymbol{r}'; \omega) = \delta(\boldsymbol{r}, \boldsymbol{r}'). \qquad (3.19)$$

In contrast to many textbooks where the general formalism of Green's function technique is built in the real-space representation $(\boldsymbol{r}, t)$ or reciprocal space $(\boldsymbol{k}, \omega)$, for our purpose it is better to work in a general basis. To simplify the notations we use $(1), (2), (3)...$ to label the set of space coordinates, time, and, possibly, spin. We label the basis functions as $\alpha, \beta, ...$ It is clear that most of the equations will not change its form in this basis set representation. But in this way we avoid some problems that arise from the assumption on a particular kind of basis function and simplify the notations. Thus, we can rewrite the last equation in the form

$$\sum_\alpha \left[\omega - H_{\gamma\alpha}^0 - \Sigma_{\gamma\alpha}(\omega) \right] G_{\alpha\beta}(\omega) = I_{\gamma\beta}, \qquad (3.20)$$

where $I_{\alpha\beta}$ is a diagonal operator. It is clear that one can get the equation for the Green function in the HF approximation diagrammatically represented on Fig. 3.1 from this equation as a particular case assuming that the self-energy takes the form

$$\Sigma^{HF}(\boldsymbol{r}t, \boldsymbol{r}'t') =$$
$$\underbrace{iv(\boldsymbol{r}, \boldsymbol{r}')G(\boldsymbol{r}t, \boldsymbol{r}'t')\delta(t - t' + \delta t)}_{H^{ex}} - \underbrace{i\delta(\boldsymbol{r}, \boldsymbol{r}') \int d^3 r'' v(\boldsymbol{r}, \boldsymbol{r}'')G(\boldsymbol{r}'' \, t, \boldsymbol{r}'' \, t + \delta t)}_{H^d} \quad (3.21)$$

Thus, we see that in the HF theory the self-energy depends self-consistently on the density matrix, or, which is the same, on the Green function in the equal time limit. In general, going beyond HF the self-energy should be regarded as a functional of G, i.e. $\Sigma = \Sigma(G)$. In

the case of any approximation the Hartree part (the second term of the above equation) of self-energy must be present. It is local in space and describes the effective potential in which the electron moves. We add it to the single-particle Hamiltonian redefining accordingly the self-energy $\Sigma(\boldsymbol{r}t, \boldsymbol{r}'t') \rightarrow \delta(\boldsymbol{r}, \boldsymbol{r}')H^d(\boldsymbol{r}) + \Sigma(\boldsymbol{r}t, \boldsymbol{r}'t')$.

Now we consider functional equations that enable us to determine the self-energy from the known Green function, and thus to close the infinite chain. The set of equations was first derived by Hedin (see Appendix C for the thorough derivation), and in the real-space representation it takes the form:

$$\Sigma(12) = i \int W(1^+3)G(14)\Gamma(42;3)d(34) \tag{3.22a}$$

$$W(12) = v(12) + \int W(13)P(34)v(42)d(34) \tag{3.22b}$$

$$P(12) = -i \int G(23)G(42)\Gamma(34;1)d(34) \tag{3.22c}$$

$$\Gamma(12;3) = \delta(12)\delta(13) + \int \frac{\delta\Sigma(12)}{\delta G(45)}G(46)G(75)\Gamma(67;3)d(4567). \tag{3.22d}$$

The plus sign here denotes the appropriate selection of the time arguments: $(1) \leftrightarrow (\boldsymbol{r_1}, t_1)$, whereas $(1+) \leftrightarrow (\boldsymbol{r_1}, t_1 + \delta t)$. The key quantity in Hedin's set of equations is the *screened interaction* W. It describes the interaction between the electrons in the electron gas. Because of the screening effects this interaction is weaker than the pure Coulomb interaction and is frequency dependent. It is connected to the Coulomb interaction via the inverse dielectric function as

$$W(12) = \int v(13)\varepsilon^{-1}(32)d(3). \tag{3.23}$$

$v(12)$ is an abbreviated notation for the Coulomb interaction

$$v(12) = v(\boldsymbol{r_1}, \boldsymbol{r_2})\delta(t_1 - t_2),$$

which, of course, is time-independent. To calculate the dielectric function one needs to know the *irreducible polarization operator* P, which is related to ε by

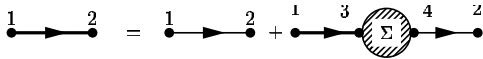$$\varepsilon(12) = \delta(12) - \int P(32)v(13)d(3). \tag{3.24}$$

Fig. 3.3: *Dyson's equation for the single-particle Green function.*

The set of Eqs. (3.22a)-(3.22d) has a very clear interpretation in terms of Feynman diagrams, see Fig. 3.4. As usually, thin and thick straight lines denote electron Green's functions of the non-interacting and interacting systems, respectively. Thin and thick wavy lines describe the screened and bare Coulomb interaction. Each connection point means integration in real space and real time. We also use the following notations: the self-energy is shown as a filled circle, the irreducible polarization operator is depicted by a filled electron loop, the irreducible vertex

part is given as a filled triangle and the functional derivative of the self-energy with respect to the Green function is displayed as a rectangle. The set of equations (4.22) should be complemented by the Dyson equation for Green's function, see Fig. 3.3

$$G(12) = G^0(12) + \int G(13)(H^d(34) + \Sigma(34))G^0(42)d(34), \tag{3.25}$$

where G^0 stands for the unperturbed Green function.

The influence of the self-energy on the properties of Green's function can be most easily understood by considering the translationally invariant homogeneous electron gas and expressing all quantities in reciprocal space. It is advantageous that in this case the non-interacting Hamiltonian $\hat{H}^0$ is diagonal, and the Green function and self-energy depend only on the $\boldsymbol{k}$-vector and frequency ω. The direct interaction part of the Hamiltonian H^d, which is diverging in this case, is cancelled by the field of the positive ion background, thus we do not include it in the following. Neglecting the spin, Dyson's equation (Eq. (3.25)) takes a simple form:
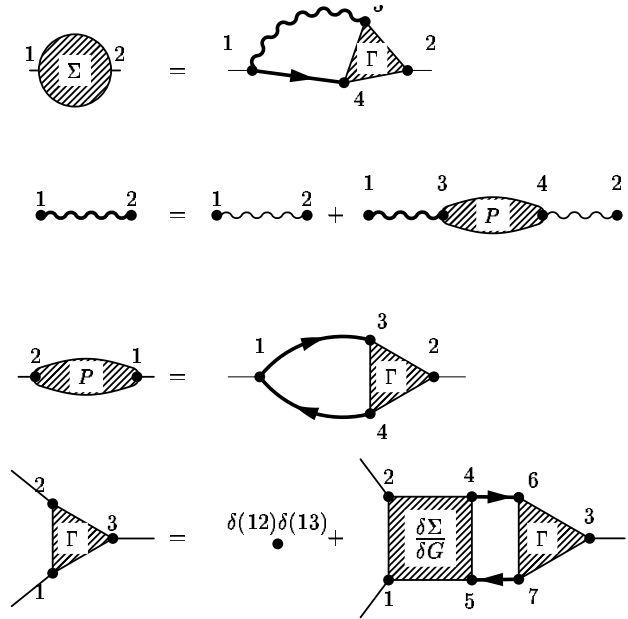
Fig. 3.4: *Hedin's equations.*

$$G(\boldsymbol{k},\omega) = G^0(\boldsymbol{k},\omega) + G(\boldsymbol{k},\omega)\Sigma(\boldsymbol{k},\omega)G^0(\boldsymbol{k},\omega).$$

From this, using the expression for G^0 (similar to Eq. (2.15))

$$G^0(\boldsymbol{k},\omega) = \lim_{\delta\to 0^+}\left[\frac{\Theta(k-k_F)}{\omega - \varepsilon_k^0 + i\delta} + \frac{\Theta(k_F - k)}{\omega - \varepsilon_k^0 - i\delta}\right]$$

one can obtain the following representation of the Green function

$$G(\boldsymbol{k},\omega) = \frac{1}{\omega - \varepsilon_k^0 - \Sigma(\boldsymbol{k},\omega)}. \tag{3.26}$$

From that one can see two effects of the self-energy (Fig. 3.6). First, it renormalizes the quasiparticle dispersion law. Instead that of the non-interacting system $\varepsilon_k^0 = \frac{k^2}{2m}$ it is now determined from the zero of the denominator[5]:

$$\omega - \frac{k^2}{2m} - \Sigma(\boldsymbol{k},\omega) = 0 \tag{3.27}$$

---

[5] Generally speaking one can have more than one solution, however, all of them except one lie in the region of energies where the imaginary part of the self-energy is large, and, thus, they are strongly damped.

The second important effect is the renormalization of the *spectral weight* of the quasiparticle peak. If we write the Green function in the vicinity of the pole in the form $G(\omega) = \frac{Z}{\omega - \varepsilon}$ we see that for the non-interacting system the spectral weight Z is exactly unity. In the interacting case we expand the self-energy around the pole as $\Sigma(\omega) = \Sigma(\varepsilon) + \frac{\partial \Sigma(\omega)}{\partial \omega}\Big|_{\omega = \varepsilon} (\omega - \varepsilon)$ and obtain the following expression for the spectral weight:

$$
\frac{Z}{\omega - \varepsilon} = \frac{1}{\omega - \varepsilon_k^0 - \Sigma(\omega)} = \frac{1}{\omega - \underbrace{(\varepsilon_k^0 + \Sigma(\varepsilon))}_{\sim \varepsilon} - \frac{\partial \Sigma(\omega)}{\partial \omega}\Big|_{\omega = \varepsilon} (\omega - \varepsilon)} =
$$

$$
1 \qquad \frac{1 + \frac{\partial \Sigma(\omega)}{\partial \omega}\Big|_{\omega = \varepsilon}}{\omega - \varepsilon}
$$
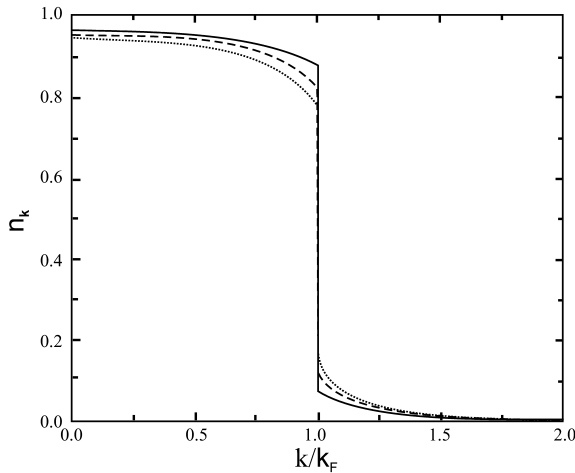
Fig. 3.5: *Momentum distribution function in the homogeneous electron gas at $r_s = 4$ a_B according to Ref. [35]. The calculations were performed on different levels of the theory: full line – GW, dashed line – GW^0, dotted line – $G^0 W^0$.*

The spectral weight is closely related to the momentum distribution function. In the case of the non-interacting electron gas the distribution is just a step function that is equal to 1 below the Fermi level and is 0 for the states with momentum larger than k_F. In the interacting case the states above the Fermi level get partially populated[6] and, as shown in Fig. 3.5, the magnitude of the discontinuity equals the strength of the quasiparticle pole at $k = k_F$.

In a similar manner Eq. (3.27) can be solved approximately to estimate the broadening $\Gamma(k)$ of the quasiparticle peak:

$$
\Gamma(k) = \frac{\Im m\, \Sigma(\boldsymbol{k}, \varepsilon(k))}{1 - \frac{\partial \Re e \Sigma(\omega)}{\partial \omega}\Big|_{\omega = \varepsilon}}.
$$

The frequency dependence of the self-energy can be understood from general principles. Such, from the existence of quasiparticles in the vicinity of the Fermi surface it follows that

---

[6] Note the similarity between the distribution function of the non-interacting electron gas at non-zero temperature and the interacting electron gas. There is, however, one important difference – at finite temperature the discontinuity at the Fermi energy disappears in the noninteracting case, whereas it is preserved in the interacting case. This has been confirmed in the work of Daniel and Vosko (Phys. Rev. **120** (1960), 2041) by considering RPA-type diagrams for the homogeneous electron gas at metallic densities. They demonstrate that the magnitude of the discontinuity is related to the Wigner-Seitz radius r_s as: $Z \sim 1 - 3.4 \frac{1}{\pi^2}(\frac{4}{9\pi})^{1/3} r_s$.

the imaginary part of the self-energy vanishes at $\omega = E_F$. In the cases when MBPT works it is possible to prove that $|\Im \Sigma(\omega)| \sim (\omega - E_F)^2$. From the fact that the discontinuity of the momentum distribution function cannot be larger than unity ($Z < 1$) a limitation of the slope of the real part of the self-energy follows $\frac{\partial \Re e\, \Sigma(\omega)}{\partial \omega} < 0$. Combining these two properties and imposing causality of the self-energy

$$\Sigma(\omega) = H^{ex} + \frac{1}{\cdot} \int \frac{|\Im \Sigma(\omega')|}{\cdot} d\omega'$$

one obtains the qualitative behavior as sh

The system of Hedin's equations (3.22) is exact and very complicated. The equations for the self-energy, screened potential, and polarization operator contain double integration over the space and time coordinates. Each of these quantities depends on two space-time variables. Even to represent them on the mesh in real space is very difficult. Let us make an estimation. For the DFT calculation one needs typically 10^5 mesh points to represent the electronic density. Let us assume that the time axis can be divided in 10^2 intervals. Thus one needs to keep at least 10^{14} real numbers for each function to capture them correctly. Double integra-
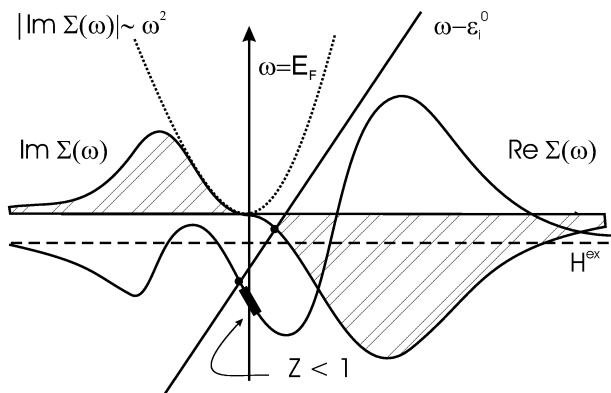

Fig. 3.6: *Anticipated behavior of the electron self-energy. Intersections of the straight line with the self-energy curves give solutions of Dyson's equation.*
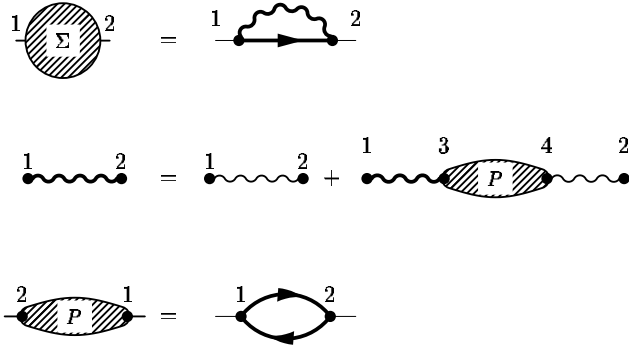
tion would require than 10^{28} floating-point operations, which are impossible now even on the most powerful supercomputers. The equation for the vertex part is even more complex. It contains the four-index quantity $\frac{\delta \Sigma}{\delta G}$ that has to be determined by a functional differentiation of the self-energy with respect to the Green function. This is very difficult to do numerically. Thus, one has to resort to approximations. The simplest one is to neglect the vertex function ($\Gamma(12;3) = \delta(12)\delta(13)$). One can consider that as a first step of the iterative solution of Hedin's equations. One starts with $\Sigma = 0$ and inserts this in Eq. (3.22d). From that we get a self-consistent set of equations to determine the single-particle electron propagator $G(\omega)$, screened interaction $W(\omega)$, dielectric function $\varepsilon(\omega)$ and irreducible polarization operator $P(\omega)$:

$$\begin{aligned}
\Sigma(12) &= iW(1^+2)G(12) \\
W(12) &= v(12) + \int W(13)P(34)v(42)d(34) \\
P(12) &= -iG(12)G(21).
\end{aligned} \qquad (3.28)$$

In the literature the set of Eqs. (3.28) is usually referred to as GW approximation, because the self-energy is a product of Green's function G and screened Coulomb interaction W. In a diagrammatic form they can be represented as shown in Fig. 3.7.

Fig. 3.7: *Hedin's equations neglecting the vertex correction.*

The system Eq. (3.28) must be solved iteratively. It means that one starts with a reasonable expression for the Green function. Normally one can build it in the quasiparticle approximation based on the results of the HF or LDA calculations[7]

$$G^{HF}(\boldsymbol{r}, \boldsymbol{r}'; \omega) = \sum_i \frac{\psi_i^*(\boldsymbol{r})\psi_i(\boldsymbol{r}')}{\omega - \varepsilon_i^0},$$

where we understand that the proper infinitesimals are included in ε_i^0 according to the rule Eq. (2.14). Here the sum is taken over all occupied and virtual states. From this Green's function one builds the polarization operator and, consequently, the screened interaction. The self-energy is then computed and is used to find a new Green function by the solution of Dyson's equation (Eq. (3.25)). The cycle is repeated until the Green functions of two consecutive steps do not differ any more. From that one can introduce further approximations, discussed in the literature. A broad review of the multitude of approaches within the framework of the GW approximation can be found in the paper of Aryasetiawan and Gunnarsson [36]. They differ by how the self-consistency loop is arranged. If one stops after the first step of iteration, thus using the Green function of the mean-field calculations to compute both the screened interaction and self-energy it is referred to as G^0W^0 approximation. Within this approach only corrections to the eigenstate energy are computed by approximately solving Dyson's equation

$$\varepsilon_i = \varepsilon_i^0 + \langle i|\Sigma(\varepsilon_i)|i\rangle.$$

This equation should be understood as a first order perturbational treatment of the self-energy function. This kind of approach is the simplest one because only the diagonal matrix elements of the self-energy are required, thus, it was the first one that has been implemented for realistic systems. However, one of the conceptual deficiencies of a non-self-consistent procedure is, of course, the dependence of the final results on the choice of initial Green's function.

One can build a partially self-consistent scheme to avoid that problem. In the GW calculations one of the major computational difficulty is the inversion of the dielectric function $\varepsilon(\omega)$, that should be performed at each frequency point. This can be facilitated by using the so called plasmon pole approximation for the dielectric function, or by taking the screened potential out of the self-consistency loop, in the so called GW^0 approximation. Therefore, the computational efficiency is improved and the method becomes less sensitive to the initial choice of Green's function.

Summarizing, in this section we started with a set of Hedin's equations that connect Green's function, polarization operator, screened potential and vertex function. Neglect

---

[7] It is easy to verify that the HF Green function satisfies Eq. (3.19) with $\Sigma = \Sigma_{HF}$ given by Eq. (3.21).

of the vertex function leads to the simplified GW approximation. Further simplification can be achieved to make the theory accessible for numerical implementations in going to the G^0W^0 or GW^0 levels. Before proceeding further with these approximations one must clarify the following points:

- For which systems and under which conditions are they valid?

- Do they conserve particle number and total energy of the system?

- What is the role of the vertex function, that is neglected in GW approach?

3.2.2   Justification of the GW approximation

One can understand how the approximation works for realistic systems by applying the method to simplified models. The most popular system to test MBPT is the homogeneous, translationally invariant electron gas. In the series of papers by Holm and von Barth [37, 35] the G^0W^0, GW^0 and GW schemes were compared. Calculations show that for the electronic density $r_s = 4\,a_{\mathrm{B}}$, which is typical for sodium, the shift of the quasiparticle energy due to the GW corrections is around 10%. The description of the bandwidth is best in the G^0W^0 scheme and deteriorates in going further to GW^0 and GW. It is known, for example, that for simple metals (e.g. sodium) experiments give the bandwidth approximately 10% narrower compared to the results of band-structure calculations employing LDA. This paradoxical result[8], that the fully self-consistent GW calculation is worse than G^0W^0 indicates the necessity of vertex corrections. The situation is opposite with the total energy: the quality of the obtained results becomes better in the full GW calculation, giving excellent agreement with results of Monte-Carlo calculations (at $r_s = 4\,a_{\mathrm{B}}$ the relative error of the energy per particle is approximately 0.6%).

In the papers [38, 39] the role of the vertex function was discussed again for the same system, for the Hubbard cluster [40] and for realistic systems like silicon or diamond [41]. Up to now it was not possible to take the vertex function into account without any simplifying approximations because a numerical treatment is possible only if the functional derivative in the Eq. (3.22d) can be evaluated analytically. A general approach how to do that within the self-consistency loop was developed in [40] and was shown to be very fruitful in describing the satellite structure, as well as in demonstrating the convergence of the $GW\Gamma$ scheme.

---

[8] The reason for that is a different distribution of the spectral weight (Z) among the quasiparticle peak and satellite structure on the different levels of theory. In the G^0W^0 scheme a Green function with non-renormalized spectral weight ($Z = 1$ – no satellites) is used to compute the dynamical part of the self-energy that partially cancels the HF contribution and produces the best result. On the GW^0 level the spectral weight of the quasiparticle peak in the Green function is already reduced because of the appearance of the satellite structure. Thus, the dynamical part of the self-energy is smaller and does not compensate the static one any more. On the fully self-consistency level the quasiparticle peak becomes sharper again (compare full and dashed lines in Fig. 3.5), thus one can expect an improvement of the cancellation and further reduce of the band-gap. This, however, is obstructed by the change of the static part of the self-energy because of the redistribution of the electronic density. The second effect is even stronger leading to an increase of the band-gap. A good discussion on this subject can be found in Ref. [35].

Fig. 3.8: *Expansion of the self-energy as a functional of the screened interaction in second order as used in Ref. [38].*

There is the general belief that there exists a cancellation of the self-consistency effect on the band gap and inclusion of the vertex correction coming from the work of Shirley [39]. He used the expansion of the self-energy to second order in the screened interaction (Fig. 3.8) to capture some effect

of the vertex function. In the paper of Ummels *et al.* [41] it was shown that higher order diagrams in both the polarization operator (to first order in W) and self-energy (to second order in W) can partially cancel. This effect is very large for P and is 35% for the self-energy.

Fig. 3.9: *Generating functional for the self-consistent GW approximation that guarantees conservation of the particle number, total energy, and momentum.*

Not all GW approaches are equivalent with respect of their conservation properties. There is a sufficient condition derived in the papers by Kadanoff and Baym [42, 43] that guarantees conservation of particle number, total energy, and momentum under a time-dependent external perturbation. It requires that the self-energy can be represented as a functional derivative $\Sigma = \delta\Phi/\delta G$ of a certain generating functional Φ with respect to Green's function G which satisfies the Dyson equation with this self-energy. In the case of the self-consistent GW approximation the functional

can be diagrammatically represented as shown in Fig. 3.9. On the other hand it is obvious that the G^0W^0 approximation is not conserving because the Green function is not determined self-consistently from the corresponding self-energy. The partially self-consistent scheme GW^0, however, conserves the total particle number, although the self-energy cannot be represented as a functional derivative of some functional. The prove of that as well as calculations that show the violation of the total particle number in the G^0W^0 approach can be found in Ref. [44]. According to this work, in the case of the homogeneous electron gas, the relative error in determining the total particle number on the G^0W^0 level ranges from 0% at $r_s = 0$ to 0.25% at an electron density of $r_s = 4.6\ a_B$.

3.2.3   Numerical implementation

In this section we describe our implementation of the GW method using localized basis functions. This approach is particulary useful for systems without translational invariance i.e. atoms, molecules and clusters. As a basis we use contracted Gaussians that have found a broad application in quantum chemistry. It might look contradictory, that in this section we use indices $i, j, k, ...$ to label basis functions. As we mentioned before indices $\alpha, \beta, \gamma...$ are reserved for this purpose, and $i, j, k, ...$ label eigenstates. However, Gaussian basis functions often contain information of limited physical relevance. For example results of the HF calculations in this basis contain a number of virtual states with high energy

that are represented very poorly. Their inclusion in further calculations will not add new features to the physical picture, but slow down the computations. Therefore it is necessary to limit the states included in the GW calculation. It is achieved by changing from the Gaussian basis to the basis of HF eigenfunctions and introducing cut-offs for highly excited and deeply lying states ($\{\alpha, \beta, \gamma...\} \rightarrow \{i, j, k, ...\}$).

It is important to represent all equations in matrix form to achieve the best performance. When transforming Hedin's equations to this form special care must be taken in order to reduce possible numerical errors due to the incompleteness of the basis set. For example one must avoid operations of the kind: $C_{\alpha\beta} = \sum_\gamma A_{\alpha\gamma} B_{\gamma\beta}$ wherever possible when the matrix C can be computed directly. As an illustration let us consider the computation of the screened interaction W from the known Green function in detail. One may do it in the following sequence of operations: first, the polarization operator is computed as $P = -iGG$, then the dielectric matrix is built using Eq. (3.24). In the next step it has to be inverted to compute the screened interaction according to Eq. (3.23). The first step can easily be done in real space where it amounts to a simple multiplication. In order to perform this operation in matrix form one must compute overlap integrals over three basis functions

$$O_k^{mn} = \int d^3r \phi_k(\boldsymbol{r})\phi_m(\boldsymbol{r})\phi_n(\boldsymbol{r}).$$

Omitting the time arguments for the sake of simplicity we then have

$$
\begin{aligned}
P(\boldsymbol{r_1}, \boldsymbol{r_2}) &= -i \int d^3r\, G(\boldsymbol{r_1}, \boldsymbol{r_2}) G(\boldsymbol{r_2}, \boldsymbol{r_1}) = \\
&\quad -i \int d^3r \sum_{k_1,k_2} \sum_{l_1,l_2} G_{k_1,k_2} \phi_{k_1}(\boldsymbol{r_1}) \phi_{k_2}(\boldsymbol{r_2}) G_{l_1,l_2} \phi_{l_1}(\boldsymbol{r_2}) \phi_{l_2}(\boldsymbol{r_1}) \\
P(\boldsymbol{r_1}, \boldsymbol{r_2}) &= \sum_{mn} P_{mn} \phi_m(\boldsymbol{r_1}) \phi_n(\boldsymbol{r_2}).
\end{aligned}
$$

Comparing both expressions we get finally

$$P_{mn} = -i \sum_{k_1,k_2} \sum_{l_1,l_2} O_m^{k_1,l_1} G_{k_1,k_2} G_{l_1,l_2} O_n^{k_2,l_2}.$$

The integration over the space coordinates needed to compute the dielectric function in the basis set representation is reduced to a simple matrix multiplication, thus

$$\varepsilon_{mn} = I_{mn} + \sum_k P_{mk} v_{kn}.$$

Here the v_{kn} are two-point matrix elements of the Coulomb interaction. However this implementation is *not* an optimal way. The last identity is true only if the basis set is complete and infinite. Performing the integration via matrix multiplication is not precise even in the case of an extended basis, because of the absence of the delocalized basis functions. One avoids this problem by introducing three-point electron repulsion integrals (ERIs)

$$V_k^{mn} = \int d^3r d^3r' \frac{\phi_k(\boldsymbol{r})\phi_m(\boldsymbol{r'})\phi_n(\boldsymbol{r'})}{|\boldsymbol{r} - \boldsymbol{r'}|}$$

and combining two steps together:

$$(\varepsilon - I)_{mn} = -i \sum_{k_1,k_2} \sum_{l_1,l_2} O_m^{k_1,l_1} G_{k_1,k_2} G_{l_1,l_2} V_n^{k_2,l_2}.$$

The crucial place of performing the 3D integration has now shifted to the computation of the 3-point ERIs, which can be done analytically in the case of Gaussian basis functions as is explained in Appendix A.

Inversion of the dielectric matrix is as well not the best way from the computational point of view because of the numerical instability. It is better to combine it with the last step by solving the system of linear equations to determine the screened potential. It is useful to split the screened potential W into two parts: the unscreened Coulomb interaction that is not frequency dependent and the contribution from the *Coulomb hole*[9] ($W_{mn}(\omega) = v_{mn} + W'_{mn}(\omega)$). The former, after convolution with Green's function, gives the exchange part of the Hartree-Fock Hamiltonian. Keeping in mind expression Eqs. (3.1, 3.8) for the Hartree-Fock Hamiltonian $\hat{H}^{HF}$ we can rewrite the system of equations in the form

$$\Sigma'_{mn}(\omega) = \frac{i}{2\pi} \int d\omega' \sum_{k_1,k_2,l_1,l_2} O_m^{k_1 l_1} G_{k_1 k_2}(\omega + \omega') W'_{l_1 l_2}(\omega') O_n^{k_2 l_2} e^{i\omega'\delta}, \quad (3.29a)$$

$$W'_{mn}(\omega) = W_{mn}(\omega) - v_{mn}, \quad (3.29b)$$

$$v_{mn} = \sum_{k,l} W_{mk}(\omega)\varepsilon_{kn}(\omega), \quad (3.29c)$$

$$(\varepsilon - I)_{mn}(\omega) = -\frac{i}{2\pi} \int d\omega' \sum_{k_1,k_2,l_1,l_2} O_m^{k_1 l_1} G_{k_1 k_2}(\omega') G_{l_2 l_1}(\omega' - \omega) V_n^{k_2 l_2}, \quad (3.29d)$$

$$G_{mn}(\omega) = [\omega I - H^{HF} - \Sigma'(\omega)]_{mn}^{-1}. \quad (3.29e)$$

This is the set of equations that forms the essence of our method. However, spin is not taken into account here (spinless fermions). According to the diagrammatic rules summation over the spin variables must be performed in the expression for the polarization operator. In the case of an equal number of spin-up and spin-down electrons an additional factor 2 results in Eq. (3.29d) on the RHS.

The computation of the polarization operator and self-energy is the major computational task. At a first glance the numerical cost of performing these convolutions is $N_\omega^2 N_{bf}^6$ proportional to the square of ω points and sixth power of the number of basis functions. In fact this estimate can be considerably reduced by making use of the fast Fourier transform (FFT) to the real time $\omega \to t$ and back. This idea is very similar to that used in the real-space implementation of the GW method for jellium and semiconductors by Godby *et al.* [45]. They define the Green function on a mesh in real space and imaginary time ($G(\boldsymbol{r}, \boldsymbol{r}', \tau)$). To compute the convolutions $P = -iGG$ and $\Sigma = iGW$ 6D-FFT with respect to space coordinates and 1D-FFT from complex time to complex energy are performed.

---

[9] When a negatively charged particle – an electron – is put into the electron gas it repels other electrons. Therefore, around it a cloud of positive charge density is build that reduces the strength of electron-electron interaction and makes it frequency dependent.
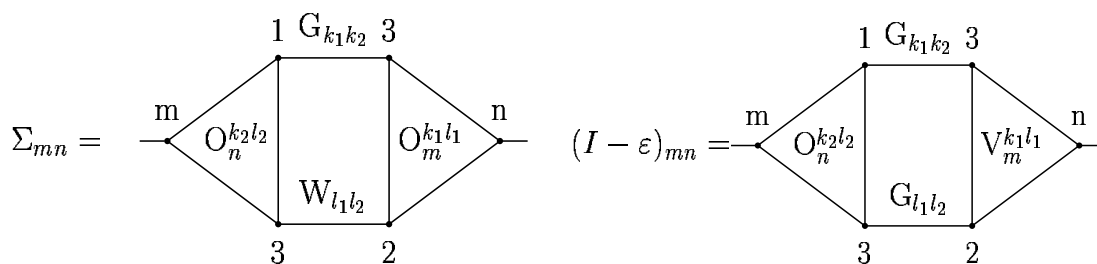
Fig. 3.10: *Computation performed in the order shown by numbers. Numerical cost of each step is proportional to N_{bf}^4*

In this new representation P and Σ are simply given as a product of the corresponding quantities. As a consequence the method asymptotically scales almost linearly with the system size. In the case of localized systems it is better to retain the basis set representation of the spacial part and use FFT to do the convolution in ω space. Convolution in the frequency domain corresponds to a simple multiplication in the time domain. The number of operations is, thus, proportional to N_ω. The conventional Fourier transform scales as N_ω^2, therefore no gain in speed is expected. The fast Fourier transform, which operates only on a certain number of mesh points[10] scales as $N_\omega \log_2(N_\omega)$ thus giving a huge acceleration. The efficient computation of the product of 2 two-indexes and 2 three-indexes quantities can be done at a cost of only N_{bf}^4 by carefully scheduling the order of operations as shown schematically in Fig. 3.10. All three steps can be done by matrix multiplications employing highly efficient mathematical libraries.

The initial Green function and dielectric function are computed from the results of the self-consistent Hartree-Fock calculation

$$G_{mn}(\omega) = \sum_{s=1}^{N_{\mathrm{bf}}} \frac{\psi_m^s \psi_n^s}{\omega - \varepsilon_s}, \tag{3.30}$$

$$(\varepsilon - I)_{mn}(\omega) = \sum_{\substack{k1,k2, \\ l1,l2=1}}^{N_{\mathrm{bf}}} \sum_{s,s'=1}^{N_{\mathrm{bf}}} \frac{n_s - n_{s'}}{\varepsilon_s - \varepsilon_{s'} - \omega} \psi_{k_1}^s \psi_{l_2}^{s'} \psi_{l_1}^{s'} \psi_{k_2}^s V_n^{k_2 l_2} O_m^{k_1 l_1}. \tag{3.31}$$

Here a small positive (negative) imaginary part has to be added to the eigenvalues below (above) the Fermi energy, according to the rule Eq. (2.14). The last expression is obtained by performing the integration in Eq. (3.29d). n_s is the occupation number of the corresponding state.

We represent all ω-dependent quantities on the *real axis* (Fig. 3.11). This has advantages and deficiencies. For example there is no need to perform an analytic continuation from the real axis to the imaginary axis and back, for which no reliable numerical algorithm exists. On the other hand, the Green function (for instance) has a complicated behavior close to the real axis because of the vicinity of the poles. This requires a larger number of mesh points compared to the imaginary axis, where the function is smooth. To overcome

---

[10] most often it is a power of 2

this problem we use *a dense mesh only in the central part*, close to the Fermi level, where all physics happens, whereas outside that region functions are rationally approximated as:

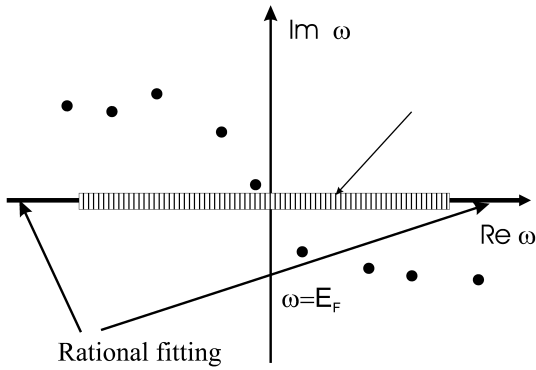$$F_{mn}(\omega) = \frac{F_{mn}^{(1)}}{\omega - \omega_1} + \frac{F_{mn}^{(2)}}{\omega - \omega_2} \tag{3.32}$$

Fig. 3.11: *Representation of the ω-dependent functions in our approach. Black dots schematically denote the poles of Green's function. In the central part a uniform mesh is used. At the edges functions are approximated by a rational expression, see Eq. (3.32).*

In contrast to the analytic continuation, for such fitting one can use a reliable least squares method[11]. The above approach reduces the memory requirements and speeds up the computations by eliminating the regions, in which functions behave predictably and smoothly anyway.

Up to now the only approximation that we used was neglecting the vertex part in the expressions for the self-energy and polarization operator. Now we discuss several approximation, that we used in order to speed up the computations.

(i) It is well known that the self-consistent approximation GW belongs to the class of conserving approximations (Ref. [42, 46]). The problems arises in the course of the self-consistent loop, when we start with the G^0W^0 approximation which is not conserving. The manifestation of the non-conservation of the particle number is the non-Hermiticity of the density matrix which is most readily obtained via integration of Green's function in the whole frequency domain

$$\rho_{mn} = \frac{1}{2}\left[I_{nm} - \frac{1}{\pi i} \int\limits_{-\infty}^{\infty} G_{nm}(\omega)d\omega \right]$$

To avoid this problem one has to symmetrize the density matrix, or, as we did to keep the density matrix on the HF level throughout the GW self-consistency loop (see Fig. 3.12 for the diagrammatic representation).

(ii) In order to speed up the computation of the polarization operator as a convolution of two Green's functions one might construct both $G_{mn}(\omega)$ and $P_{mn}(\omega)$ by solving the Dyson equation approximately (path (a) on the flowchart Fig. 3.13 compared to the exact solution of Dyson's equation, that is shown as path (b)). Instead of computing the Green function as the inverse of the non-local Hamiltonian one may try to solve the eigenvalue

---

[11] In fact such fitting is done in two stages. First the least squares-method is used to find the coefficients of $F_{mn}(\omega) = \frac{A_{mn}^{(1)}\omega + A_{mn}^{(0)}}{B^{(2)}\omega^2 + B^{(1)}\omega + B^{(0)}}$. Then this is transformed to the above form by factorizing the denominator.

problem close to each expected pole of the Green function. As the Hamiltonian due to the self-energy correction is non-Hermitian we must consider left end right eigenfunctions.

$$\varepsilon_n \quad \sim \quad \varepsilon_n^{HF} + \Sigma_{nn}(\varepsilon_n) \tag{3.33a}$$

$$\left[H^{HF} + \Sigma'(\varepsilon_n) \right] \psi_n^L \quad = \quad \varepsilon_n \psi_n^L \tag{3.33b}$$

$$\left[H^{HF} + \Sigma'^\dagger(\varepsilon_n) \right] \psi_n^R \quad = \quad \varepsilon_n \psi_n^R \tag{3.33c}$$

The Green function is then constructed (approximately) similar to Eq. (3.30)

$$G_{mn}(\omega) = \sum_{s=1,N_{\text{bf}}} \frac{\psi_m^{Rs} \psi_n^{Ls}}{\omega - \varepsilon_s}. \tag{3.34}$$

The dielectric function is built then in analogy to Eq. (3.31). However this method is not suitable when the poles of the Green function are close one to another.

Our computational approach permits an efficient parallelization for the multi- or vector-processors machines in the most time-demanding stages, namely, convolutions of two Green's functions or Green's function and screened interaction. After FFT the problem consists of many independent tasks of computing the self-energy or polarization operator for each time point according to the schemes of Fig. 3.10. This is shown schematically on Fig. 3.13 by multi-lines.
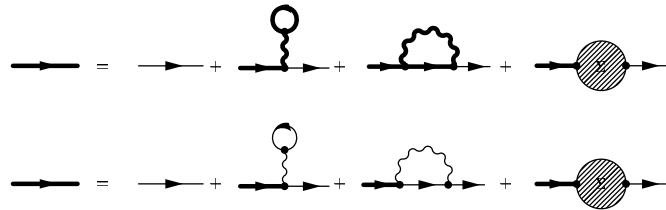
Fig. 3.12: *Dyson's equation, two approximations: top – fully self-consistent GW. The Σ' as well as direct and exchange terms are updated from the Green function of the previous step. Bottom – the direct and exchange energies are kept on the HF level (first iteration).*

3.3 Differences and similarities between HF, LDA, and GW

The notion of electronic states is the cornerstone of solid-state physics and quantum chemistry. With the exception of several models, where analytic solutions are known, one has to rely on different approximations to deal with the many-body nature of the problem. Here we would like to concentrate on the question how electron-electron interaction (this, actually, makes the problem a many-body one) is described on the single-particle level in different approximations, such as HF, LDA, and GW. Several aspects have to be addressed:

- To which extent are results of HF, LDA, and GW comparable ?

- How do these methods describe electronic correlations ?

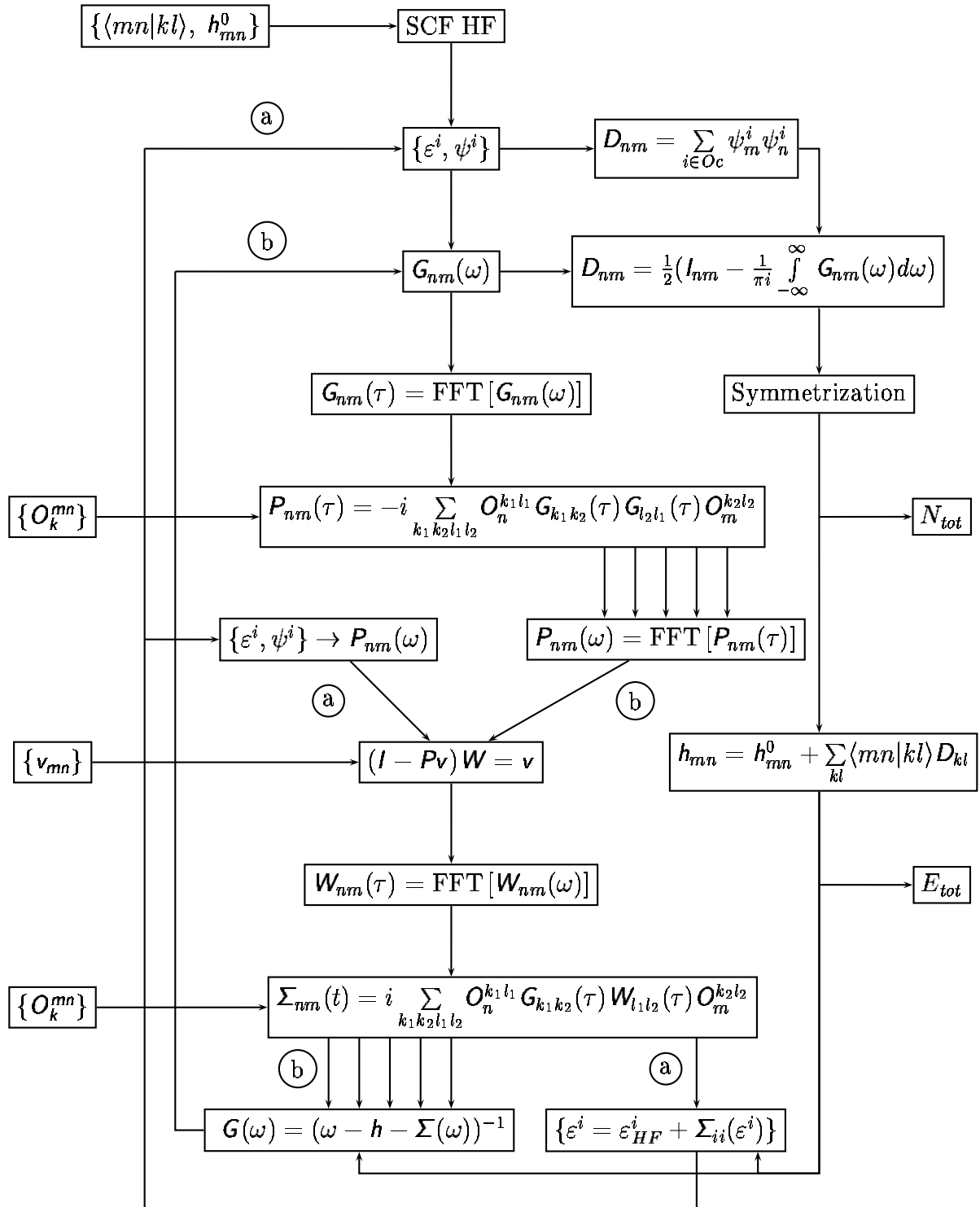- How is the non-local two-body Coulomb interaction treated within a one-body scheme ?

Fig. 3.13: *Flow chart of the self-consistent GW calculation. (a) denotes the path, when Dyson's equation is solved approximately, (b) — Dyson's equation is solved by the inversion of the non-local Hamiltonian at each ω point.*

For the HF and LDA approaches or their time-dependent counterparts the result is always single-particle wave-functions and their energies. In contrast, the GWA operates mainly with Green's functions. However, as we showed by Eqs. (3.33a-3.33c, 3.34), even in the case of a non-Hermitian problem that arises due to the self-energy corrections the Green function can still be built based on the single-particle eigenstates. But the analogy with HF and LDA is not complete – one must consider left and right eigenfunctions.

By definition electronic correlations are not accounted on the HF level. In the case of DFT one can, in principle, calculate them completely, but the exchange-correlation functional is known only for a few model systems. In the case of realistic systems one has to resort to various approximations. The first and most obvious one is the simplified spatial dependence of the exchange-correlation potential in the LDA (their are also cases were the gradient correction is needed). The second is the simplified treatment of correlation used to build the exchange-correlation functional. As a consequence the results of the calculations done for the same system using different functionals may differ slightly.[12] The GW approximation has several advantages in this respect by accounting for correlations more fully and allowing even for the life-time determination that is not possible within the LDA approach.

Regarding the properties of the effective Coulomb interaction entering the eigenvalue problem in all three cases one sees a similarity between the HF and GW approaches, which is different from the LDA. In the latter case the exchange-correlation functional that describes electron-electron interaction is local in space similar to the direct interaction in HF, LDA, and GWA. By contrast, the exchange interaction in the HF approach as well as the self-energy in the GW are *non-local in space*, i.e. they depend on two space variables $(\boldsymbol{r}, \boldsymbol{r'})$. In the GW scheme the self-energy additionally depends on the energy. The non-locality of the self-energy is very important and can be illustrated on the example of dynamical mean-field theory (DMFT) [47]. Within this approach, which gives an explicit analytical solution for the infinite-dimensional Hubbard model [48] and well describes the Mott transition in model and realistic systems, the correlational problem on the lattice is reduced to a single-site problem which has to be solved via the $\boldsymbol{k}$-integrated Dyson equation. For the one-site problem the self-energy is, of course, local. The iterative mapping between the lattice and the one-site problem, which is given by the Anderson impurity model, is necessary to account for spatial variations and, thus, to obtain a solution for a bulk system. This last step shows the importance of spatial resolution, which, in contrast, is achieved in the GW approach by explicitly constructing the non-local self-energy.[13]

---

[12] For quantum chemical calculations examples of commonly used functionals are: correlational functionals of Vosko, Wilk, and Nusair (Canadian J. Phys. **58**, 1200 (1980), the gradient corrected functional of Lee, Yang and Parr (Phys. Rev. B **37**, 785(1988)) employed together with exchange functional of Becke (Phys. Rev. A **38**, 3098(1988)) or the Perdew and Wang exchange-correlational functional (Phys. Rev. B **54**, 16533 (1996)).

[13] For realistic materials the DMFT approach can be combined with the GWA (P. Sun and G. Kotliar, Phys. Rev. B **66**, 085120 (2002)) or with the LDA (K. Held I. A. Nekrasov, N. Blümer, V. I. Anisimov, and D. Vollhardt, Int. J. Mod. Phys. B **15**, 2611 (2001)).

3.4   SHG

In Section. 2.2.3 we derived the plasmon dispersion from the equation of motion for the density matrix. As a starting point we used perturbational theory and computed the variation of the electronic density due to some time-dependent external potential (Eq. (2.18)) in first order. One can put a question: What will give us the inclusion of the higher orders into the perturbational treatment? Analogously to Eq. (2.18) we can obtain the expression for the second order correction to the density matrix:

$$\rho_{kk'}^{(2)}(2\omega) = \frac{1}{\varepsilon_{kk'} - 2\omega} \sum_l V_{kl} V_{lk'} \left[\frac{n_{kl}}{\varepsilon_{kl} - \omega} - \frac{n_{lk'}}{\varepsilon_{lk'} - \omega} \right], \tag{3.35}$$

where we introduce the notations $n_{kl} = n_k - n_l$ and $\varepsilon_{nk} = \varepsilon_n - \varepsilon_k$. The summation is performed over all eigenstates of the single particle Hamiltonian. The superscript "(2)" indicates that the expression corresponds to second-order perturbation theory and the argument 2ω explicitly shows that in this order we have response only on the double frequency (second harmonic generation). We introduce the second order susceptibility tensor $\rho_{kk'}^{(2)}(2\omega)$ according to:

$$\boldsymbol{P}_{2\omega}^{(2)\,i} = \chi^{ijk}(2\omega)\boldsymbol{E}_\omega^j \boldsymbol{E}_\omega^k \tag{3.36}$$

as a quantity that shows the dipole response of the system $\boldsymbol{P}_{2\omega}^{(2)}$ at frequency 2ω to the electric field $\boldsymbol{E}_\omega$ at frequency ω. With

$$\begin{aligned} \boldsymbol{P}_{2\omega}^{(2)} &= \sum_{kl} \boldsymbol{d}_{kl} \rho_{lk}^{(2)}(2\omega) \\ V_{kl} &= (\boldsymbol{d}, \boldsymbol{E}_\omega)_{kl} = (\boldsymbol{d}_{kl}, \boldsymbol{E}_\omega) \end{aligned}$$

Eq. (3.35) enables us to express the susceptibility tensor via internal parameters of the system as

$$\chi^{ijk}(2\omega) = \frac{1}{2} \frac{\partial^2}{\partial \boldsymbol{E}^j \partial \boldsymbol{E}^k}\bigg|_{\boldsymbol{E}^j = \boldsymbol{E}^k = 0} \sum_{kl} \boldsymbol{d}_{kl}^i \rho_{lk}^{(2)}(2\omega). \tag{3.37}$$

$\boldsymbol{d}$ denotes the vector of the dipole moment. Performing the differentiation we finally obtain:

$$\chi^{ijk}(2\omega) = \sum_{lmn} \frac{\boldsymbol{d}_{lm}^i \overline{\boldsymbol{d}_{ln}^j \boldsymbol{d}_{nm}^k}}{\varepsilon_{lm} - 2\omega} \left[\frac{n_{ln}}{\varepsilon_{ln} - \omega} - \frac{n_{nm}}{\varepsilon_{nm} - \omega} \right], \tag{3.38}$$

where the overline denotes symmetrization:

$$\overline{\boldsymbol{d}_{ln}^j \boldsymbol{d}_{nm}^k} = \frac{1}{2}(\boldsymbol{d}_{ln}^j \boldsymbol{d}_{nm}^k + \boldsymbol{d}_{ln}^k \boldsymbol{d}_{nm}^j).$$

In order to make sense of the formula close to the poles small imaginary parts should be added to the eigenvalue energies according to the rule Eq. (2.14). In SI units the expression for the second order susceptibility tensor reads [49]:

$$\chi^{ijk}(2\omega) = \frac{\rho_0}{\varepsilon_0} \sum_{lmn} \frac{\boldsymbol{d}_{lm}^i \overline{\boldsymbol{d}_{ln}^j \boldsymbol{d}_{nm}^k}}{\varepsilon_{lm} - 2\hbar\omega} \left[\frac{n_{ln}}{\varepsilon_{ln} - \hbar\omega} - \frac{n_{nm}}{\varepsilon_{nm} - \hbar\omega} \right], \tag{3.39}$$

where ε_0 is the permittivity of free space and ρ^0 denotes the unperturbed electronic density. Let us check the dimension of the formula:

$$\chi^{ijk}[\text{m/V}] = \chi^{ijk}\left[\frac{\text{e}\cdot\text{s}^2}{\text{kg}\cdot\text{m}}\right] =$$

$$\frac{\rho^0[1/\text{m}^3]}{\varepsilon_0[\text{e}^2\cdot\text{s}^2/(\text{kg}\cdot\text{m}^3)]}\frac{(d[\text{e}\cdot\text{m}])^3}{(E[\text{J}])^2} = \frac{\rho^0[1/\text{m}^3]}{\varepsilon_0[\text{e}^2\cdot\text{s}^2/(\text{kg}\cdot\text{m}^3)]}\frac{d^3[\text{e}^3\cdot\text{m}^3]}{(E[\text{kg}\cdot\text{m}^2/\text{s}^2])^2} = \left[\frac{\text{m}}{\text{V}}\right].$$

This second order susceptibility tensor $\chi^{ijk}(2\omega)$ possesses a number of symmetry properties. Obviously, it is symmetric with respect to the interchange of the two last indices

$$\chi^{ijk}(2\omega) = \chi^{ikj}(2\omega). \tag{3.40}$$

This reflects the equivalence of the two incident photons. In the static case ($\omega = 0$) the tensor is symmetric with respect to the interchange of the first and second (third) indices (so-called Kleinman symmetry [50]):

$$\chi^{ijk}(0) = \chi^{jik}(0). \tag{3.41}$$

To prove that let us rewrite Eq. (3.38) in the form:

$$\chi^{ijk}(2\omega) = \sum_{lmn} \boldsymbol{d}_{lm}^i \overline{\boldsymbol{d}_{ln}^j \boldsymbol{d}_{nm}^k} F(lmn),$$

where the function $F(lmn)$ in the limit $\omega = 0$ is:

$$F(lmn) = \frac{n_{ln}}{\omega_{ln}\omega_{lm}} - \frac{n_{nm}}{\omega_{nm}\omega_{lm}}.$$

Upon changing indexes $i \leftrightarrow j$ we have:

$$\chi^{jik}(0) = \sum_{lmn} \boldsymbol{d}_{lm}^j \overline{\boldsymbol{d}_{ln}^i \boldsymbol{d}_{nm}^k} F(lmn) = \sum_{lmn} \boldsymbol{d}_{lm}^i \overline{\boldsymbol{d}_{ln}^j \boldsymbol{d}_{nm}^k} F(lnm).$$

Thus, we need to prove the following symmetry property $F(lmn) = F(lnm)$. We proceed with transformations:

$$F(lmn) = \frac{n_{ln}}{\varepsilon_{ln}\varepsilon_{lm}} - \frac{n_{nm}}{\varepsilon_{nm}\varepsilon_{lm}} = \frac{1}{\varepsilon_{lm}}\left[\frac{n_{lm} - n_{nm}}{\varepsilon_{lm} - \varepsilon_{nm}} - \frac{n_{nm}}{\varepsilon_{nm}}\right]$$

$$= \frac{1}{\varepsilon_{lm}}\frac{n_{lm}\varepsilon_{nm} - n_{nm}\varepsilon_{lm}}{\varepsilon_{nm}\varepsilon_{ln}} = \frac{n_{lm}}{\varepsilon_{lm}\varepsilon_{ln}} - \frac{n_{nm}}{\varepsilon_{nm}\varepsilon_{ln}} = \frac{n_{lm}}{\varepsilon_{lm}\varepsilon_{ln}} - \frac{n_{mn}}{\varepsilon_{mn}\varepsilon_{ln}} = F(lnm).$$

$$\textbf{Q.E.D.}$$

In summary, we discussed in this chapter the theoretical ideas well-known from the literature and our new implementations of:

- the TDHF method to study electron dynamics in real time.

- the GW method to study the electronic structure of the system and its decay processes in the frequency domain.

- the computation of the second harmonic response.

Chapter 4

Results I: Electron dynamics from TDHF theory

In this chapter we apply the TDHF method previously developed by us to realistic systems: Na_4, Na_9^+, and Pt_3 clusters. The small number of electrons, the simple electronic structure, the similarity to the homogeneous electron gas make the first two clusters accessible to a large variety of methods. Both static and dynamical calculations were reported in the literature. Na clusters can also easily be produced in experiment. Important information that can be measured is the optical absorption spectrum. This quantity characterizes the excitation spectrum of the system. In small metallic clusters collective excitations are very pronounced. Depending on the geometry of the clusters the plasmon peak can have a regular shape (single peak) or can split because of the absence of axial symmetry. Besides the position of the plasmon resonance we are interested in its broadening due to electron-electron interaction. It contains important information about the dynamics and relaxation processes in the system.

The situation with the Pt_3 cluster is much more complicated. Because of the strongly localized d-electrons and the complicated electronic structure this system differs very much from the jellium model. Due to the incomplete d-shell, and, as a consequence, the high density of states close to the Fermi level, electron-electron scattering is very important for the relaxation It reduces the plasmon life-time from 200 fs in the closed shell transition metals to 70 fs in Pt.

The structure of this chapter is as follows. First we apply the TDHF method to the simple, molecule-like systems in order to better understand the time evolution in this approach and to test the numerical precision of our method. As an example regimes of low and high frequency excitations are considered and compared with the adiabatic solution. On the second step we study properties of the collective excitations by analyzing the power spectrum of the metallic clusters subject to an ultrafast laser pulse. Our aim is to obtain information about the plasmon decay and compare it with available experimental data. This task looks very controversial in the framework of the TDHF approach. One may argue that the direct and exchange interaction taken into account in the method are not sufficient to describe a finite life-time, and one needs to consider correlations on the higher level of the theory. We give a thorough explanation of this paradox using a model system

as an example.

As is shown in the theory section our method is fully *ab initio*. Input parameters for the calculations are only the geometry of the cluster, number of electrons and parameters of the laser pulse. Geometry optimization of all clusters explored in the present work was done on the HF level by means of the GAUSSIAN 98 quantum chemistry package. The initial guess of the geometry was taken from the publications and will be cited below. All systems we consider are closed-shell, i.e. the number of electrons with spin up and spin down is equal. Therefore we performed restricted HF calculations for the systems in the singlet state. Triplet states require spin-polarized calculations and will not be considered here.

4.1 Deviation from adiabaticity

We start our investigation with Na_4 (Fig. 4.1) – one of the most widely studied cluster in the literature. A small number of atoms made it accessible to almost all known *ab initio* methods including CI [51], GW [5] and TDLDA [52].

The cluster geometry is a planar rhombus with D_{2h} symmetry. The result of the geometry optimization for this cluster is also widely reported in the literature, predicting this isomer as the most stable one. However, the bond lengths differ slightly depending on the level of theory and the basis set. The length of the rhombus side ranges from 3.27 Å in the LDA calculation [53] to 3.74 Å in the HF approach [54]. The length of the shorter diagonal is 2.87 Å and 3.25 Å respectively. Geometry optimization on a higher level of the theory gives similar results that fall inside these extremes.

We study the behavior of the Na_4 cluster within the TDHF and adiabatic approaches [compare Fig. 2.6(a)(c)]. At time $t = t_0$ the system is excited by a laser pulse with a temporal intensity distribution [55]

$$I(t) = I_0 \cdot \mathrm{sech}^2(\frac{t - t_0}{\sigma}) \qquad (4.1)$$

of a fixed duration and different photon frequencies. The results of the spectral analysis of the dipole response (power spectrum) and the excitation pulse are given in Fig. 4.2. The Fourier transform of the laser pulse peaks around the photon frequency and its width is inversely
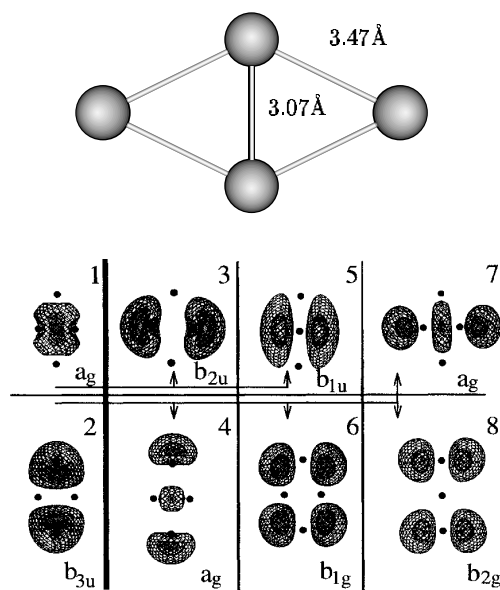

Fig. 4.1: *Top – geometry of the Na_4 cluster. Bottom – electronic density of the two highest occupied (1-2) and six lowest unoccupied (3-8) orbitals according to Ref. [5]. The two surfaces correspond to the constant density of, approximately, 0.001 a.u.$^{-3}$ and 0.002 a.u.$^{-3}$ Arrows denote allowed dipole transitions.*

proportional to the duration of the pulse (see Fig. 4.4, dashed line). Thus, when the temporal width of the pulse is large compared to the period of one oscillation, the main contributions to the electron dynamics take place at the photon frequency. We follow the time evolution of the total energy of the system (Eq. (3.15)) and the number of the electrons (Eq. (3.13)) in the initially highest occupied (HOMO – $1b_{3u}$, see Fig. 4.1) and lowest unoccupied (LUMO – $1b_{2u}$) molecular orbital states). The initial stationary HF calculation was done by employing the Los Alamos effective core potential (ECP) that replaces 8 inner electrons and use double zeta basis functions that contain two s and two p orbitals for each of the atoms. Thus we are left with 4 active electrons, that are described by 32 basis functions. In Fig. 4.1 two occupied and six lowest unoccupied eigenstates states are shown. Arrows denote allowed dipole transitions among the states. The adiabatic electron dynamics is obtained by performing the self-consistent solution of the HF equation with the perturbation operator for each of the time points.
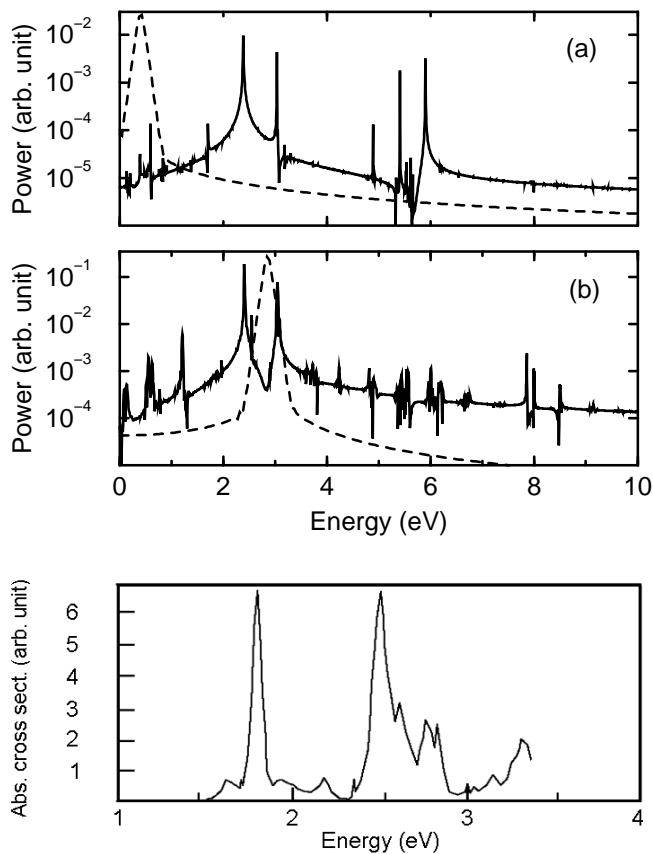
Fig. 4.2: *Top: Fourier transform of the laser pulse (dashed line) and power spectra (solid line) of the Na_4 cluster in two regimes: (a) low frequency excitation; (b) high frequency excitation. Bottom: optical absorption spectrum measured in experiment (Ref. [56]).*

The HOMO-LUMO gap in our approach is quite large (3.7 eV) and reflects the general feature of the Hartree-Fock method to overestimate the band gap. This is, however, consistent with a previous HF result (3.4 eV) reported in Ref. [51]. The LDA clearly fails in this case giving a band gap of only 0.55 eV. However GW calculation performed on top of LDA yields a systematically improved value of 3.0 eV [5]. The HOMO-LUMO gap gives only a crude approximation to the energy of the first excited state. Thus, information from the time-dependent calculation is required. The power spectrum that has been computed from the time-dependent calculations (Fig. 4.2, top) shows results similar to the experimental optical absorption spectrum (Fig. 4.2, bottom). In particular our calculation shows two strongly pronounced peaks at 2.3 and 3.1 eV observed as well in experiment at slightly lower energy. As is shown in a supercell GW calculation for this cluster they result from the transitions (see Fig. 4.1)

$1b_{3u} - 2a_g$ (2-4); $1a_g - 1b_{2u}$ (1-3) and $1b_{3u} - 1b_{1g}$ (2-6); $1a_g - 1b_{1u}$ (1-5), respectively. In general, our calculations agree well with CI [51], GW [5] and TDLDA [52] calculations of excited states in the Na_4 cluster. A small shift to higher energies does not necessary mean a systematic tendency of TDHF to overestimate excited state energies. As we have shown above even stationary HF calculations can differ in predicting the HOMO-LUMO gap by up to 0.3 eV depending on numerical details, such as basis set size, use of the ECP, etc.

The difference between the power spectra obtained from high and low frequency excitations is only quantitative: the magnitude of the peaks increases approximately by one order of magnitude when the laser frequency approaches the resonance, preserving, however, their position. But, a completely different behavior has been found comparing the time evolution of the populations of the eigenstates and the total energy of the system. For excitations of an energy considerably lower than the energy of transitions between different states the dynamics of the system (Fig. 4.3) obtained from the full time-dependent treatment differs only slightly from that in the adiabatic approach.
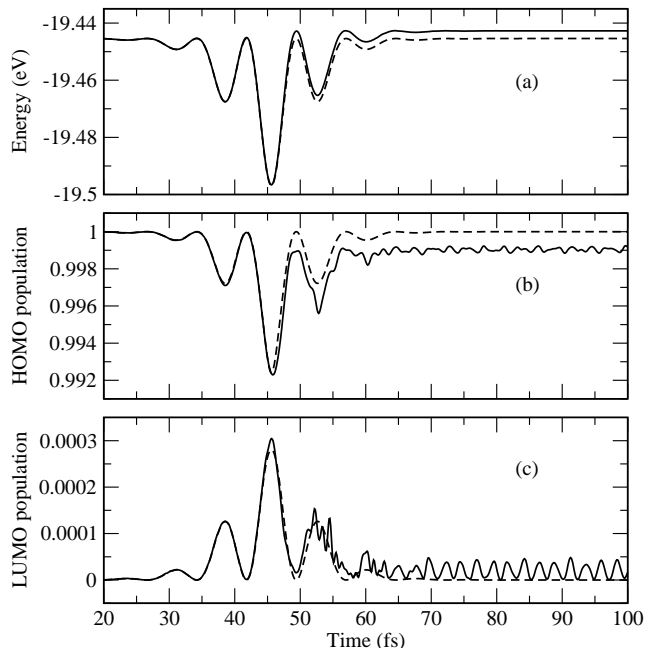
Fig. 4.3: *The Na_4 cluster in the regime of low frequency excitation. Solid line – TDHF, dashed line – adiabatic solution. Time evolution of: (a) total energy; (b) number of the electrons in the HOMO state; (c) number of the electrons in the LUMO state.*

After the excitation it returns almost to the initial state, preserving only some small oscillations. By contrast, a completely different behavior is found at higher frequencies (Fig. 4.4). Our calculations indicate that, in the case of a Na_4 cluster, for an excitation energy above 0.5 eV [Fig. 4.2(b)] the adiabatic approximation ceases to be valid and one has to resort to methods that explicitly account for the time dependence [compare Fig. 3.13(a) — adiabatic approximation and Fig. 3.13(c) — TDHF]. After the HOMO level is partially depopulated, it remains in that state forever, which, of course, is an effect, that cannot be observed on the adiabatic level. The time-dependence of the total energy reveals another feature of the method – energy conservation. After the perturbation is switched off the energy remains constant. This also provides a good test for the numerical precision of the ordinary differential equations (ODE) solvers that we used to propagate wave-functions in time. We have tested both Runge-Kutta and Bulirsch-Stoer methods with adaptive step-size. They give a perfect agreement and conserve total energy

and particle number on the scale of hundreds of femtosecond with an accuracy of 10^{-6}. Another possibility to study the high-frequency case would be to use Floquet theory [57], where the time-dependent Hartree-Fock or DFT equation is recast into a generalized eigenvalue problem. But as we found numerically it is very difficult to solve this kind of equation self-consistently.
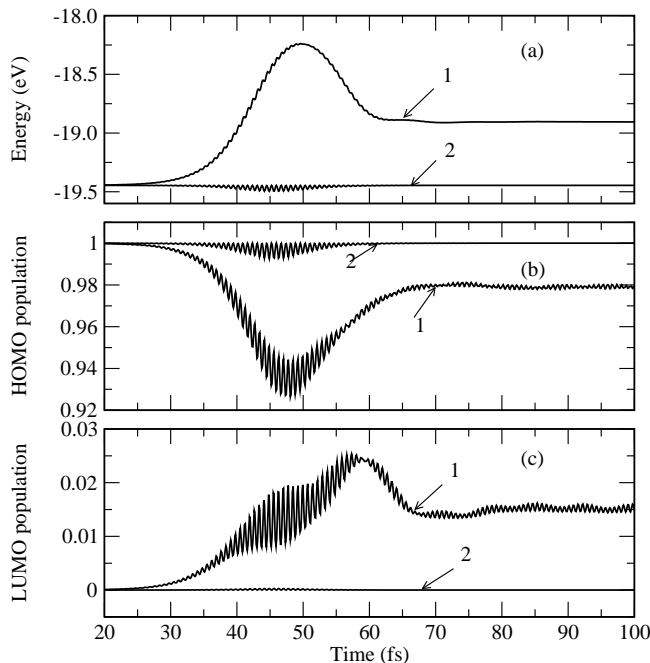
4.2   SHG response

Fig. 4.4: *The Na$_4$ cluster in the regime of high frequency excitation. Line 1 – TDHF, line 2 – adiabatic solution. Time evolution of: (a) total energy; (b) number of the electrons in the HOMO state; (c) number of the electrons in the LUMO state.*

In Sec. 3.4 we have derived the second order nonlinear susceptibility $\chi_{ijk}^{2\omega}$ using perturbation theory for the density matrix. In contrast to the linear response it is very sensitive to the geometry of the system, quality of the wave-functions and eigenenergies involved in the calculation. In particular, from the symmetry analysis one expects no second harmonic generation on systems with inversion symmetry. From an experimental point of view SHG is a valid method for the characterization of nanostructures and clusters. Recent investigations have examined, for example, the transient properties of SHG in silver island films [58], in specially designed silver particles [59] and Na clusters [60]. Employing observation of the size-dependence of the nonlinear response of Ref. [61] one can use the SHG measurements to characterize the distribution of the cluster size. Recently, the femtosecond time-resolved SHG from alkali metal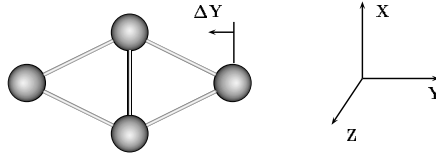 clusters [62, 63, 64] was used to find life-times of the plasmon excitations. Compared to other techniques, such as linear optical measurements, the SHG scheme has the distinct advantage of eliminating the role of the substrate since the bare surface does not give an appreciable second harmonic response.

Here we would like to check the absence of SHG in the case of system with inversion symmetry and its appearance when the symmetry is broken by employing the eigenstates of the HF Hamiltonian used for the time-dependent calculation on the example of a Na$_4$ cluster. In order to break the inversion symmetry of the equilibrium geometry (D_{2h}) we allow for the displacement of one of the atoms of the cluster (Fig. 4.5). Apparently, this

Fig. 4.5: *Displacement of one the atom in Na$_4$ cluster that breaks inversion symmetry and, therefore, enables nonzero SHG response. See text.*

kind of distortion has no physical substantiation, serving only for the purpose to show the possibility to accurately compute the SHG response from clusters with broken inversion symmetry. However, one can expect a non-zero SHG signal even from the cluster with inversion symmetry at finite temperature due to the phonon distortion of the geometry[1]. Another possibility of getting non-zero response is to assume a situation close to experiment, where clusters are deposited on a substrate. This situation was theoretically studied in Ref. [34] by means of TDLDA.

In our case the HF equation is solved for each value of Δy in order to obtain the eigenenergies and wave-functions, which are subsequently used to compute the SHG response according to Eq. (3.38). We find that at zero displacement of the Na atom from the minimal energy position all matrix elements of $\chi^{2\omega}_{ijk}(\omega)$ are zero within machine precision. At nonzero displacement we distinguish three groups of tensor elements:

- non-zero — $|\chi^{2\omega}_{ijk}(\omega)| > 1.0 \cdot 10^{-6}$ (shown with bold face)

- almost zero — $1.0 \cdot 10^{-6} > |\chi^{2\omega}_{ijk}(\omega)| > 1.0 \cdot 10^{-8}$ (shown with normal face)

- vanishing — $1.0 \cdot 10^{-8} > |\chi^{2\omega}_{ijk}(\omega)|$ (are not shown).

$$\chi^{2\omega}_{ijk}(\omega) = \begin{pmatrix} & (yyy) & (yzz) & \Big| & (xxy) & & (\mathbf{xzx}) \\ (\mathbf{zxx}) & (\mathbf{zyy}) & (\mathbf{zzz}) & \Big| & & (\mathbf{yyz}) & \\ & & & \Big| & & (zyz) & \end{pmatrix}$$

Our calculations show the reliability of the results of the HF calculation numerically fulfilling the selection rules with a high precision (the magnitude of non-zero tensor elements contradicting the selection rules is on the noise level, the smoothness of the graphs indicates a high precision of computing the dipole moments). A strong SHG response is observed in the region of energies from 2 eV to 6 eV in accordance with [34], where optimal frequency of the incident light is stated to be at 1/2 and 1 times the plasmon frequency.

As a possible development of the present technique two approaches are possible: using many-body wave-functions and excited states from the CI calculation to compute the SHG response according to the perturbation formula and performing a TDHF calculation. The present method, although being very simple, correctly accounts for the selection rules and, thus, can be used to describe future experiments. At the present time experiments are only possible on larger Na clusters of a size of tens of nanometers [62, 64].

---

[1] SHG is also possible for systems with inversion symmetry when quadrupole transitions are taken into account.
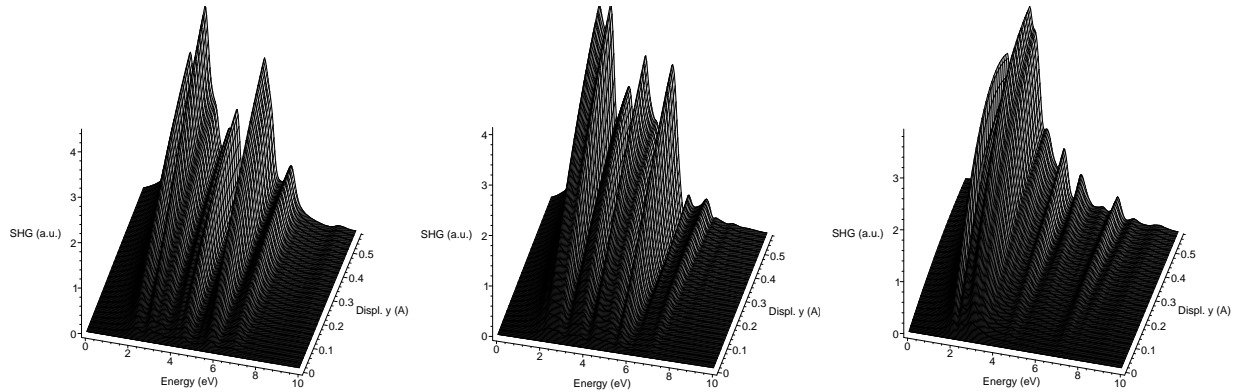
Fig. 4.6: *SHG response of the Na_4 cluster resolved as a function of displacement of one of the atoms. Absolute values of χ_{zxx}, χ_{zyy} and χ_{zzz} are shown.*

4.3 Finite life-time from TDHF theory

From the beginning we would like to distinguish two different approximations that form the essence of the time-dependent Hartree-Fock (TDHF) method. In the first step the stationary HF equation is solved in order to get the unperturbed ground state of the system. It contains no Coulomb correlation by definition. The Hartree-Fock Hamiltonian is Hermitian. It means that the energy of the quasi-particle states (eigenvalues of the HF equation) are pure real numbers, i.e. there is no imaginary part that would be responsible for the decay. In the second step the time evolution of the system is monitored by solving the TDHF equation Eq. (2.24). This equation does not only describe ground-state properties, but also excited states: particle-hole (ph) excitation and collective excitation — the plasmon.
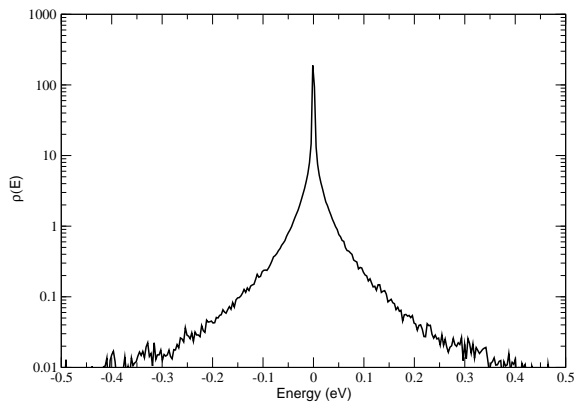
Fig. 4.7: *Distribution of the matrix elements of the Coulomb interaction for the Na_9^+ cluster.*

To better understand how one can extract a finite *life-time for the particle-hole* states from the time-dependent HF calculations we continue to investigate the random interaction model described by the Hamiltonian Eq. (2.17), that contains $m = 5$ particles distributed over the $n = 10$ states. The one-particle energies are uniformly distributed in the energy interval $[-10, ..0]$ and the two-particle interaction is given by a random Gaussian-shaped distributed potential with standard deviation $\sigma = 1$.

The model is not a completely abstract object having no relation to realistic systems. Just on the contrary, a simple glance on the distribution of the matrix elements of the Coulomb interaction in clusters (Fig. 4.7) shows that they exhibit a great amount of
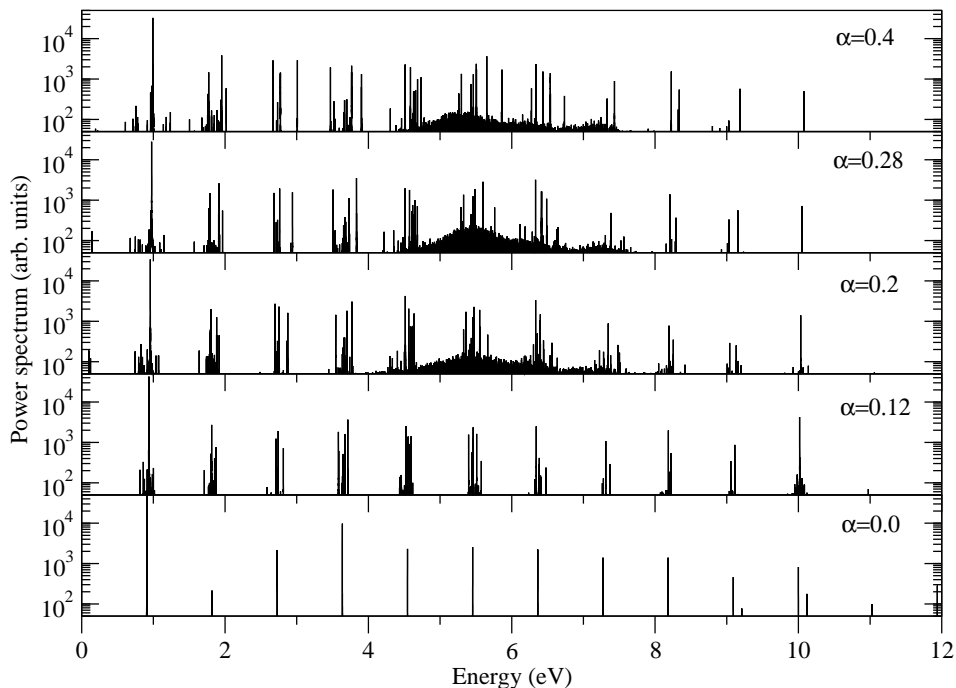
Fig. 4.8: *Power spectra for the model (Eq. 2.17) with different interaction strength α.*

the randomness in their electronic properties. This fact leads to the idea that one can understand some general features of their spectra (Ref. [65]), as well as in other complicated systems like heavy nuclei Ref. [66] or mesoscopic quantum dots Ref. [67] on the basis of random matrix theory (Ref. [68]). We performed a series of time-dependent calculations for this model at different interaction strengths. The system is excited by changing the sign of interaction ($\alpha \rightarrow -\alpha$) at time $t = 0$.

As one can see from Fig. 4.8 at low interaction strength the power spectrum (Fig. 4.8) consists of a set of single peaks that correspond to the transitions of the particles between one-particle states. These states are degenerate, and increasing the interaction strength α leads to their splitting. Thus, at high resolution one sees a large number of δ peaks around each one-particle state. With low resolution, they essentially merge into one peak of non-zero width. Selecting an appropriate theoretical model, for example a Lorentzian for the decaying particle, one can fit the shape of this peak to that predicted from the model and obtain a finite life-time of the state. Thus one always has a choice in interpreting the results of a calculation or experimental observation. The only criterion that justifies a certain choice for the interpretation is the requirement that the natural width of the single peak in the envelope must be less than the distance between peaks, forming the envelope.

The situation with the *plasmon life-time* requires a more careful consideration. It was found long time ago that the collective-resonance states are composed as a coherent superposition of many 1 *ph* states, in other words as a constructive interference [18, 69]. On the other hand, as we mentioned above, the time-dependent Hartree approximation (TDHF without exchange) in the limit of linear response is equivalent to the random

System	Fig.	N_{bf}	N_{e}	$I_0[10^{11}W/m^2]$	N_{ECP}	basis set ref.
Na_9^+	4.10	72	4	107.6	10	[71]
Pt	4.10	72	24	2.1	30	[72]
Pt	4.11	72	24	1.4-2.8	30	[72]
Pt	4.12	15-25	5-10	0.0	30	[72]

Tab. 4.1: *Parameters of the time-dependent calculation. As all systems are closed-shell N_{e} means the number of spin-compensated electron pairs. N_{ECP} is the number of electrons replaced by the effective core potential.*

phase approximation (RPA) of many-body perturbation theory [9]. The RPA dielectric function for the 3D uniform electron gas first derived by Lindhard [10] and its zeros, which are situated in the complex plane describe the electronic excitations in the system. There are two kinds of excitations in this approximation: particle-hole contributions and the plasmon. The life-time of the particle-hole excitations is finite on the RPA level and it explains why we are able to see a broadening in the above model. The plasmon excitation has no decay below a certain critical wave-vector q. But both the TDHF method and the RPA may yield a finite life-time for the plasmon. The Lindhard dielectric function is obtained from the RPA expression assuming an equilibrium electron distribution. In the case of finite temperature or an electron distribution away from equilibrium (*which was studied in our case*) the dielectric function must be evaluated in the whole complex plane. The plasmon frequency and decay can then be found at the intersection of the $\Re e\,(\varepsilon) = 0$ and $\Im m\,(\varepsilon) = 0$ curves [12, 13, 70]. In our manuscript we study a situation close to experiment (such as described in Ref. [55]). The laser pulse interacts with a cluster and part of the photon energy is absorbed. The electron distribution becomes different from a step function and can be approximately treated introducing some effective non-zero temperature. For this case we expect to obtain a finite plasmon life-time from the TDHF method by analogy with the RPA result.

We believe that the shown illustrative examples clearly indicate the existence of a finite life-time of both the plasmon and the single-particle excitations in the time-dependent Hartree-Fock description of electron dynamics.

4.4   Power spectra of Na_9^+ and Pt_3 metal clusters

In simple systems, such as Na_4, the electronic density of states is small. This leads to a power spectrum with well separated peaks that correspond to one particle-hole ($1ph$) excitations. Considering more complicated systems such as Na_9^+ and Pt_3 (see Tab. 4.1 for the information about the number of basis functions, electrons in the active space and laser pulse parameters and Fig. 4.9), with a larger number of electrons, a new feature in their power spectra can be observed. Because of the dense level scheme in these clusters many $1ph$ states merge and form a collective excitation — a plasmon — due to their constructive interference. In contrast to one-particle excitations, the oscillator strength of

the plasmon is very high and it manifests itself as a strong peak in the power spectrum of the dipole moment. In contrast to the response function, which only characterizes the internal properties of the system, such as the energies and the oscillator strengths of the excited states, the power spectrum depends as well on the parameters of the external excitation. To study intrinsic properties of the system one has to minimize the role of the second factor. This can be done by putting the system initially in some nonequilibrium state and then following its relaxation [18] or one uses very short pulses, that embrace a large frequency interval.

We performed a series of calculations on Na$_9^+$ cluster for pulses of the mean photon frequency $\omega^* = 2.25$ eV and different durations [Fig. 4.10 (left panel)]. The polarization of the electric field is taken to be along the axis of axial symmetry of the cluster. When the frequency width of the pulse is small predominantly states that correspond to the absorption of one, two, and three photons (denoted by vertical lines) are well pronounced. The plasmon peak at 2.7 eV is almost invisible [see Fig. 4.10 (left panel: a)]. Shorter pulses lead to a broader region of energies in which absorption can take place and thus excitations of the states that are further away from the resonance, but of higher oscillator strength become possible. Our value for the position of the plasmon peak, determined as a excitation with the highest oscillator strength that can be excited off-resonantly [Fig. 4.10 (left panel: c)] ($\omega_{pl} = 2.7$ eV) of the Na$_9^+$ cluster is in good agreement with results obtained within the real-space implementation of TDLDA (Refs. [18, 73, 74, 75, 29]). In spite of this its oscillator strength is consid-

Fig. 4.9: *Structures of Na$_9^+$ and Pt$_3$ clusters studied in this work. The numbers indicate the bond lengths in units of Å.*

erably lower in our approach. We think that this may be caused by the difference in the excitation mechanisms used (initial dipole shift of the entire electron cloud vs. excitation with certain frequency and time profile) and the number of electrons, taken into account. The plasmon, as a collective effect, is very sensitive to the density of virtual states in the system. Replacing part of the inner electrons with an effective potential may have small impact on the ground state properties, but may imply a sophisticated analysis in the case of excited states.

To better understand the possibility of the non-resonant plasmon excitation and in order to estimate the plasmon lifetime we apply our technique to the previously experimentally
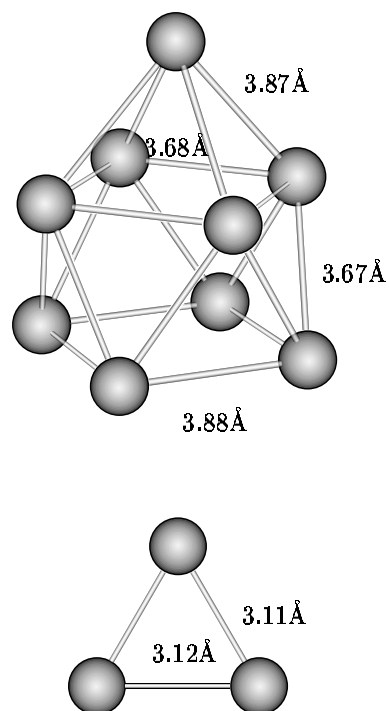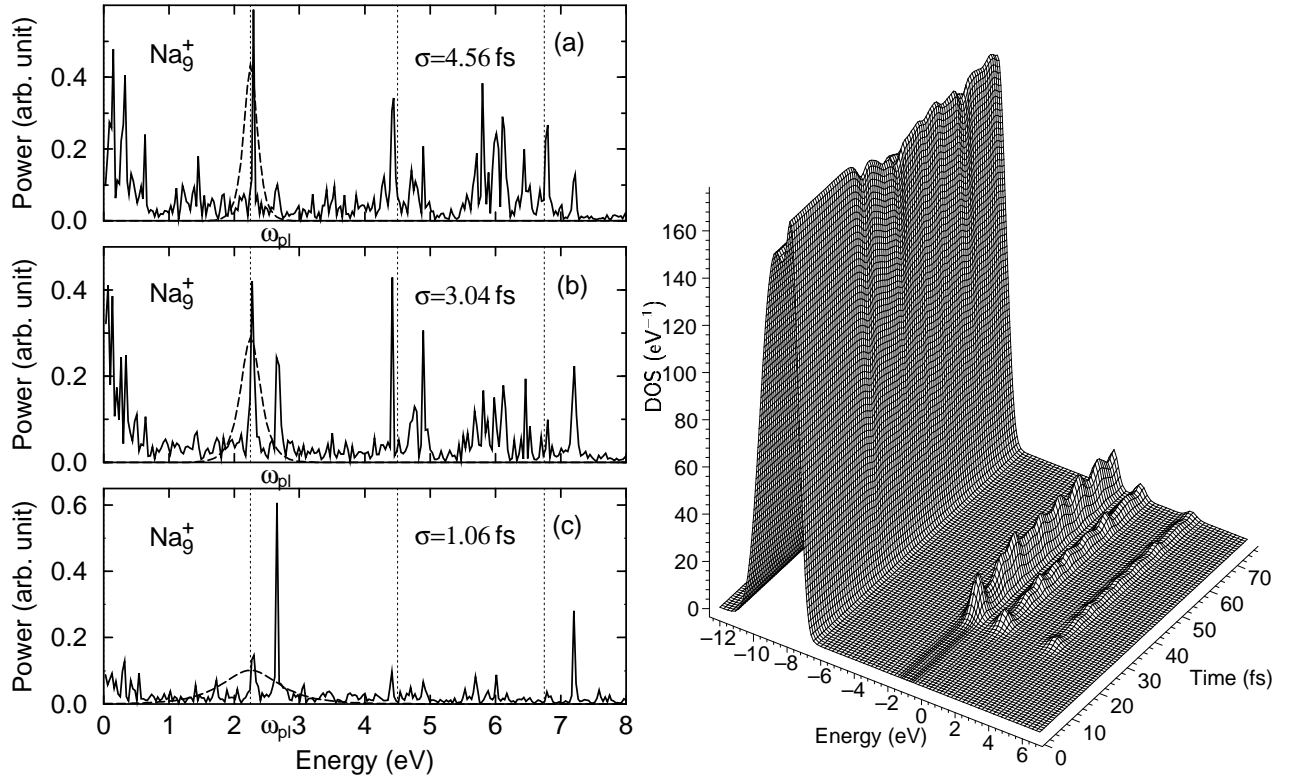
Fig. 4.10: *Left panel. Power spectra of the Na_9^+ cluster, excited with laser pulses of the same photon energy and different pulse width. Dashed line shows the Fourier transform of the pulses of different duration: (a) $\sigma = 4.56$ fs, (b) $\sigma = 3.04$ fs, (c) $\sigma = 1.06$ fs. Vertical lines denote energies, that correspond to the one-, two-, and three-photon processes.*
Right panel. Time-resolved density of states of the Pt_3 cluster, excited by a laser pulse with $\omega^* = 3.125$ eV. Gaussian broadening of width 0.27 eV has been used.

studied cluster Pt_3 (Eberhardt and coworkers, Ref. [55]). It has been shown that the cluster possesses a very dense metallic like energy-level structure [76], leading to the enhancement of electron-electron scattering processes. The latter causes an effective energy transfer from one $1ph$ state to another, thus considerably reducing the plasmon lifetime in open-shell transition-metal clusters compared to noble or alkali-metal clusters. In calculations we use pulses of the same duration $\sigma = 0.76$ fs and different photon energies in a range from $\omega^* = 2.625$ eV to $\omega^* = 3.625$ eV that is in either case below the plasmon energy (Fig. 4.11). Polarization of the electric field is perpendicular to the plane of Pt_3 cluster. A typical time evolution of the density of occupied states, computed according to Eq. (3.14) is shown in Fig. 4.10 (right panel) ($n_i(t)$ is computed according to Eq. (3.13)). A transition of part of the electronic population from the occupied states close to Fermi level to previously unoccupied states occurs shortly after applying the laser pulse and leads to complicated oscillations. The use of very short pulses, although at present experimentally not feasible allows us to cover a very large energy range and to study fast processes far from resonance.

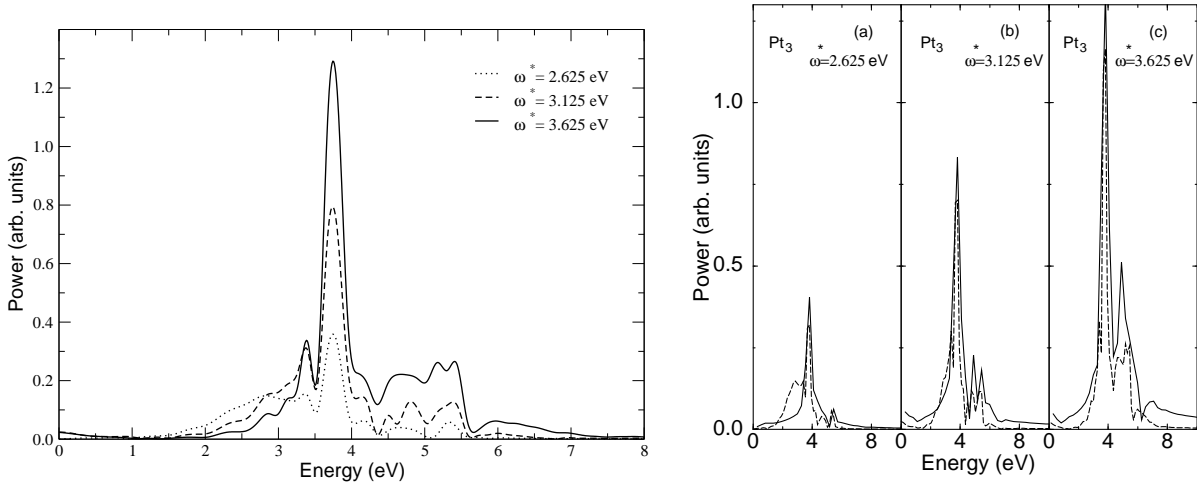One can see (Fig. 4.11) a redistribution of the spectral weight of the peaks with the

Fig. 4.11: *Power spectra of the Pt_3 cluster, excited with laser pulses of the same width and different photon energies: dotted line – $\omega^* = 2.625$ eV; dashed line – $\omega^* = 3.125$ eV; solid line – $\omega^* = 3.625$ eV. Right panel: comparison of the power spectra computed on different time intervals. Solid lines denote power spectra, calculated on the time interval after excitation took place, and dashed lines – power spectra on the whole time interval.*

change of the excitation energy. The magnitude of the plasmon peak strongly depends on the vicinity of the photon frequency to the plasmon pole. The spectral weight of the shoulder in the region of energies 2-3.5 eV decreases when ω^* approaches the plasmon resonance at ω_{pl}=3.7 eV. On the right panel of Fig. 4.11 for comparison power spectra computed in two different time domains are plotted. Dashed lines corresponds to that on the left panel, where power spectra are computed on the whole time interval: during the excitation and after it. Solid lines show power spectra computed on the second, relaxation period. One can see, that in this case the spectral weight is even more concentrated in the in plasmon peak, shoulders become less pronounced.

As mentioned above, the plasmon is a collective effect that originates from the strong enhancement of the one-particle excitations due to their constructive interference [18, 69]. If a time-dependent calculation is performed on very long time scales, it would be possible to resolve the plasmon peak as a very dense structure of individual $1ph$ peaks of very small width. In the higher-order correlation treatment these peaks will be smeared out to form one envelope that will resemble the plasmon peak at the present level of the theory (for the discussion of the plasmon width as a result of fragmentation of the resonance into nearby $1ph$ states and comparison with another mechanism — broadening due to the thermal fluctuations see Ref. [77]). That is why it is natural to use information from mean-field calculations in order to extract information about plasmon lifetime. The plasmon peak can be viewed as a Lorentzian or Gaussian peak. The first case describes a $e^{-\frac{t}{\tau}}$ decay of the quasiparticle in the many-body system, while the second one corresponds to the inhomogeneous broadening of the peak. The decay law is then $e^{-\frac{t^2}{\tau^2}}$. The lifetime can

differ up to a factor of 2π depending on the choice of the model[2]. We perform a non-linear fitting of the power spectrum by a set of Lorentzians (a similar idea can be found in the recent work of Molina *et al.* Ref. [78]):

$$P(\omega) = \sum_i \frac{A_i}{2\pi} \frac{\delta_i}{(\omega - \omega_i)^2 + \delta_i^2} \qquad (4.2)$$

and find the width of the plasmon peak to be $\delta_{pl} = 0.17$ eV that corresponds to a lifetime of approximately $\tau_{pl} = 24$ fs ($\tau_{pl} = 3.8$ fs in the case of a Gaussian model). This result should be compared with experimental data of Eberhardt and coworkers, [55] who determined the lifetime to be less than 70 fs and attributed it solely to electron-electron scattering.
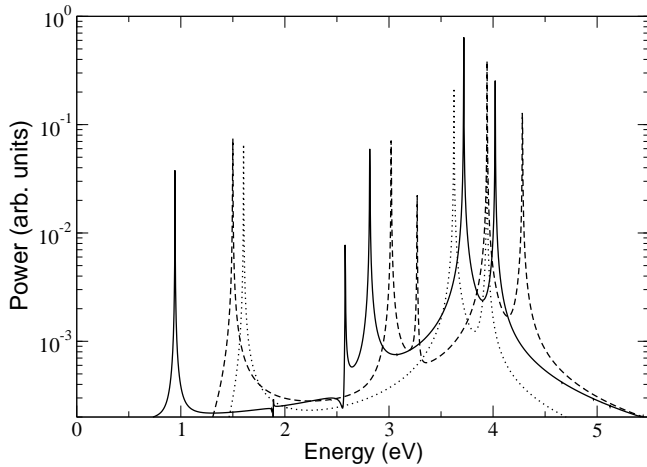
Fig. 4.12: *Power spectrum of the Pt_3 cluster, for different numbers of electrons and basis functions: dotted line — $N_e = 5, N_{bf} = 15$; dashed line — $N_e = 10, N_{bf} = 20$; solid line — $N_e = 10, N_{bf} = 25$.*

Up to now we were interested only in the properties of the system, excited in a way similar to the experiment. For comparison the *clean* (contains only the information about the properties of the system, but not of the laser pulse) power spectrum has been computed. To move the system out of equilibrium we used, as an initial configuration, the eigenstates of the HF Hamiltonian at elevated temperature ($T = 0.005$ a.u.). We propagate this solution during a very long time interval (several *ps*) to get a fine resolution for the spectra. A different number of basis functions and electrons has been included in the active space in order to understand its role on the formation of the plasmon peak (Fig. 4.12). Comparing this with the calculations using a larger basis set (Fig. 4.11), shows that only a small number of basis functions ($N_{bf} \sim 15 - 25$) is needed to get the correct position of the plasmon. However the fine details of the spectrum are quite sensitive to the size of the active space. Another important feature of the *clean* spectra is the presence of the peaks at 1-2 eV, not available for the case, when the system is excited by a laser pulse, which shows that some transitions might be forbidden for the particular polarization of the light, and can be excited only thermally.

Summarizing, in this chapter we demonstrated the application of a new computational scheme for the investigation of the electron dynamics in clusters under the influence of the external field within the mean-field approach. The application of the TDHF method to the Na_9^+ cluster, previously intensively studied theoretically with different methods,

---

[2] For the Lorentzian model one has $Et = 2\pi\hbar$. This gives the relation $E[\text{eV}]t[\text{fs}] = \frac{6.6260755 \times 10^{-34}}{1.602188 \times 10^{-19} \cdot 10^{-15}} = 4.135642$. In the case of a Gaussian model $Et = \hbar$. Thus $E[\text{eV}]t[\text{fs}] = \frac{6.6260755 \times 10^{-34}}{2 \cdot 3.141593 \cdot 1.602188 \times 10^{-19} \cdot 10^{-15}} = 0.658208$.

and the Pt$_3$ cluster already accessible to experimental investigation revealed the following capabilities of our approach:

- The method is able to accurately predict the position of the plasmon peak for the Na$_9^+$ cluster, although its oscillator strength differs considerably from the TDLDA result.

- The calculation on the open-shell transition metal cluster Pt$_3$ allowed us not only to determine the position of the plasmon resonance, but also to estimate its life-time by fitting the power spectrum to a set of Lorentzians. Our value for the decay constant supports the experimental evidence in favor of a bulk-like lifetime of the electronic excitations in this cluster despite an electronic structure that strongly differs from bulk Pt.

- The calculation on the TBRIM supports the possibility to determine the life-time of collective excitations from the time-dependent mean-field theory.

Chapter 5

Results II: Numerical results of GW calculations

In this chapter we continue the *ab initio* investigation of metal clusters and the model system by many-body perturbation theory. Besides the systems considered before we apply our method to a row of larger sodium clusters up to a maximum size of 25 atoms.

The GW approach is much more complicated than TDHF. The latter is based on two well developed numerical techniques: the self-consistent solution of the stationary problem and the propagation of this solution in time by using ordinary differential equations (ODE) solvers. Both have no adjustable parameters and can be completely automatized. The GW calculation consists of more stages: building an initial approximation for the Green function from the HF results, calculating the polarization operator and consequently the screened potential. Finally the self-energy has to be computed and the improved Green function has to be found by the solution of Dyson's equation. If one wants to obtain self-consistent results the above scheme has to be repeated until convergence is achieved. On each stage of the calculations input and output quantities are frequency dependent. This means, that in addition of requiring of convergence of results with respect to the basis set size one must also pay attention to the density of the frequency mesh and energy cut-offs. FFT that we introduced for the computation of convolutions must be applied to very large data sets, that hardly fit the memory of state of the art workstations. The calculations even on medium sized systems require parallelization of the entire scheme and balancing data transfer traffic.

But not only numerical problems have to be solved. There are two principal difficulties of physical origin. First, the results of the G^0W^0 computational scheme, which is the simpler one, depend strongly on the initial guess, besides the approximation is non-conserving. On the other hand, to achieve full convergence in the spirit of the GW scheme, which is conserving and gives results independent of the initial guess, one has to go through the stages, where the density matrix of the system is not Hermitian because of non-conservation of the total particle number. To avoid that problem we developed a partially self-consistent scheme, where the frequency independent part of self-energy is kept on the initial level, while the dynamical part is involved in the iteration loop. We start by comparing the G^0W^0 and GW schemes for our model system with random interactions. We use this experience

to perform calculations on real systems in order to determine the improved eigenstate energies, the life-time of quasiparticles and to obtain information about collective excitations – plasmons.

5.1 Comparison of G^0W^0 and GW approaches

5.1.1 Na_9^+ cluster

In this section we continue the investigation of the Na_9^+ cluster, initiated on the TDHF level. As was explained in the theory part (Sec. 3.2), on the first stage of calculation the polarization operator $P_{\alpha\beta}(\omega)$ has to be computed from the known initial approximation to Green's function (Here we neglect numerical details, considering just the physical side of the problem). The polarization operator renormalizes the electron-electron interaction by accounting for virtual electronic transitions between occupied and unoccupied states. Consequently, we have here an additional complication compared to the conventional electronic structure methods. While the latter only require a good knowledge of the occupied states, computations according to the GW scheme require also an adequate description of the virtual states. Therefore we spent additional efforts to understand the role of the basis set employed to represent the system. It was found that standard basis set used for the quantum chemical calculations, indeed only represent the occupied states well. In order to improve the representation of the virtual states we extended the `laln2dz` basis set with additional diffusive functions as explained in Appendix B. For this particular cluster we use a basis set (referred to as `laln2dz2`) containing 15 functions for each sodium atom. As before an effective core potential is employed to eliminate the deeply lying core states not important for our discussion. Thus, initially our system is described by 135 basis functions and contains four spin-up, spin-down electron pairs. After the HF equation is solved to produce an initial guess for Green's function we do not use the gaussian basis any more and change to the eigenstates basis. Furthermore we have the possibility to vary the number of states included in the GW calculations and compare the results obtained for different sizes. On Fig. 5.1 the real and imaginary parts of the state average self-energies ($\langle \text{HOMO}|\Sigma(\boldsymbol{rr'},\omega)|\text{HOMO}\rangle$ and $\langle \text{LUMO}|\Sigma(\boldsymbol{rr'},\omega)|\text{LUMO}\rangle$) of the cluster are shown for different numbers of basis functions. We found very good agreement among calculations with different basis size in the region of energies close to Fermi level. Augmenting the basis set only affects states at the edges of the spectrum, indicating their incipient poor representation. Not only self-energies have to be compared. Another important feature that indicates the convergence of the results with respect to the number of states is the HOMO-LUMO gap (Fig. 5.2). Starting with almost a toy system containing only 10 basis states and increasing the size up to 50 states we observed a steady reduction of the gap. At $N_{bf} = 50$ results differ already slightly from the previous step, indicating the convergence towards $\Delta E = 3.7$ eV.

In what follows we will be concerned only with the case $N_{bf} = 50$, which balances between physical relevance and good numerical performance. The computational time depends as well on the density of the frequency mesh on which all functions are represented
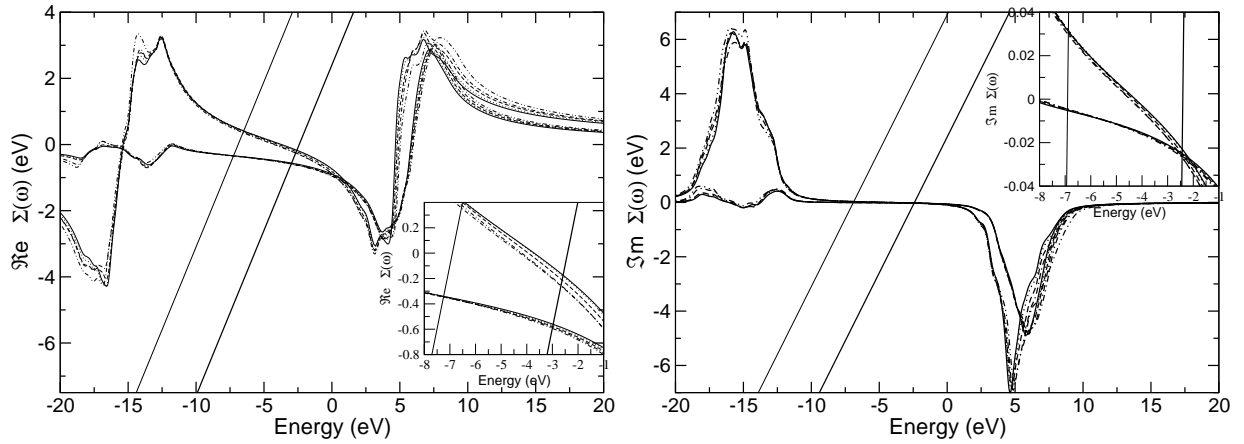
Fig. 5.1: *The real and imaginary part of the self-energy for the Na_9^+ cluster. Diagonal matrix elements of HOMO and LUMO states are shown for a different number of basis functions: solid line —- 54, dotted — 56, dashed —58, dash-dotted — 60. The intersections of the straight lines with the self-energy show the solutions of the Dyson equation.*

and their energy cut-offs[1]. The former must be at least one order of magnitude smaller than the details of fine structure of the functions, while the latter should be large enough to cover regions of energy, where poles of functions are contained. For the present calculation we use symmetrical energy intervals (E_{min}=-E_{max}) for the representation of the functions and for the Fourier transforms. Typical parameters of our calculations are given in Tab. 5.1. The density of such a mesh is sufficient to capture details of the order $5 \cdot 10^{-3}$ eV.

Function	Mesh representation		Rational fitting	FFT	
	E_{max} (eV)	N_{max}	E_{max} (eV)	E_{max}	N_{max}
G	108.8	20000	217.6	356.3	65536
W	122.4	22500	272.0	356.3	65536
Σ	163.2	30000	326.4	356.3	65536

Tab. 5.1: *Tabulation of the key parameters for the GW calculation.*

Here we tried here the simplest approach to go beyond the G^0W^0 level of the theory and to close the self-consistency loop (follow (a)-path on the scheme Fig. 3.13). After the self-energy is computed, we approximately solve the Dyson equation to get improved values of the energies for the quasiparticle states. After that a new Green function is computed based on the initial Hartree-Fock wave-functions and on the new eigenenergies. Our calculations indicate that already on the fourth cycle a satisfactory convergence of all quantities (band-gap, screened interaction, self-energy, Green's function) is achieved.

---

[1] Typically the computational time for one SC cycle of GW calculation comprises 2.5 hours on the 2 CPU (21264 `Alpha` chip) `AlphaStation DS20E` (parallelization of some processes are allowed). This time comprises the solution of Dyson's equation (9%), the computation of the screened potential (1%), the simultaneous FFT of the Green function and screened potential (21%), the multiplication in the time domain (56%) and FFT transform of the self-energy back to the frequency domain (13%).
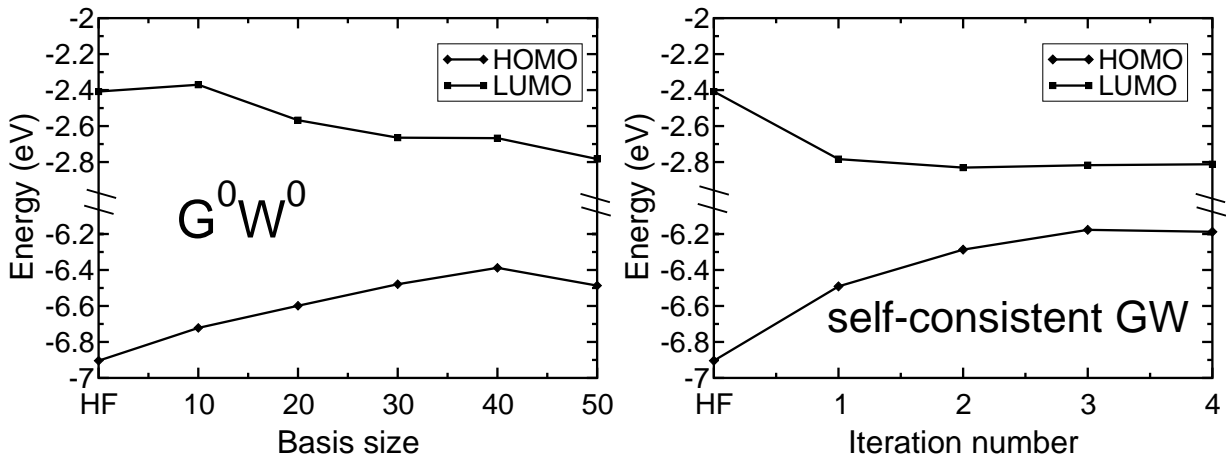
Fig. 5.2: *Energy of the HOMO and LUMO states of Na_9^+ cluster at different levels of theory. On the left panel the dependence on the number of basis function included in the G^0W^0 calculation is shown. On the right panels their evolution in the course of the self-consistent GW calculation is displayed.*

We observe that in the course of the self-consistency loop the band-gap reduces further (Fig. 5.2) tending towards the value of 3.37 eV. Such a reduction of the gap influences all other quantities, above all, the Green function and the screened Coulomb interaction (Fig. 5.3). The latter reflects the frequency behavior of the inverse dielectric function. In Sec. 2.2.3 we have shown that for metallic systems a plasmon peak is a typical feature of its spectrum. In the case of clusters we have a deviation from this picture due to the presence of the HOMO-LUMO gap. Modifying the derivation of the Lindhard formula for the dielectric function for the systems with a gap one can show that the plasmon peak in this case must be positioned at $\Delta_{\mathrm{HOMO-LUMO}} + \omega_{\mathrm{pl}}$, the sum of the plasmon frequency for the gapless system and the HOMO-LUMO gap. Thus, in the case of clusters one expects to find a strong peak in the inverse dielectric function at $\Delta_{\mathrm{HOMO-LUMO}} + \omega_{\mathrm{s.pl}}$, where $\omega_{\mathrm{s.pl}}$ is the surface plasmon frequency. This was indeed observed in our calculations. At every step of the iteration perfect agreement between the RPA position ($\omega_{\mathrm{s.pl}} = 2.5 - 2.6$ eV) of the surface plasmon from our calculation and the experimental [79, 80] or TDLDA values [32] was found. The peak itself changes its position from approximately 7 eV to 6 eV due to the reduction of the HOMO-LUMO gap. Besides that it narrows due to the renormalization of the broadening of the quasiparticle states. Its half-maximum width ($\Delta\omega_{\mathrm{s.pl}} = 2$ eV) corresponds to the plasmon life-time of approximately 4.1 fs, which is in fact very short. Recent experiments [63], however, support this result by estimating the life-time of the plasmon resonance in Na_{93}^+ to be about 10 fs in agreement with time-resolved SHG measurements [62] on larger surface-bound Na clusters where the same life-time was obtained for a cluster size of about 25 nm.

As well as the screened Coulomb potential, the self-energies obtained in our approach fit the anticipated behavior very well (compare Fig. 5.4 with schematic expectation on
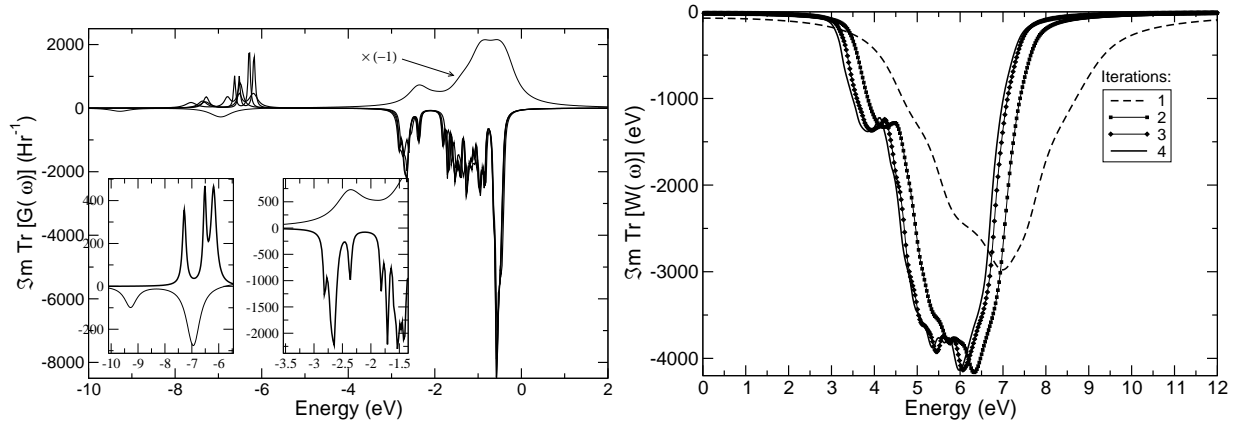
Fig. 5.3: *Sum of the diagonal matrix elements of the imaginary part of Green's function and screened interaction for the Na_9^+ cluster. On the left panel insets compare the initial Green function with that on the fourth step, for which convergence is already achieved.*
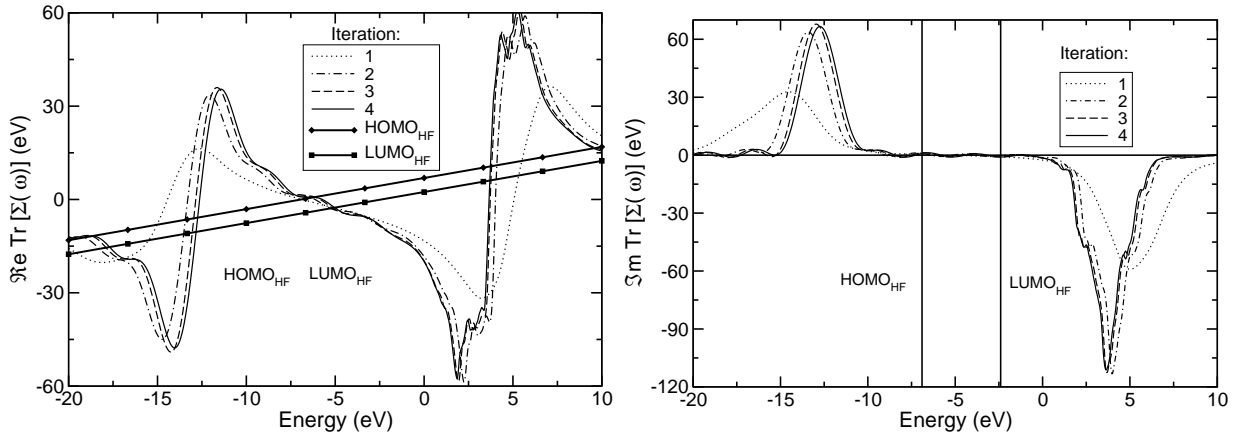

Fig. 5.4: *Sum of the diagonal matrix elements of the self-energy for the Na_9^+ cluster.*

Fig. 3.6)[2]. One sees, that in the region of energies, where all quasiparticle states are located, the real part of the self-energy has a negative slope, leading to the shrinking of the gap and pushing all quasiparticle states towards the Fermi energy. Its imaginary part has two peaks below and above the Fermi energy, where it changes the sign. It corresponds to the strong damping of the quasiparticle states far away from the gap. The different sign of the function above and below the Fermi energy indicates the existence of particles (holes) respectively, and is a pre-requisite of particle number conservation. Despite being qualitatively correct, the imaginary part of the self-energy does not come out very well quantitatively. From Fig. 5.4 (right panel) we see that its absolute value for the HOMO and LUMO states is very small (life-time tends to infinity). This makes

---

[2] It is necessary, however, to say, that the above figure has only illustrative character, without a direct physical meaning. As we explained above all physical quantities involved in the calculation have a matrix form. Representing their trace on the graph is only the way to display their average properties and does not reflect the properties of a certain state.
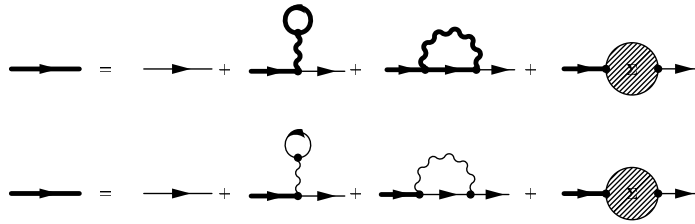
Fig. 5.5: *Dyson's equation, two approximations: top — fully self-consistent GW. The Σ' as well as direct and exchange terms are updated from the Green function on the previous step. Bottom — direct and exchange energy is kept on the HF level (first iteration).*

these quasiparticle states too narrow to represent them correctly on the frequency mesh, and prevents the determination of their life-time from the self-consistent calculation. To remedy this situation we apply an additional broadening of the states with a width below a certain critical value.

As a conclusion, our partially self-consistent scheme is successful in eliminating the dependence of the final results on the initial guess for the Green function. It yields fast convergence, further reduces the HOMO-LUMO gap and shifts the plasmon peak in the inverse dielectric function to lower energies. The Na_9^+ cluster, however, is too small a system to observe the finite life-time of the quasiparticle state due to the electron-electron interaction. Thus, we analyze the role of self-consistency on the life-time of quasiparticle excitation for our model system.

5.1.2   Two-body random interaction model

Albeit the G^0W^0 method has widely been applied for various systems in most of the cases the self-energy is evaluated only close to the poles of the initial Green function thus yielding a correction to the quasiparticle energies. The corrections to the wave-functions are normally neglected. However there were also attempts to perform a fully self-consistent GW calculation. The results for the electron gas on this level [35, 40, 38] show the necessity to include the vertex correction in order to get the correct bandwidth. The description of the satellite structure is reasonable only on the G^0W^0 and GW^0 levels. Here we would like to extend the discussion to clarify the role of self-consistency for the life-times obtained from G^0W^0 and GW.

We continue here the investigation of the random-interaction model, described by the Hamiltonian Eq. (2.17). As we explained in Sec. 3.2, besides the $V_{ij,lk}$ we also need three other matrix elements V_i^{lk}, $V_{i,l}$, O_i^{lk} to perform a GW calculation. Although all matrix elements of the interaction are random quantities, we must generate them consistently. Thus we randomly generate two-point interactions $V_{i,l}$ and three-point overlap O_{lk}^i matrix elements, make a transformation and normalize O_i^{lk} in order to fulfill the orthogonality condition

$$\sum_{lk} O_i^{lk} O_j^{lk} = \delta_{ij} \tag{5.1}$$

and then generate the rest of matrix elements according to:

$$V_i^{kl} = \sum_j V_{i,j} O_j^{kl} \tag{5.2}$$

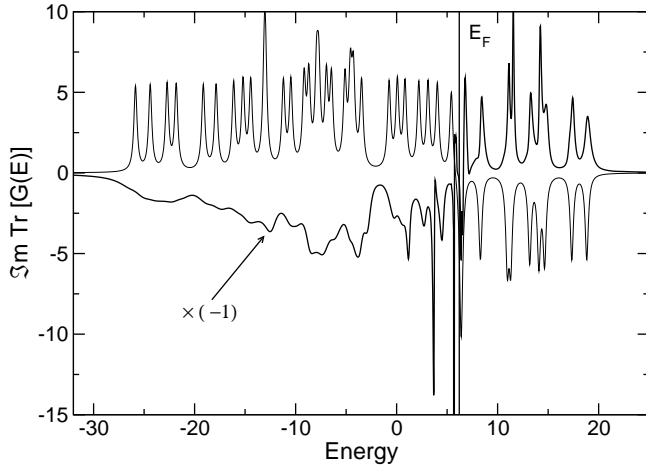$$V_{ij,lk} = \sum_{mn} O_m^{ij} V_{m,n} O_n^{kl}. \tag{5.3}$$

Fig. 5.6: *Sum of diagonal elements of $\Im$m $G(\omega)$ for the system with $m = 30, n = 40$. Thin line — HF Green's function, Thick line — forth iteration.*

Finally, the distribution of the four-point Coulomb matrix elements is close to a Gaussian with standard deviation 1.

First we performed several fully self-consistent GW cycles on the small system $m = 30, n = 40$. In order to avoid the possible errors in the density matrix obtained via the integration of the Green function over ω due to the small values of the self-energy $\Sigma(\omega)$ around the Fermi energy[3] we kept the direct and exchange part of the Hamiltonian on the HF level (Fig. 5.5). This stabilizes the calculation while it does not affect the imaginary part of the self-energy $\Im$m $\Sigma(\omega)$ very much.

The initial Green function has been computed using the eigenstates of the convergent Hartree-Fock Hamiltonian and applying the broadening $|\delta| = 0.19$ (Fig. 5.6). Our calculations show the rapid convergence of the self-energy (Fig. 5.7) in the course of the self-consistent GW loop. There is a considerable difference between the zeroth-order self-energy and consecutive iterations due to the homogeneous broadening that has been applied initially. In the beginning all peaks in Green's function have the same height and they give the same contribution to the self-energy. On the next iteration, instead of artificial broadening, the imaginary part of self-energy gives a finite width to the peaks. According to the results of MBPT the imaginary part of self-energy must vanish in the vicinity of the Fermi level. Thus the peaks become very narrow close to the Fermi energy, increasing their width for the deeply lying or highly excited states. This shows, that the excitation, when the electron moves only slightly above Fermi level is long lived and can be called a quasiparticle. By contrast, removing an electron with a low energy or putting an electron to a highly excited state leads to its fast recombination. The life-time of this kind of excitation is very small. The excitation cannot be described as a quasiparticle.

---

[3] A small imaginary part of the self-energy leads to very narrow peaks in the Green function. In order to correctly integrate it one must use a very fine mesh. This increases both memory and CPU-time requirements. Besides that, one must keep in mind that the intermediate steps in the GW interaction procedure are not conserving the number of particles. In order to get a physically correct, Hermitian Hartree-Fock Hamiltonian one must start with a Hermitian density matrix, thus its symmetrization is required, which is difficult to substantiate physically.
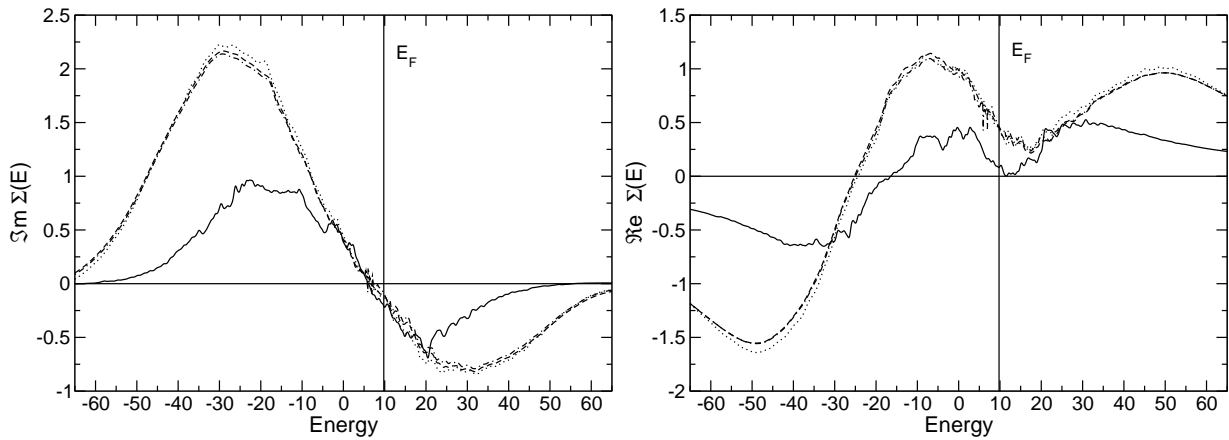
Fig. 5.7: *Average diagonal elements of $\Im\mathrm{m}\,\Sigma(\omega)$ and $\Re\mathrm{e}\,\Sigma(\omega)$ for the system with $m = 30, n = 40$. Iterations: 1—solid, 2—dotted, 3—dashed, 4 — dash-dotted.*

Already the second iteration gives good convergence of the self-energy. Moreover, the self-energies at any cycle are physically relevant, for they satisfy three major requirements:

(i) $\Im\mathrm{m}\,\Sigma(E_F) \sim 0$

(ii) $[\partial\Re\mathrm{e}\,\Sigma(\omega)/\partial\omega]_{\omega=E_F} < 1$

(iii) $\Im\mathrm{m}\,\Sigma(E_F)$ is positive for particles and negative for holes.

During the self-consistency loop a change in the inverse dielectric function compared to the RPA (first step) can be observed (on Fig. 5.8 the screened Coulomb interaction that reflects the frequency dependence of the dielectric function is shown). One can anticipate two peaks in its spectrum: a small bump at low energies associated with particle-hole scattering and a strong plasmon peak due to collective excitations. However the zeroth order dielectric function for the system exhibits a deviation from this prediction. There are several peaks at low energy. In the course of the self-consistent GW calculation they move to the higher energies, merge and form a broad bulge, that may be attributed to the existence of a hardly pronounced plasmon in this disordered system.
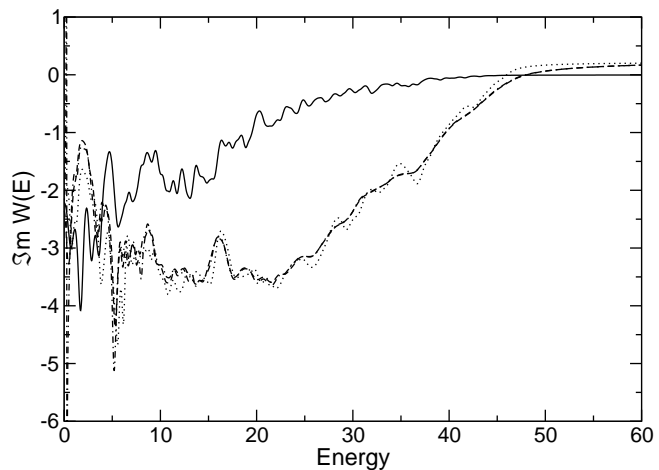

Fig. 5.8: *Average diagonal elements of $\Im\mathrm{m}\,W(\omega)$ for the system with $m = 30, n = 40$. Iterations: 1—solid, 2—dotted, 3—dashed, 4 — dash-dotted.*

From the comparison of the GW calculations on the different stages we conclude that G^0W^0 generally overestimates the life-time of the quasiparticle states far from the Fermi level. But taking into account the good agreement of the self-energy in the vicinity of the Fermi level and the complexity of the self-consistent GW calculation we perform the further investigation on the G^0W^0 level.
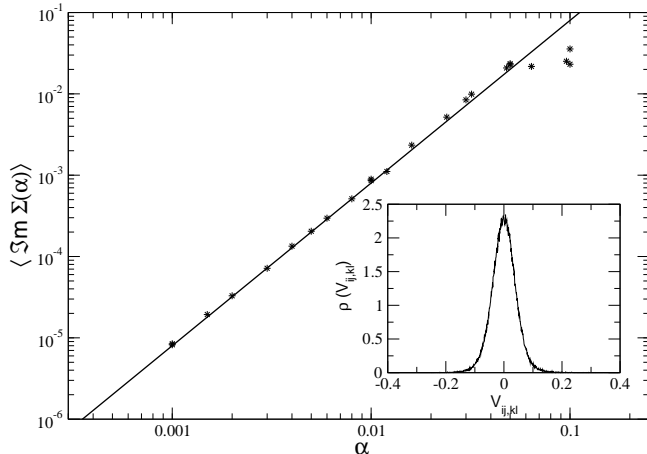

Fig. 5.9: *Dependence of the average $\Im m\, \Sigma(\omega)$ for the system with $m = 25, n = 50$ on the interaction strength. The line shows a quadratical dependence. In the inset a typical distribution of the Coulomb matrix elements is shown.*

Now we would like to put the random interaction model in closer relation to the experimental situation. As we showed before (Fig. 4.7) the distribution of the matrix elements of the Coulomb interaction in clusters has a random character and can be described by a regular shape. Increasing the number of the atoms in the cluster only enhances its randomness. This fact leads to the idea that one can understand some general features of their spectra (Ref. [65]), as well as in other complicated systems like heavy nuclei Ref. [66] or mesoscopic quantum dots Ref. [67] on the basis of random matrix theory (Ref. [68]). We use the two-body random interaction model (TBRIM, Ref. [81]) described above, which was widely studied before in the connection with the Poisson to Wigner-Dyson transition in the distribution of the level spacing ($P(E)$, Ref. [82]), to study the influence of the interaction strength on the life-time of the quasiparticle states. The life-time of the quasiparticle states is closely related to the $P(E)$. Several results are known for the TBRIM (Ref. [83]). There are some analytical estimates as well as numerical evidences from the diagonalization of the large many-body Hamiltonian matrices that the life-time

$$1/\tau \sim \Gamma \sim U^2 \tag{5.4}$$

is inversely proportional to the square of the interaction strength. However, numerical results were obtained so far for the systems with the number of many-body states not exceeding $10^5 - 10^6$. Here we would like to use the perturbative approach (GWA) to go far beyond that. In order to check the theoretical prediction Eq. (5.4) the calculation on the TBRIM with $m = 25, n = 50$ (number of the many-body states $\sim 10^{15}$) has been performed for the various interaction strength ranging from 10^{-3} to 10^{-1}. The self-energy has been averaged over the states. The averaging over the energy was done as well in the energy window in which all states are contained. The results in Fig. 5.9 show excellent agreement with the theoretical estimate and serve as a proof of the correctness of using this perturbational approach for a disordered system. Interesting is the small deviation of the

Cluster	HOMO-LUMO gap (eV)			Broadening(eV)		Life-time(fs)	
	HF	LDA	G^{0}W^0	HOMO	LUMO	HOMO	LUMO
Na$_9^+$	4.50	2.03	3.7 (3.47^a)	$< 5 \cdot 10^{-3}$	$> -5 \cdot 10^{-3}$	>827	>827
Na$_{15}^+$ (a)	3.98	1.55	2.91	0.056	-0.016	74	258
Na$_{15}^+$ (b)	3.49	1.28	3.13	0.022	-0.011	188	376
Na$_{17}^+$	2.86	0.82	2.34	0.018	-0.016	606	258
Na$_{21}^+$ (a)	2.95	0.83	2.11	0.022	-0.021	188	197
Na$_{21}^+$ (b)	2.71	0.67	2.05	0.030	-0.009	138	460
Na$_{25}^+$	2.71	0.82	2.42	0.021	-0.004	197	1034
Pt$_3$	6.36	0.40	5.16	0.059	-0.19	70	22

Tab. 5.2: *Comparison of the HOMO-LUMO gap of Na and Pt clusters from different methods.*
^{a} *Result of self-consistent calculation.*

broadening of the states from the quadratic law at the interaction strength around 10^{-1}. This saturation was observed as well before in Ref. [83] on the TBRIM with $m = 3, n = 130$ and $n = 4, m = 60$. And the fact of such a good agreement can serve as an additional evidence in favor of the GW approach.

5.2   Sodium clusters Na$_N^+$, N from 15 to 25

In this section we present our result for the quasiparticle life-time and the HOMO-LUMO gap correction (Tab. 5.2) from the non-self-consistent (G^{0}W^0) calculation. The geometry of clusters (Fig. 5.10-5.16) has been optimized on the HF level using the Gaussian 98 package [84]. The idea of the initial configurations for the sodium clusters has been taken from the work of Reinhard (Ref. [32]). Two isomers of the Na$_{21}^+$ cluster are supposed to be very stable due to the completion of the $2s$ shell (This is reflected in the high ionization potential for the neutral Na$_{20}$ cluster or, which is the same, the high electron affinity for Na$_{21}^+$, see Fig. 2.2).

We use the `lanl2dz` basis set for the Na$_{17}^+$, Na$_{21}^+$, Na$_{25}^+$ clusters while for smaller clusters we use the extended `lanl2dz` basis set (referred to in Appendix B as `lanl2dz1`) that consists of three s-type and three p-type functions. Basis functions were optimized to well represent the wave-functions of unoccupied states, which is important for the computation of, for example, the polarization operator. The effective core potential replaces 10 inner electrons. Therefore, our active space contains one electron described by 8 (12) basis functions for each sodium atom.

As we explained above the inversion of the dielectric function is avoided in our implementation because we compute the screened potential directly by solving the system of linear equations for each ω point. Thus, we use this quantity to show the behavior of the inverse dielectric function. In the plasmon-pole approximation the inverse dielectric function is said to consist of a single peak. Its position and strength can be determined directly from the boundary conditions. However, the above example shows that it is an
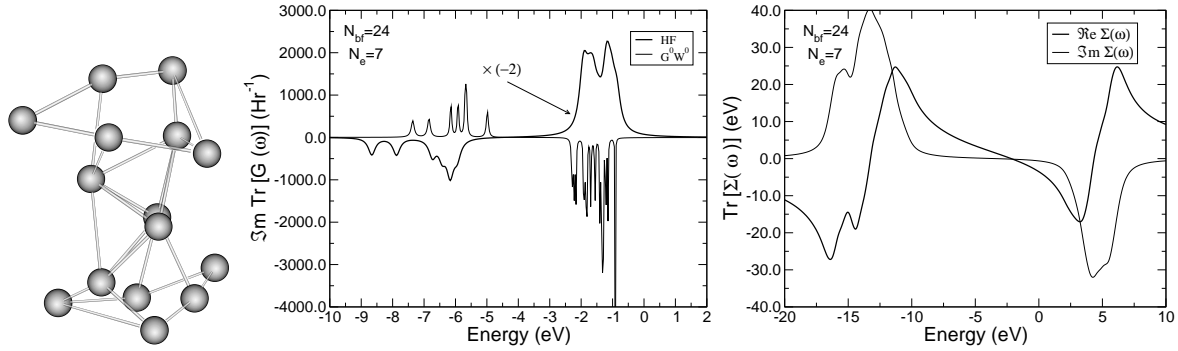
Fig. 5.10: Na_{15}^+ (a) cluster: geometry, density of states from HF and G^0W^0 theory, trace of self-energy matrix
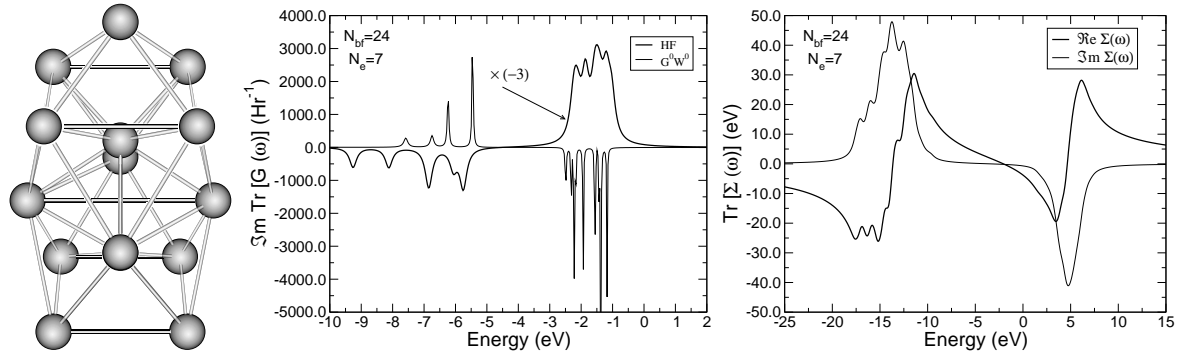

Fig. 5.11: Na_{15}^+ (b) cluster: geometry, density of states from HF and G^0W^0 theory, trace of self-energy matrix

oversimplification. In the case of clusters with irregular shape or elongated clusters the inverse dielectric function consists of several peaks.

Our calculation shows that for all sodium clusters we consider the dominant plasmon peak is positioned in the region of energies from 6 to 8 eV. According to the explanation in Sec. 5.1.1 an energy of the HOMO-LUMO gap must be subtracted from this value in order to obtain the surface plasmon resonance observed in the optical absorption spectrum. Comparing Fig. 5.17 and Tab. 5.2 shows that our RPA value for the surface plasmon energy (around 3 eV) agrees well with experimental data [79, 80] as well as with theoretical results from TDLDA theory [32].

In our calculations we initially applied a broadening $\delta = 0.136$ eV to each of the Hartree-Fock states. In order to reduce the computational effort and to make the calculations comparable for different systems the GW calculation was done in the HF basis by restricting the number of basis functions N_{bf} to 24.

Geometry optimization of the Na_{15}^+, performed without imposing any symmetry restrictions, shows, besides the lowest energy isomer (Fig. 5.11) found in the work of Reinhard *et al.*, a low symmetry cluster (Fig. 5.10) with even smaller total energy ($\Delta E = 0.36$ eV). Such an irregular shape of the cluster stipulates a complicated frequency dependence of
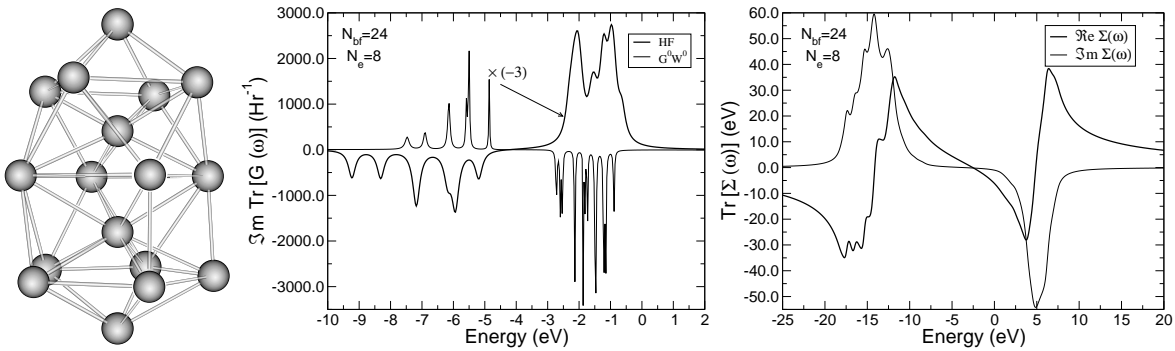
Fig. 5.12: *Na$_{17}^+$ cluster: geometry, density of states from HF and G^{0}W^0 theory, trace of self-energy matrix*

the screened potential $W(\omega)$ (Fig. 5.17). The composite plasmon peak is very broad (approximately 3 eV) and splits into two pronounced peaks around 5.9 eV and 7.5 eV. The structure of the screened potential in the case of another isomer of Na$_{15}^+$ is more compact. The total width is approximately 2 eV with a main maximum around 6.6 eV.

It is interesting to observe the effect of the GW correction on the band gap in these two clusters (Tab. 5.2). Both HF and LDA calculations show a larger HOMO-LUMO gap in the case of the first isomer. This is consistent, also, with its higher stability. On the contrary, GW calculations show a larger reduction of the band gap in the first case due to the correction to the HOMO state (the shift is around 0.96 eV, while for the second isomer it is only 0.30 eV). This makes the band gap for this cluster even smaller (2.91 eV) than for the second isomer (3.13 eV) (unoccupied states are less affected by the GW approximation). The density of states for the Na$_{15}^+$(b) cluster serves as a perfect illustration of the results of Fermi liquid theory. One sees, that approaching the Fermi level the width of the quasiparticle states reduces monotonically, or, in other words, their life-time increases.
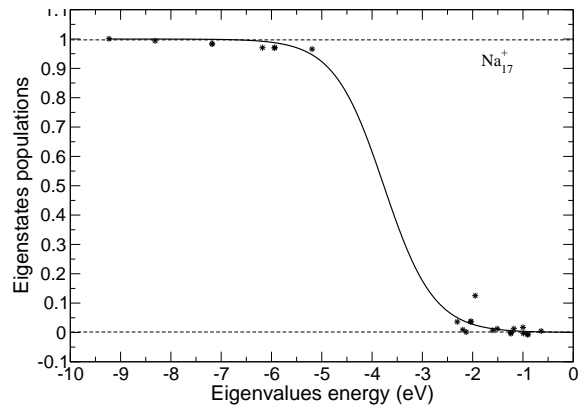

Fig. 5.13: *Distribution of the electrons over the eigenstates of the density matrix for a Na$_{17}^+$ cluster. Solid line is shown as a guide for eyes and was obtained by fitting the data by means of Fermi distribution.*

The structure of the Na$_{17}^+$ cluster (Fig. 5.12) has been optimized imposing the symmetry restriction, that puts 4 atoms on the main axis with the planes containing $5-4-4$ atoms in between. In order to check the quality of the final Green function we perform a numerical integration along the ω axis to determine the density matrix (Eq (3.12)). The diagonalization of the density matrix gives the occupation numbers for the quasiparticle states
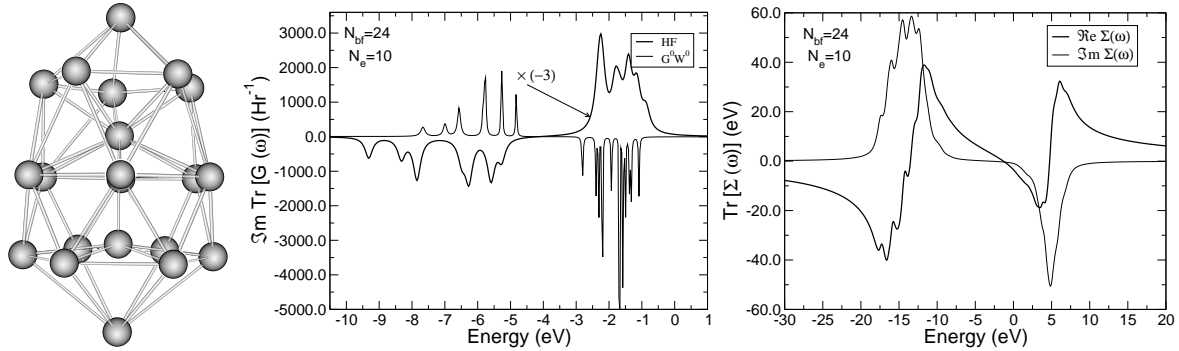
Fig. 5.14: Na_{21}^+ (a) cluster: geometry, density of states from HF and G^0W^0 theory, trace of self-energy matrix
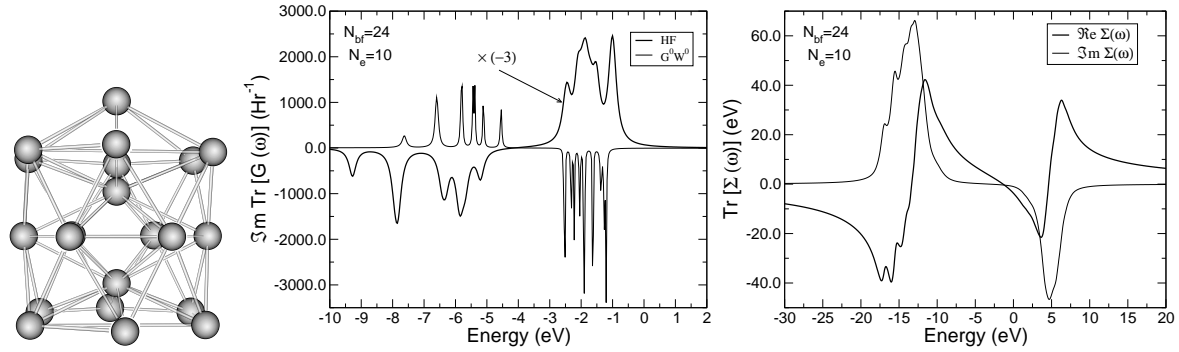

Fig. 5.15: Na_{21}^+ (b) cluster: geometry, density of states from HF and G^0W^0 theory, trace of self-energy matrix

(Fig. 5.13). One sees that according to the basic principles of many-body perturbation theory, the electron distribution differs from a step function when electronic correlations are taken into account. Summing up the eigenvalues of the density matrix gives the total number of electrons in the system. Our calculation produces a result of 8.12 (should be exactly 8), which shows the precision of the G^0W^0 method. This small error has two origins: physically the method is not conserving and, second, numerical errors occur due to the convolution and integration.

Geometry optimization for the Na_{21}^+ cluster gives two isomers when starting with configurations $1 - 5 - 1 - 6 - 1 - 6 - 1$ (Fig. 5.14)and $1 - 6 - 1 - 6 - 1 - 6$ (Fig. 5.15). The first one has a slightly lower energy ($\Delta E = 0.10$ eV). This is consistent with a result of Reinhard *et al.*, where the difference in energy between these structures was found to be almost negligible ($\Delta E = 0.10$eV).

Both clusters show similar results for the electronic properties: the main peak of the screened potential is situated at 6.8 eV and 6.5 eV respectively, the HOMO-LUMO gap is reduced by approximately 25% compared to the HF value.

The geometry of the Na_{25}^+ cluster is very elongated[4]. Its electronic density (Fig. 5.16) has

---

[4] Splitting of the plasmon resonance in elongated clusters can be estimated considering the Mie theory for
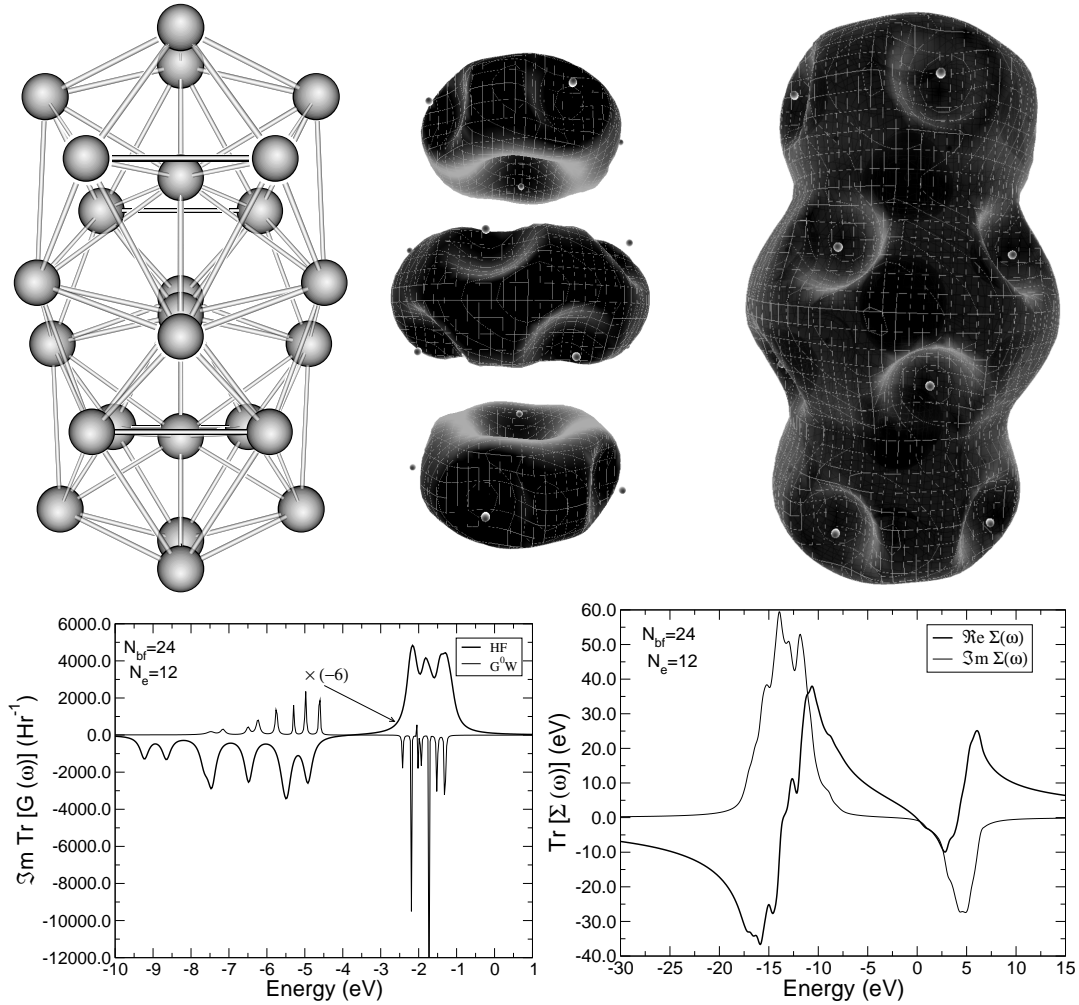
Fig. 5.16: *Na$_{25}^+$ cluster. Top: geometry and surfaces of the electronic density 0.004 a.u.$^{-3}$ (left) and 0.003 a.u.$^{-3}$ (right) are shown. Bottom: density of states from HF and G^0W^0 theory, trace of self-energy matrix.*

a spatial extent along the symmetry axis by approximately 26 Å, while in the perpendicular direction it is considerably smaller 14 Å. This results in a splitting of the plasmon resonance (Fig. 5.17) into two peaks at 5.1 eV and 6.4 eV. Contrary to the lighter clusters, the reduction of the band gap is small. This could result from the small number of virtual states ($N_e = 12$, $N_{bf} = 24$) taken into account and thus requires further investigation with a larger basis set.

On the figures Figs. 5.18 and 5.19 the self-energy of the HOMO and LUMO states are plotted as a function of energy for all clusters. Drawing straight lines $E = \omega - \varepsilon_i$, the

---

the ellipsoidal particles characterized by 3 geometric parameters R_x, R_y and R_z such that $R_x \cdot R_y \cdot R_z = R_0^3$, where R_0 is the average radius of the cluster. The surface plasmon correspondingly has three peaks at $\omega_i = \omega_{s.pl} \left[1 - \frac{3}{5} \frac{R_i - R_0}{R_0} \right]$. Putting realistic parameters for this cluster $R_1 = R_2 = 7$ Å, $R_3 = 13$ Å, $R_0 = 8.5$ Å, $\omega_{s.pl} = 2.7$ eV we obtain the splitting $\Delta\omega_{s.pl} = \omega_{s.pl} \frac{3}{5} \frac{R_3 - R_1}{R_0} = 1.1$ eV.
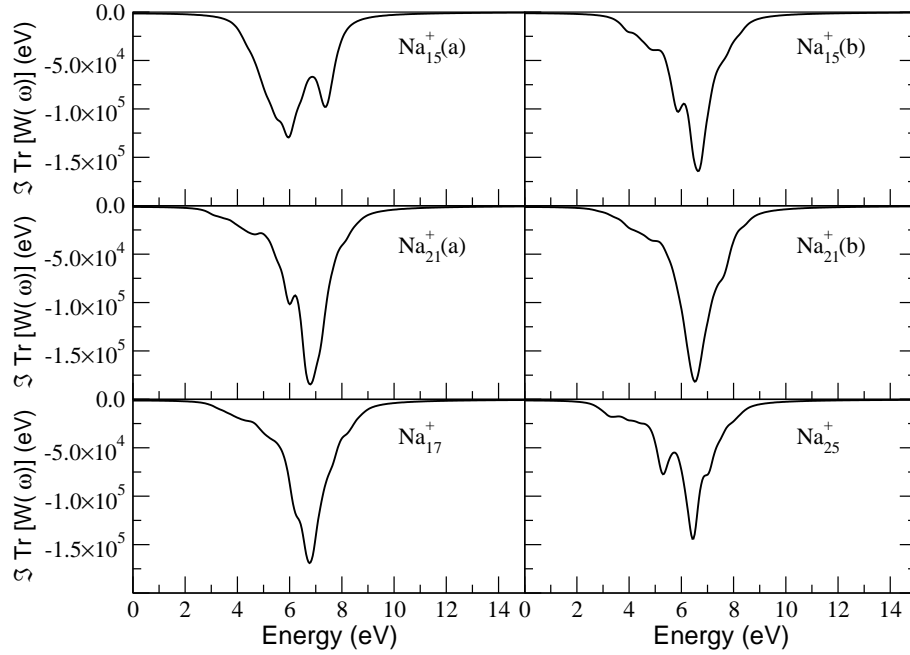
Fig. 5.17: *Imaginary part of the trace of the screened potential that shows the frequency dependence of the inverse dielectric function for sodium clusters.*

intersections show a schematic solution of the Dyson equation. The imaginary part of the self-energy gives a broadening of the quasiparticle states and, as a result, their life-time due to the electronic correlations.

The results of our calculations – band-gap, broadening of the quasiparticle states – are collected in Tab. 5.2. It is desirable for us to confirm them experimentally. Using time-resolved second-harmonic generation via femtosecond pump-probe studies [62] or analyzing photofragmentation of sodium clusters [63] the life-time of the surface plasmon can be obtained. It was found that for the cluster sizes from 5 to 55 nm plasmon life-time ranges from 3 fs to 10 fs. A similar result (10 fs) was also found for a system of much smaller size, viz. the Na_{96}^{+} cluster. This is consistent with the plasmon broadening from the RPA (Fig. 5.17) obtained during the G^0W^0 calculation, when initially constant broadening of the eigenstate energies was applied. One can see that the width of the plasmon peak is approximately 2 eV, which corresponds to life-times of a few femtoseconds. To obtain a more precise value the exact knowledge of the broadening of the quasiparticle states and a fully self-consistent GW calculation is required. The first is the main result of our calculation (Tab. 5.2, last two columns), it requires further experimental confirmation. The fully self-consistent calculation is the possible subject of our future work.

Fig. 5.18: *Real part of the self-energy for the HOMO (solid lines) and LUMO (dashed lines) states of the sodium clusters. Intersections of the straight lines with the curves denoted by the dots show the solution of the Dyson equation, which gives the real part of the energy of the HOMO and LUMO quasiparticle states.*

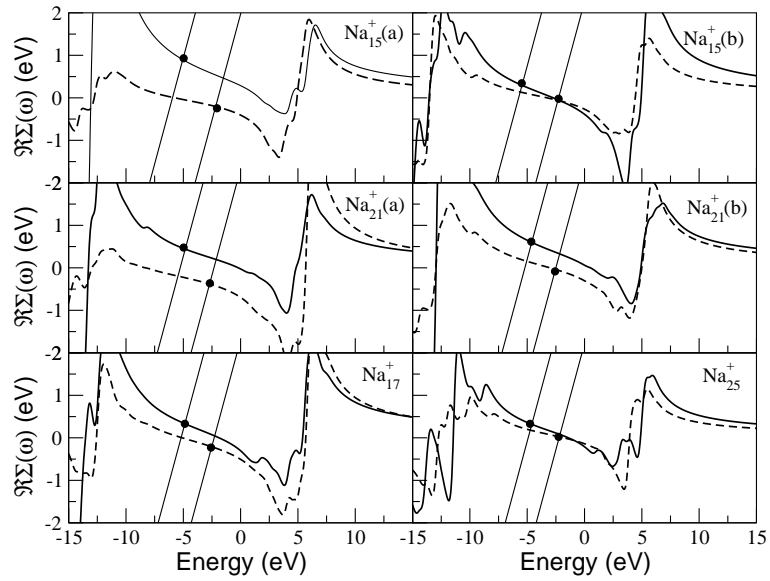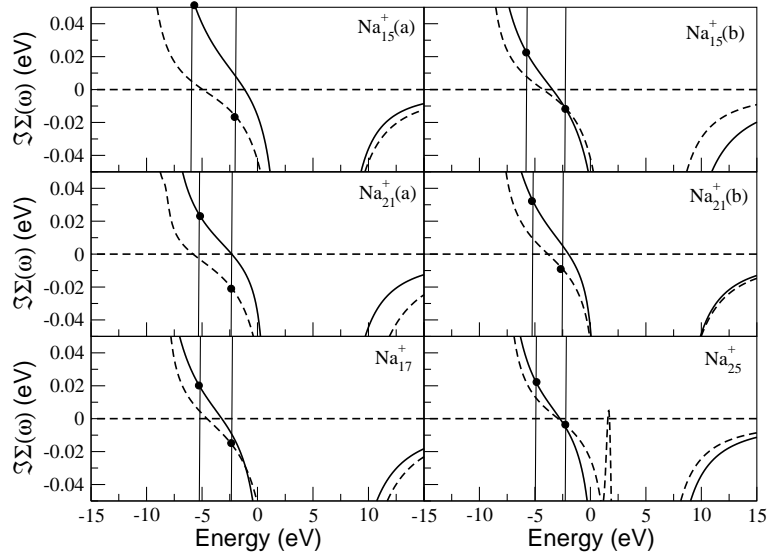Fig. 5.19: *Imaginary part of the self-energy for the HOMO (solid lines) and LUMO (dashed lines) states of the sodium clusters. Intersections of the straight lines with the curves denoted by the dots show the solution of the Dyson equation, which gives the imaginary part of the energy of the HOMO and LUMO quasiparticle states.*
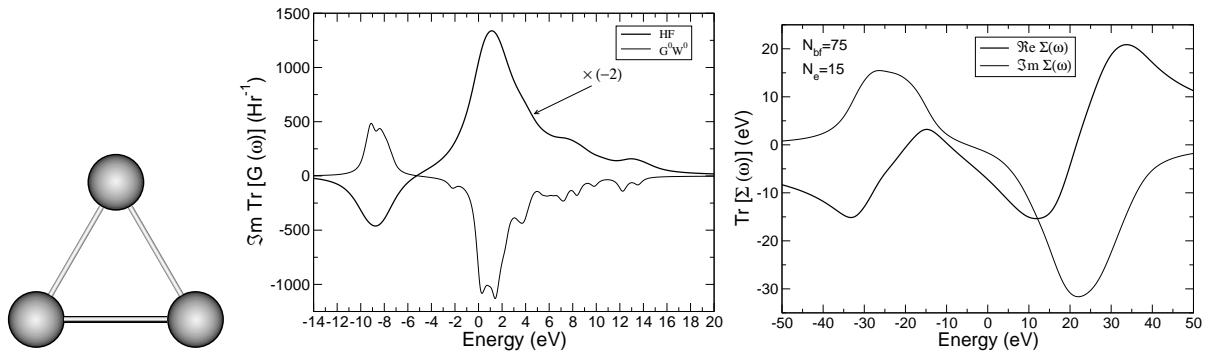
Fig. 5.20: *Pt$_3$ cluster: geometry, density of states from HF and G^0W^0 theory, trace of self-energy matrix.*

5.3   Pt$_3$ cluster

The Pt$_3$ cluster represents a system with complicated electronic structure. This is a consequence of the open shell (d^9s^1) configuration of the platinum atom, the importance of the spin-orbit coupling (to the extent that it even changes the ground state configuration [85]), and correlation effects [86]. The large discrepancy between the HOMO-LUMO gap from the HF and LDA approaches (Tab. 5.2) indicates the necessity of using the many-body perturbation technique. We found this system also to be a very difficult case for the GW calculations. The use of only a small number of basis functions leads to physically incorrect results, mostly due to the wrong sign of the imaginary part of self-energy for some states. This leads to the exchange of particle and hole states and to the wrong density matrix, obtained from the integration of the Green function. One can improve the situation only by adding a large number of eigenstates and increasing the energy cut-offs. We were able to obtain physically relevant results by considering 75 eigenstates and 15 electrons (Fig. 5.20). This is the largest system that we have studied sofar with our G^0W^0 approach.

To give an idea about the real amount of calculations, needed to obtain these results we illustrate our contribution with the self-energy, resolved along both energies axis (Fig. 5.21). The first one, parallel to the observation plane shows the usual dependence of this quantity on the frequency, that is the argument in the formulas. The second axis, perpendicular to the plane, shows the energy of the eigenstates, to which the self-energy belongs. Thus, it numbers the diagonal matrix elements. To obtain a smooth graph small broadening has been applied. Although the figure contains more information than just a trace of the self-energy that we use to plot, it does not reveal its off-diagonal matrix elements.

The interesting observation, coming from our calculations is a very large broadening of the HOMO and LUMO quasistates (0.058 and 0.19 eV respectively). The last one is almost one order of magnitude larger than for the sodium clusters and indicates fast damping of the LUMO state. The time resolved two-photon photoemission method (TR-2PPE) [55] gives a possibility to check that prediction directly in the experiment. The experiment comprises two pulses (Fig. 5.22): pump and probe. The pump pulse generates electron-hole pairs in the cluster. The photon energy must be chosen to be lower than the
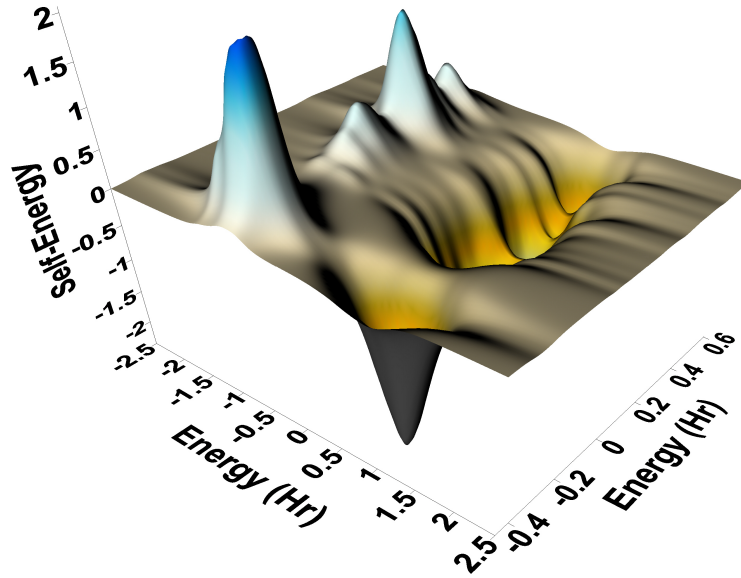
Fig. 5.21: *Imaginary part of the self-energy for the Pt₃ cluster. It is plotted as a function of ω and is resolved as a function of the eigenstates energies.*

work function, so that no electrons are emitted. During the life-time of the excitation, a second photon from the probe laser pulse can be absorbed. The excited electron can be photoemitted, and, hence, the cluster becomes ionized. The efficiency of the second process is proportional to the population of the excited state. Thus, if it is decaying with a certain time constant, this can be monitored by varying the time delay between the pulses. In Sec. 4.4 we estimated the life-time of the collective excitation (plasmon) and compared it with this type of experiments, considering that the extremely short life-time (70 fs as an upper limit) observed in experiment Ref. [55] can be attributed with the same rate of persuasion to both collective and single-particle excitations. Our GW calculation also demonstrates the second possibility.
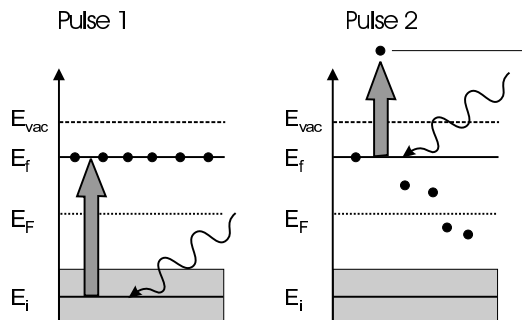
Fig. 5.22: *Schematic figure of two-photon processes involved in the TR-2PPE experiments.*

Summarizing, among the most important results of this chapter are:

- a partially self-consistent GW calculation on Na_9^+ cluster that enables us to improve HOMO-LUMO gap (4.5 eV – HF, 3.7 eV – G^0W^0, 3.37 eV GW) and to determine plasmon width and life-time (2 eV and 4.1 fs respectively).

- a fully self-consistent GW calculation on the TBRIM that helps us to understand the importance of the quasiparticle life-time renormalization and to check with a high precision the theoretical prediction that the life-time of the quasiparticle states is inversely proportional to the square of the interaction strength.

- the G^0W^0 calculation on a series of sodium clusters (Na_N^+, N=15-25) to improve their electronic structure obtained on the HF level and to estimate quasiparticles life-times.

- the G^0W^0 calculation on the Pt_3 cluster that reveals an extremely short life-time of the HOMO and LUMO states in striking agreement with the experimental observation and shows the capability of the method to treat large systems.

Conclusions

Our work was devoted to ultrafast electron dynamics in metallic clusters. Nontrivial (not just a change of the phase of the wave-function, which is not observable) electron dynamics is a consequence of electronic correlations in the system. It manifests itself as a transition of electrons between states or an excitation during the interaction with an external field and, as relaxation or equilibration of the system due, first, to electron-electron collisions and, then, due to electron-phonon interaction. In our work we use two approaches to investigate what happens to the system on the femtosecond time-scale. First, we employ the time-dependent Hartree-Fock equation to observe phenomena resolved in real time. We were able to see electron transitions among the states, plasmon oscillations and even plasmon damping. This approach also enables us to compute excited states of the system by analyzing the power spectrum of the dipole moment and compare it with optical absorption experiments. The first one, namely, damping of the electronic excitations is also nowadays within experimental reach. We find good agreement between our estimate of the plasmon life-time and experiment on platinum clusters. Platinum is not the only direction of our work. While it shows its outreach power in the treatment of small systems with complicated electronic structure that contains strongly localized d-functions, sodium clusters give examples of large systems, which, however, are closest to the theoretical idealization of the homogeneous electron gas model. We also illustrate our work with the example of the two-body random interaction model, which is more flexible in the sense that it is easier to vary its parameters to see the evolution from the non-interacting to the strongly correlated electron system and, thus, it is easier to see the origin of many phenomena.

The second part of our work followed the line of many-body perturbational theory with, seemingly, no direct relation to the time evolution. This is, however, not true! Even the smallest step beyond the mean-field treatment (to include correlations), made in a proper way by taking into account a certain class of diagrams leads to improvement of, first, our knowledge of the electronic structure, and, second, describes the damping of the states by a set of life-times. They manifest themselves as an imaginary part of the eigenenergy of any electronic state, quasiparticle, or plasmon, and describe their decay due to the electron-electron interaction. The complexity of the method (there is no realistic system for which it has been applied in full extent at the present time) gives many approximate ways to its implementation. For large systems, like the series of clusters from Na_{15}^+ to Na_{25}^+ it was reasonable to stop on the simplest G^0W^0 level, which is commonly used at present to correct the electronic structure of solids. Smaller clusters are described by fewer basis functions allowing for the self-consistent extension of the method. The advantage is the independence of the results on the initial guess of the Green function, which bears some reminiscence of the Hartree-Fock or DFT calculations.

A lot still remains to be done. The first approach, being almost perfect from the computational point of view can now be applied to a larger class of materials and allows for the exploration of a variety of experimental situations, such as four-wave mixing, second harmonic generation, etc. The second approach requires its further development in seeking the best computational scheme, comparing different additional approximations and finding the optimal level of the theory for each particular class of clusters. Only then its routine application for the design of new materials is possible.

Appendix A

Computation of some integrals over Gaussian basis functions

In order to make this thesis self-explanatory we present here recursive formulae for the computation of two, three, and four-point integrals. The derivation of most of the formulae given here can be found in Ref. [87]. The recursive expressions for the two- and three-point electron repulsion integrals are presented here for the first time. We write the unnormalized Cartesian Gaussian functions with the origins at $\boldsymbol{R}$ as

$$\phi(\boldsymbol{r}; \zeta, \boldsymbol{n}, \boldsymbol{R}) = (x - R_x)^{n_x}(y - R_y)^{n_y}(z - R_z)^{n_z} \exp[-\zeta(\boldsymbol{r} - \boldsymbol{R})^2] \tag{A.1}$$

The three-center overlap integrals over unnormalized Cartesian Gaussian functions are of the form:

$$(\boldsymbol{a}|\boldsymbol{c}|\boldsymbol{b}) = \int d\boldsymbol{r}\phi(\boldsymbol{r}; \zeta_a, \boldsymbol{a}, \boldsymbol{A})\phi(\boldsymbol{r}; \zeta_c, \boldsymbol{c}, \boldsymbol{C})\phi(\boldsymbol{r}; \zeta_b, \boldsymbol{b}, \boldsymbol{B}). \tag{A.2}$$

The recurrence formula reads:

$$(\boldsymbol{a} + \boldsymbol{1}_i|\boldsymbol{c}|\boldsymbol{b}) = (G_i - A_i)(\boldsymbol{a}|\boldsymbol{c}|\boldsymbol{b}) + \frac{1}{2(\zeta + \zeta_c)}[N_i(\boldsymbol{a})(\boldsymbol{a} - \boldsymbol{1}_i|\boldsymbol{c}|\boldsymbol{b})$$
$$+ N_i(\boldsymbol{b})(\boldsymbol{a}_i|\boldsymbol{c}|\boldsymbol{b} - \boldsymbol{1}) + N_i(\boldsymbol{c})(\boldsymbol{a}_i|\boldsymbol{c} - \boldsymbol{1}|\boldsymbol{b})] \tag{A.3}$$

where the following notations have been introduced:

$$\xi = \frac{\zeta_a\zeta_b}{\zeta_a + \zeta_b}, \tag{A.4}$$

$$\zeta = \zeta_a + \zeta_b, \tag{A.5}$$

$$\boldsymbol{P} = \frac{\zeta_a\boldsymbol{A} + \zeta_b\boldsymbol{B}}{\zeta_a + \zeta_b}, \tag{A.6}$$

$$\boldsymbol{G} = \frac{\zeta\boldsymbol{P} + \zeta_c\boldsymbol{C}}{\zeta + \zeta_c} \qquad . \tag{A.7}$$

The integral over s-type functions is given by

$$(\boldsymbol{0}_A|\boldsymbol{0}_B|\boldsymbol{0}_C) = (\frac{\zeta}{\zeta + \zeta_c})^{3/2}(\boldsymbol{0}_A|\boldsymbol{0}_B) \exp\left[-\frac{\zeta\zeta_c}{\zeta + \zeta_c}(\boldsymbol{P} - \boldsymbol{C})^2\right]. \tag{A.8}$$

This is expressed via the overlap of two s functions:

$$(\mathbf{0}_A|\mathbf{0}_B) = \frac{\pi^{3/2}}{\zeta} \exp\left[-\xi(\mathbf{A}-\mathbf{B})^2\right]. \tag{A.9}$$

Our next target is the computation of four-point ERIs

$$\begin{aligned}(\mathbf{ab},\mathbf{cd}) = \int d\mathbf{r}_1 \int d\mathbf{r}_2 [\phi(\mathbf{r}_1;\zeta_a,\mathbf{a},\mathbf{A})\phi(\mathbf{r}_1;\zeta_b,\mathbf{b},\mathbf{B})]\\ \times|\mathbf{r}_1-\mathbf{r}_2|^{-1}[\phi(\mathbf{r}_2;\zeta_c,\mathbf{c},\mathbf{C})\phi(\mathbf{r}_2;\zeta_d,\mathbf{d},\mathbf{D})].\end{aligned} \tag{A.10}$$

Introducing parameters similar to those given in the Eqs. (A.4,A.5,A.6,A.7)

$$\eta = \zeta_c + \zeta_d, \tag{A.11}$$

$$\rho = \frac{\zeta\eta}{\zeta+\eta}, \tag{A.12}$$

$$\mathbf{Q} = \frac{\zeta_c\mathbf{C} + \zeta_d\mathbf{D}}{\zeta_c + \zeta_d}, \tag{A.13}$$

$$\mathbf{W} = \frac{\zeta\mathbf{P} + \eta\mathbf{Q}}{\zeta+\eta} \tag{A.14}$$

the recursive expression for the ERI can be obtained:

$$\begin{aligned}[(\mathbf{a}+\mathbf{1}_i)\mathbf{b},\mathbf{cd}]^{(m)} =&\ (P_i - A_i)(\mathbf{ab},\mathbf{cd})^{(m)} + (W_i - P_i)(\mathbf{ab},\mathbf{cd})^{(m+1)}\\ &+\frac{1}{2\zeta}N_i(\mathbf{a})\left\{[(\mathbf{a}-\mathbf{1}_i)\mathbf{b},\mathbf{cd}]^{(m)} - \frac{\rho}{\zeta}[(\mathbf{a}-\mathbf{1}_i)\mathbf{b},\mathbf{cd}]^{(m+1)}\right\}\\ &+\frac{1}{2\zeta}N_i(\mathbf{b})\left\{[\mathbf{a}(\mathbf{b}-\mathbf{1}_i),\mathbf{cd}]^{(m)} - \frac{\rho}{\zeta}[\mathbf{a}(\mathbf{b}-\mathbf{1}_i),\mathbf{cd}]^{(m+1)}\right\}\\ &+\frac{1}{2(\zeta+\eta)}N_i(\mathbf{c})[\mathbf{ab},(\mathbf{c}-\mathbf{1}_i)\mathbf{d}]^{(m+1)}\\ &+\frac{1}{2(\zeta+\eta)}N_i(\mathbf{d})[\mathbf{ab},\mathbf{c}(\mathbf{d}-\mathbf{1}_i)]^{(m+1)}(i=x,y,z).\end{aligned} \tag{A.15}$$

Here, the ERI $(\mathbf{ab},\mathbf{cd})$ is a special case of the auxiliary electron repulsion integral defined as

$$(\mathbf{ab},\mathbf{cd})^{(m)} = \frac{2}{\pi^{1/2}}\int_0^\infty du\left(\frac{u^2}{\rho+u^2}\right)^m(\mathbf{ab},\mathbf{cd}) \tag{A.16}$$

when $m=0$.

To perform the calculation according to the given formula one needs to know the expression for the auxiliary ERI over s function:

$$\begin{aligned}(\mathbf{0}_A\mathbf{0}_B,\mathbf{0}_C\mathbf{0}_D)^{(m)} =&\ 2(\frac{\rho}{\pi})^{1/2}(\mathbf{0}_A|\mathbf{0}_B)(\mathbf{0}_C|\mathbf{0}_D)F_m(T)\\ =&\ (\zeta+\eta)^{-1/2}K(\zeta_a,\zeta_b,\mathbf{A},\mathbf{B})K(\zeta_c,\zeta_d,\mathbf{C},\mathbf{D})F_m(T)\end{aligned} \tag{A.17}$$

where

$$F_m(T) = \int_0^1 dt\, t^{2m} \exp[-Tt^2], \tag{A.18}$$

$$T = \rho(\boldsymbol{P} - \boldsymbol{Q})^2, \tag{A.19}$$

$$K(\zeta, \zeta', \boldsymbol{R}, \boldsymbol{R}') = 2^{1/2} \frac{\pi^{5/4}}{\zeta + \zeta'} \exp\left[-\frac{\zeta\zeta'}{\zeta + \zeta'}(\boldsymbol{R} - \boldsymbol{R}')^2\right] \qquad . \tag{A.20}$$

For the GW calculations it is also necessary to have formulae for the computation of the three point electron repulsion integral defined as:

$$(\boldsymbol{a}, \boldsymbol{cd}) = \int d\boldsymbol{r}_1 \int d\boldsymbol{r}_2 \phi(\boldsymbol{r}_1; \zeta_a, \boldsymbol{a}, \boldsymbol{A})|\boldsymbol{r}_1 - \boldsymbol{r}_2|^{-1}[\phi(\boldsymbol{r}_2; \zeta_c, \boldsymbol{c}, \boldsymbol{C})\phi(\boldsymbol{r}_2; \zeta_d, \boldsymbol{d}, \boldsymbol{D})]. \tag{A.21}$$

Two recursive formulae can be obtained from Eq. (A.15) by putting $\boldsymbol{b} = \boldsymbol{0}$ and $\zeta_b = 0$.

$$[(\boldsymbol{a} + \boldsymbol{1}_i), \boldsymbol{cd}]^{(m)} = (\bar{W}_i - A_i)(\boldsymbol{a}, \boldsymbol{cd})^{(m+1)}$$
$$+ \frac{1}{2\zeta_a} N_i(\boldsymbol{a}) \left\{ [(\boldsymbol{a} - \boldsymbol{1}_i), \boldsymbol{cd}]^{(m)} - \frac{\bar{\rho}}{\zeta_a}[(\boldsymbol{a} - \boldsymbol{1}_i), \boldsymbol{cd}]^{(m+1)} \right\}$$
$$+ \frac{1}{2(\zeta_a + \eta)} N_i(\boldsymbol{c})[\boldsymbol{a}, (\boldsymbol{c} - \boldsymbol{1}_i)\boldsymbol{d}]^{(m+1)} + \frac{1}{2(\zeta_a + \eta)} N_i(\boldsymbol{d})[\boldsymbol{a}, \boldsymbol{c}(\boldsymbol{d} - \boldsymbol{1}_i)]^{(m+1)}, \tag{A.22}$$

$$[\boldsymbol{0}, (\boldsymbol{c} + \boldsymbol{1}_i)\boldsymbol{d}]^{(m)} = (Q_i - C_i)(\boldsymbol{0}, \boldsymbol{cd})^{(m)} + (\bar{W}_i - Q_i)(\boldsymbol{0}, \boldsymbol{cd})^{(m+1)}$$
$$+ \frac{1}{2\eta} N_i(\boldsymbol{c}) \left\{ [\boldsymbol{0}, (\boldsymbol{c} - \boldsymbol{1}_i)\boldsymbol{d}]^{(m)} - \frac{\bar{\rho}}{\eta}[\boldsymbol{0}, (\boldsymbol{c} - \boldsymbol{1}_i)\boldsymbol{d}]^{(m+1)} \right\}$$
$$+ \frac{1}{2\eta} N_i(\boldsymbol{d}) \left\{ [\boldsymbol{0}, \boldsymbol{c}(\boldsymbol{d} - \boldsymbol{1}_i)]^{(m)} - \frac{\bar{\rho}}{\eta}[\boldsymbol{0}, \boldsymbol{c}(\boldsymbol{d} - \boldsymbol{1}_i)]^{(m+1)} \right\}. \tag{A.23}$$

The auxiliary integrals are defined as before (Eq. (A.16)) with the replacement $\rho \to \bar{\rho}$, and we used the notations:

$$\bar{\rho} = \frac{\zeta_a \eta}{\zeta_a + \eta}, \tag{A.24}$$

$$\bar{W} = \frac{\zeta_a \boldsymbol{A} + \eta \boldsymbol{Q}}{\zeta + \eta}. \tag{A.25}$$

The three point electron repulsion integral over s functions is given by

$$(\boldsymbol{0_A}, \boldsymbol{0_C 0_D})^{(m)} = 2(\frac{\bar{\rho}}{\pi})^{1/2}(\frac{\pi}{\zeta_a})^{3/2}(\boldsymbol{0_C}|\boldsymbol{0_D})F_m(\bar{T})$$
$$= 2^{1/2} \frac{\pi^{5/4}}{\zeta_a}(\zeta_a + \eta)^{-1/2}K(\zeta_c, \zeta_d, \boldsymbol{C}, \boldsymbol{D})F_m(\bar{T}) \tag{A.26}$$

with

$$\bar{T} = \bar{\rho}(\boldsymbol{A} - \boldsymbol{Q})^2. \tag{A.27}$$

The third kind of electron repulsion integrals we need is a two point integral:

$$(\boldsymbol{a}, \boldsymbol{b}) = \int d\boldsymbol{r}_1 \int d\boldsymbol{r}_2 \phi(\boldsymbol{r}_1; \zeta_a, \boldsymbol{a}, \boldsymbol{A})|\boldsymbol{r}_1 - \boldsymbol{r}_2|^{-1}\phi(\boldsymbol{r}_2; \zeta_b, \boldsymbol{b}, \boldsymbol{B}). \tag{A.28}$$

Putting $\boldsymbol{b} = \boldsymbol{0}$, $\zeta_b = 0$, $\boldsymbol{c} = \boldsymbol{0}$, $\zeta_c = 0$ in Eq. (A.15) and changing variables from $\boldsymbol{d}$ to $\boldsymbol{b}$ we get the recursive formula:

$$[(\boldsymbol{a} + \boldsymbol{1}_i), \boldsymbol{b}]^{(m)} = (\bar{P}_i - A_i)(\boldsymbol{a}, \boldsymbol{b})^{(m+1)}$$

$$+ \frac{1}{2\zeta_a} N_i(\boldsymbol{a}) \left\{ [(\boldsymbol{a} - \boldsymbol{1}_i), \boldsymbol{b}]^{(m)} - \frac{\bar{\xi}}{\zeta_a} [(\boldsymbol{a} - \boldsymbol{1}_i), \boldsymbol{b}]^{(m+1)} \right\}$$

$$+ \frac{1}{2\zeta} N_i(\boldsymbol{b}) [\boldsymbol{a}, (\boldsymbol{b} - \boldsymbol{1}_i)]^{(m+1)}. \tag{A.29}$$

Computations are initialized by the integral over the s functions

$$(\boldsymbol{0_A}, \boldsymbol{0_B})^{(m)} = 2(\frac{\xi}{\pi})^{1/2}(\frac{\pi}{\zeta_a})^{3/2}(\frac{\pi}{\zeta_b})^{3/2} F_m(\tilde{T}) \tag{A.30}$$

$$\tilde{T} = \xi(\boldsymbol{A} - \boldsymbol{B})^2, \tag{A.31}$$

and auxiliary integrals are similar to Eq. (A.16), with ξ instead of ρ. From the given formulae we can see that all integrals can be evaluated analytically by means of the recursion relations Eqs. (A.3, A.15, A.22, A.23, A.29). We use the two stage method of Head-Gordon and Pople (Ref. [88]) to implement the recurrence relation Eq. (A.15) via vertical (VRR) and horizontal (HRR) recurrence relations. The three point ERIs are also computed in two stages. The computation of the electron repulsion integrals also requires a fast algorithm for the calculation of the non-elementary function $F_m(t)$. We refer to Ref. [87] for further explanation.

Appendix B

Optimization of basis functions

Two improve the representation of the virtual states close to Fermi level we add diffusive functions to the lanl2dz (Ref. [72]) basis sets for Na and Pt atoms. Short information about them is given in Tab. B.1. In Fig. B.1 the trace of the imaginary part of Green's function for Na_9^+ and Pt_3 clusters is shown for different basis sets.

Fig. B.1: *Left panel: the trace of Green's function for the Na_9^+ cluster computed from the quasiparticle states in the HF approximation. Dash-dotted line — lanl2dz basis set, dashed line — lanl2dz1, solid line — lanl2dz2. R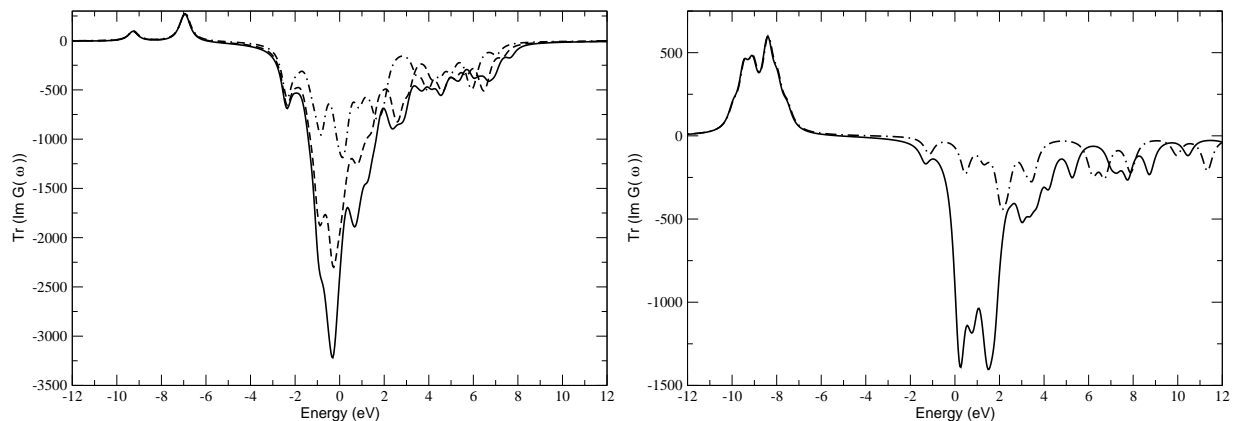ight panel: the trace of Green's function for the Pt_3 cluster computed from the quasiparticle states in HF approximation. Dash-dotted line — lanl2dz basis set, solid line — lanl2dz1.*

Basis functions were optimized by performing a series of HF calculations for different scaling parameters of the gaussian exponents and comparing the density of states above the Fermi level.

Atom	Name	Number	Type	Exp.	Contr.Coeff.
Na	lanl2dz	8	S	0.4972 0.56	-0.2753574 1.0989969
			S	0.0221	1.0
			P	0.6697 0.0636	-0.06833845 1.014055
			P	0.0204	1.0
	lanl2dz1	12	lanl2dz		
			S	0.005525	1.0
			P	0.009996	1.0
	lanl2dz2	15	lanl2dz		
			S	0.011187 0.00126	-0.2753574 1.0989969
			S	0.031075 0.0035	-0.2753574 1.0989969
			S	0.00447525	1.0
			S	0.00668525	1.0
			P	0.009996	1.0
Pt	lanl2dz	24	S	2.547 1.614 0.5167	-1.473918 1.911572 0.3922319
			S	2.547 1.614 0.5167 0.2651	1.438817 -2.091182 -1.092132 1.34266
			S	0.058	1.0
			P	2.911 1.836 0.5982	-0.5247438 0.9671884 0.5438632
			P	0.6048 0.0996	-0.1061438 1.03831
			P	0.029	1.0
			D	1.243 0.4271	0.559815 0.551109
			D	0.137	1.0
	lanl2dz1	37	lanl2dz		
			S	0.00522	1.0
			P	0.00261	1.0
			P	0.054432 0.008964	-0.1061438 1.03831
			D	0.01233	1.0

Tab. B.1: *Basis sets for Na and Pt atoms. The largest basis set for Na was used only for small clusters Na_N ($N \leq 9$).*

Appendix C

Simplified derivation of Hedin's equations

The system of Hedin's equations is obvious from their diagrammatic representation, following then just from the rules for summation of the infinite sequences of certain graphs. This approach, also being very useful in deriving further approximations and building relations with mathematics, bears little information about the physics of the problem. To lend physical meaning to each of the functions entering the Hedin's equation it is helpful to use the method of functional differentiation. We closely follow the work of Hedin (Ref. [16]), however using our notations and completing missing places in the derivations. The main idea (similar to what was used to derive the expression for the dielectric function p. 20) of the approach is to consider the system subject to some vanishing time-dependent external potential $\phi(\boldsymbol{r_1}, t_1) = \phi(1)$. It is only an auxiliary quantity and should be set equal to zero in the final expressions. We start from the most general equation of motion for the single-particle Green function in the presence of the auxiliary external potential $\phi(1)$. Its rigorous derivation is quite long and lies beyond the scope of this appendix (The interested reader is referred to the original work of Martin and Schwinger Ref. [89]).

$$\left(i\frac{\partial}{\partial t_1} - H^0(1) - V(1)\right) G(12) - i \int v(1^+3)\frac{\delta}{\delta\phi(3)}G(12)d(3) = \delta(12) \qquad \text{(C.1)}$$

Here $V(1)$ is the average potential that acts on the electrons of the system. It consists of the external potential $\phi(1)$ and the contribution due to the total electronic density, in other words, just the direct term of the Hartree-Fock potential introduced before (p. 26, p. 35).

$$V(1) = \phi(1) + H^d(1) = \phi(1) - i \int v(13)G(33^+)d(3) \qquad \text{(C.2)}$$

The next equation is the generalization of Eq. (3.19) for the presence of the external potential:

$$\left(i\frac{\partial}{\partial t_1} - H^0(1) - V(1)\right) G(12) - \int \Sigma(13)G(32)d(3) = \delta(12). \qquad \text{(C.3)}$$

To obtain an explicit expression for the self-energy we also need the inverse Green function, defined as:

$$\int G(13)G^{-1}(32)d(3) = \delta(12).\tag{C.4}$$

From the chain-rule differentiation we obtain the identity:

$$\frac{\delta G(12)}{\delta\phi(3)} = -\int G(14)\frac{\delta G^{-1}(45)}{\delta\phi(3)}G(52)d(45).\tag{C.5}$$

Putting the last expression into Eq. (C.1) and comparing it with Eq. (C.3) we arrive at:

$$\Sigma(12) = -\int v(13^+)G(14)\frac{\delta G^{-1}(42)}{\delta\phi(3)}d(34)\tag{C.6}$$

Now we proceed in a similar way to obtain the expression for the screened Coulomb interaction. Before (p. 20) we defined the dielectric function as a quantity that shows the change of the average potential in the system due to the change of the external potential. Therefore we can rewrite it in functional form as:

$$\varepsilon^{-1}(1,2) = \frac{\delta V(1)}{\delta\phi(2)}.\tag{C.7}$$

The screened potential $W(12)$ was defined (p. 36) as a frequency dependent quantity that describes the interaction between the electrons, surrounded by the electron gas. One can consider it as the average potential that acts on the electron as if the Coulomb interaction were an external field:

$$W(12) = \int v(13)\varepsilon^{-1}(32)d(3) = \int v(13)\frac{\delta V(2)}{\delta\phi(3)}d(3).\tag{C.8}$$

Using Eqs. (C.2), (C.2) and (C.2) we can write $W(12)$ as

$$W(12) = v(12) + i\int v(13)v(24)G(45)\frac{G^{-1}(56)}{\delta\phi(3)}G(64^+)d(3456).\tag{C.9}$$

Using the identity

$$\frac{\delta}{\delta\phi(1)} = \int \frac{\delta V(2)}{\delta\phi(1)}\frac{\delta}{\delta V(2)}d(2),\tag{C.10}$$

$W(12)$ can be written

$$W(12) = v(12) + \int W(13)P(34)v(42)d(34),\tag{C.11}$$

where

$$P(34) = i\int G(45)G(64^+)\frac{\delta G^{-1}(56)}{\delta V(3)}d(56).\tag{C.12}$$

Introducing the vertex function $\Gamma(12,3)$,

$$\Gamma(12,3) = -\frac{\delta G^{-1}(12)}{\delta V(3)} = \delta(12)\delta(13) + \frac{\delta\Sigma(12)}{\delta V(3)},\tag{C.13}$$

we finally obtain the following expressions (compare p. 36) for Σ and P:

$$\Sigma(12) = i \int W(1^+3)G(14)\Gamma(42;3)d(34) \tag{C.14}$$

$$P(12) = -i \int G(23)G(42^+)\Gamma(34,1)d(34). \tag{C.15}$$

The functional derivative of Green's function with respect to the average potential follows from Eq. (C.5) by replacing $\phi(3)$ with $V(3)$ and using the definition of the vertex function Eq. (C.13):

$$\frac{\delta G(12)}{\delta V(3)} = \int G(14)G(52)\Gamma(45,3)d(45). \tag{C.16}$$

This identity can be used to complete the system of Hedin's equations. Using the chain-differentiation rule and the fact that the self-energy can be regarded as a functional of Green's function only (p. 36) we can express the vertex function as:

$$
\begin{aligned}
\Gamma(12,3) \quad = \quad & \delta(12)\delta(13) + \frac{\delta\Sigma(12)}{\delta V(3)} = \\
= \; & \delta(12)\delta(13) + \int \frac{\delta\Sigma(12)}{\delta G(45)}\frac{\delta G(45)}{\delta V(3)} \\
= \; & \delta(12)\delta(13) + \int \frac{\delta\Sigma(12)}{\delta G(45)}G(46)G(75)\Gamma(67,3)d(4567).
\end{aligned} \tag{C.17}
$$

Q.E.D.

Bibliography

[1] J. J. Quinn and R. A. Ferrell. *Electron Self-Energy Approach to Correlation in Degenerate Electron Gas.* Phys. Rev. **112** (1958), 812.

[2] Migdal. *Interaction between electrons and lattice vibrations in a normal metal.* Sov. Phys. JETP (English Translation) **7** (1958), 996.

[3] D. E. Gray, editor. *American Institute of Physics handbook* (New York, NY: McGraw-Hill, 1963), 2 edition.

[4] E. Merzbacher. *Quantum mechanics* (Wiley, New York, 1970), 2 edition.

[5] G. Onida, L. Reining, R. W. Godby, R. D. Sole, and W. Andreoni. *Ab initio Calculations of the Quasiparticle and Absorption Specra of Clusters: The Sodium Tetramer.* Phys. Rev. Lett. **75** (1995), 818.

[6] W. Ekardt. *Dynamic Polarizability of Small Metal Particles: Self-Consistent Spherical Jellium Background Model.* Phys. Rev. Lett. **52** (1984), 1925.

[7] W. A. de Heer. *The physics of simple metal clusters: experimental aspects and simple models.* Rev. Mod. Phys. **65** (1993), 611.

[8] E. D. Palik. *Handbook of Optical Constants of Solids* (Academic Press, San Diago, California, 1985).

[9] L. Hedin and S. Lundqvist. *Effects of Electron-Electron and Electron-Phonon Interactions on the One-Electron States of Solids.* Solid State Phys. **23** (1969), 1.

[10] J. Lindhard. *On the properties of a gas of charged particles.* Dan. Math. Phys. Medd. **28** (1954).

[11] I. I. Rabi. *Space Quantization in a Gyrating Magnetic Field.* Phys. Rev. **51** (1937), 652.

[12] N.-H. Kwong and M. Bonitz. *Real-Time Kadanoff-Baym Approach to Plasma Oscillations in a Correlated Electron Gas.* Phys. Rev. Lett. **84** (2000), 1768.

[13] M. Bonitz, J. W. Dufty, and C. S. Kim. *BBGKY Approach to Non-Markovian Semiconductor Bloch Equations.* Phys. Stat. Sol. (b) **206** (1998), 181.

[14] T. Dittrich, P. Hänggi, G.-L. Ingold, B. Kramer, G. Schön, and W. Zwerger. *Quantum transport and dissipation* (Wiley-VCH, Weinheim, 1998).

[15] P. A. M. Dirac. *Time dependent Hartree-Fock approximation.* Proc. Cambridge Philos. Soc. **26** (1930), 376.

[16] L. Hedin. *New Method for Calculating the One-Particle Green's Function with Application to the Electron-Gas Problem.* Phys. Rev. **139** (1965), A796.

[17] W. H. Press, S. Teukolsky, W. Vetteling, and B. Flannery. *Numerical Recipes in Fortran 77 the Art of Scientific Computing* (Cambridge University Press, 1997), 2 edition.

[18] F. Calvayrac, P. G. Reinhard, and E. Suraud. *Spectral Signals from Electronic Dynamics in Sodium Clusters.* Annals of Physics **255** (1997), 125.

[19] D. Pines. *Electron interaction in metals.* Solid State Phys. **1** (1955), 367.

[20] P. Hohenberg and W. Kohn. *Inhomogeneous Electron Gas.* Phys. Rev. **136** (1964), B864.

[21] E. Runge and E. K. U. Gross. *Density-Functional Theory for Time-Dependent Systems.* Phys. Rev. Lett. **52** (1984), 997.

[22] A. Zangwill and P. Soven. *Density-functional approach to local-field effects in finite systems: Photoabsorption in the rare gases.* Phys. Rev. A **21** (1980), 1561.

[23] M. J. Stott and E. Zaremba. *Linear-response theory within the density-functional formalism: Application to atomic polarizabilities.* Phys. Rev. A **21** (1980), 12.

[24] M. Brack. *The physics of simple metal clusters: self-consistent jellium model and semiclassical approaches.* Rev. Mod. Phys. **65** (1993), 677.

[25] E. K. U. Gross and W. Kohn. *Local Density-Functional Theory of Frequency-Dependent Linear Response.* Phys. Rev. Lett. **55** (1985), 2850.

[26] S. J. A. van Gisbergen, F. Kootstra, P. R. T. Schipper, O. V. Gritsenko, J. G. Snijders, and E. J. Baerens. *Density-functional-theory response-property calculations with accurate exchange-correlation potentials.* Phys. Rev. A **57** (1998), 2556.

[27] M. Madjet, C. Guet, and W. R. Johnson. *Comparative study of exchange-correlation effects on the electronic and optical properties of alkali-metal clusters.* Phys. Rev. A **51** (1995), 1327.

[28] K. Yabana and G. F. Bertsch. *Time-dependent local-density approximation in real time.* Phys. Rev. B **54** (1996), 4484.

[29] F. Calvayrac, P. G. Reinhard, and F. Suraud. *Nonlinear plasmon response in highly excited metallic clusters.* Phys. Rev. B **52** (1995), R17056.

[30] K. Yabana and G. F. Bertsch. *Time-dependent Local-density Approximation in Real Time: Application to Conjugated Molecules.* Int. J. of Quant. Chem. **75** (1999), 55.

[31] K. Yabana and G. F. Bertsch. *Optical response of small carbon clusters.* Z. Phys. D **42** (197), 219.

[32] S. Kümmel, M. Brack, and P.-G. Reinhard. *Ionic and electronic structure of sodium clusters up to N = 59.* Phys. Rev. B **62** (2000), 7602.

[33] F. Calvayrac, P. G. Reinhard, E. Suraud, and C. A. Ullrich. *Nonlinear electron dynamics in metal clusters.* Physics Report **337** (2000), 493.

[34] C. Kohl, E. Suraud, and P.-G. Reinhard. *Second harmonic generation in deposited clusters.* Eur. Phys. J. D **11** (2000), 115.

[35] B. Holm and U. von Barth. *Fully self-consistent GW self-energy of the electron gas.* Phys. Rev. B **57** (1998), 2108.

[36] F. Aryasetiawan and O. Gunnarsson. *The GW method.* Rep. Prog. Phys. **61** (1998), 237.

[37] U. von Barth and B. Holm. *Self-consistent GW_0 results for the electron gas: Fixed screened potential W_0 within the random-phase approximation.* Phys. Rev. B **54** (1996), 8411.

[38] Y. Takada. *Inclusion of the Vertex Corrections in the Self-Consistent Calculation of Quasipaticles in Metals.* Phys. Rev. Lett. **87** (2001), 226402.

[39] E. L. Shirley. *Self-consistent GW and higher-order calculations of the electron states in metals.* Phys. Rev. B **54** (1996), 7758.

[40] A. Schindlmayr and R. W. Godby. *Systematic Vertex Corrections through Iterative Solution of Hedin's Equation Beyond the GW Approximation.* Phys. Rev. Lett. **80** (1998), 1702.

[41] R. T. M. Ummels, P. A. Bobbert, and W. van Haeringen. *First-order corrections to random-phase approximation GW calculations in silicon and diamond.* Phys. Rev. B **57** (1998), 11962.

[42] G. Baym and L. P. Kadanoff. *Conservation Laws and Correlation Functions.* Phys. Rev. **124** (1961), 287.

[43] G. Baym. *Self-Consistent Approximation in Many-Body Systems.* Phys. Rev. **127** (1962), 1391.

[44] A. Schindlmayr, P. García-González, and R. W. Godby. *Diagrammatic self-energy approximations and the total particle number.* Phys. Rev. B **64** (2001), 235106.

[45] H. N. Rojas, R.W. Godby, and R.J. Needs. *Space-Time Method for Ab Initio Calculations of Self-Energies and Dielectric Response Functions of Solids.* Phys. Rev. Lett. **74** (1995), 1827.

[46] F. Green, D. Neilson, and J. Szymanski. *Conserving dynamical theory for the electron gas.* Phys. Rev. B **31** (1985), 2779.

[47] A. Georges, G. Kotliar, W. Krauth, and M. J. Rosenberg. *Dynamical mean-field theory of strongly correlated fermion systems and the limit of infinite dimensions.* Rev. Mod. Phys. **68** (1996), 13.

[48] W. Metzner and D. Vollhardt. *Correlated Lattice Fermions in $d = \infty$ Dimensions.* Phys. Rev. Lett. **62** (1989), 324.

[49] W. Hübner and K.-H. Bennemann. *Nonlinear Magneto-Optical Kerr Effect on a Nickel Surface.* Phys. Rev. B **40** (1989), 5973.

[50] D. A. Kleinman. *Nonlinear Polarization in Optical Media.* Phys. Rev. **126** (1962), 1977.

[51] V. Bonacic-Koutecky, P. Fantucci, and J. Koutecky. *An ab initio configuration interaction study of the excited states of the Na_4 cluster: Assignment of the absorption spectrum.* Chem. Phys. Lett. **166** (1990), 32.

[52] I. Vasiliev, S. Öğüt, and J. R. Chelikowsky. *Ab initio Excitation Spectra and Collective Electronic Response in Atom and Clusters.* Phys. Rev. Lett. **82** (1999), 1919.

[53] I. Moullet, J. L. Martins, F. Reuse, and J. Buttet. *Static electric polarizabilities of sodium clusters.* Phys. Rev. B **42** (1990), 11598.

[54] V. Bonačić-Koutecký, P. Fantucci, and J. Koutecký. *Systematic ab initio configuration-interaction study of alkali-metal clusters. II. Relation between electronic structure and geometry of small sodium clusters.* Phys. Rev. B **37** (1988), 4369.

[55] N. Pontius, P. Bechthold, M. Neeb, and W. Eberhardt. *Ultrafast Hot-Electron Dynamics Observed in Pt_3^- Using Time-Resolved Photoelectron Spectroscopy.* Phys. Rev. Lett. **84** (2000), 1132.

[56] C. Wang, S. Pollack, D. Cameron, and M. M. Kappes. *Optical absorption spectroscopy of sodium clusters as measured by collinear molecular beam photodepletion.* J. Chem. Phys. **93** (1990), 3787.

[57] D. A. Telnov and S.-I. Chu. *Floquet formulation of time-dependent density functional theory.* Chem. Phys. Lett. **264** (1997), 466.

[58] D. Steinmüller-Nethl, A. Höpfel, E. Gornik, A. Leitner, and F. R. Aussenegg. *Femtosecond relaxation of localized plasma excitations in Ag islands.* Phys. Rev. Lett. **68** (1992), 389.

[59] B. Lamprecht, A. Leitner, and F. R. Aussenegg. *Femtosecond decay-time measurement of electron-plasma oscillation in nanolithographically designed silver clusters.* Appl. Phys. B **64** (1997), 269.

[60] A. Assion, B. Lang, M. Simon, S. Voll, F. Träger, and G. Gerber. Proc. SPIE (Soc. Photo-Opt. Instrum. Eng. **15** (1998), 3272.

[61] Th. Müller, P. H. Vaccaro, F. Balzer, and H.-G. Rubahn. *Size dependent optical second harmonic generation from surface bound Na clusters: comparison between experiment and theory.* Optics Communications **135** (1997), 103.

[62] J.-H. Lein-Wiele, P. Simon, and H.-G. Rubahn. *Size-Dependent Plasmon Lifetimes and Electron-Phonon Coupling Constants for Surface Bound Na Clusters.* Phys. Rev. Lett. **80** (1998), 45.

[63] R. Schlipper, R. Kusche, B. von Issendorff, and H. Haberland. *Multiple Excitation and Lifetime of Sodium Cluster Plasmon Resonance.* Phys. Rev. Lett. **80** (1998), 1194.

[64] M. Simon, F. Träger, A. Assion, B. Lang, S. Voll, and G. Gerber. *Femtosecond time-resolved second-harmonic generation at the surface of alkali metal clusters.* Chem. Phys. Lett. **296** (1998), 579.

[65] V. M. Akulin, C. Bréchignac, and A. Sarfati. *Quantum Shell Effect on the Dissociation Energies, Shapes, and Thermal Properties of Metallic Clusters from the Random Matrix Model.* Phys. Rev. Lett. **75** (1995), 220.

[66] V. V. Flambaum, A. A. Gribarkina, G. F. Gribarkin, and M. G. Kozlov. *Structure of compound states in the chaotic spectrum of the Ce atom.* Phys. Rev. A **50** (1994), 267.

[67] U. Sivan, F. Milliken, K. Milkove, S. Rishton, Y. Lee, J. Hong, *et al.. Spectroscopy, electron-electron interaction, and level statistics in a disordered quantum dot.* Europhys. Lett. **25** (1994), 605.

[68] Thomas Guhr, Axel Müller-Groeling, and Hans A. Weidenmüller. *Random-matrix theories in quantum physics: common concepts.* Phys. Reports **299** (1998), 189.

[69] D. J. Rowe. *Nuclear Collective Motion* (Methuel, London, 1968).

[70] M. Bonitz. *Quantum kinetic theory* (Stuttgart, Teubner, 1998).

[71] T. H. Dunning and P. J. Hay. *Modern Theoretical Chemistry* (Plenum, New York, 1976).

[72] P. J. Hay and W. R. Wadt. *Ab initio effective core potentials for molecular calculations. Potentials for main group elements Na to Bi.* J. Chem. Phys. **82** (1985), 284.

[73] E. Gilio, P.-G. Reinhard, and E. Suraud. *Semiclassical approach to metal cluster dynamics.* Elsevier. Computational Materials Science **17** (2000), 534.

[74] E. Gilio, P. G. Reinhard, and E. Suraud. *Semiclassical approach to metal cluster dynamics.* J. Phys. B: At. Mol. Opt. Phys. **33** (2000), L333.

[75] L. Féret, E. Suraud, F. Calvayrac, and P. G. Reinhard. *On the electron dynamics in Na_9^+ metal cluster: a Vlasov approach.* J. Phys. B: At. Mol. Opt. Phys. **29** (1996), 4477.

[76] H. Wang and E. Carter. *Metal-metal bonding in transition-metal clusters with open d shell: Pt_3.* J. Phys. Chem. **96** (1992), 1197.

[77] B. Montag and P.-G. Reinhard. *Width of the plasmon resonance in metal clusters.* Phys. Rev. B **51** (1995), 14686.

[78] R. A. Molina, D. Weinmann, and R. A. Jalabert. *Oscillatory size dependence of the surface plasmon linewidth in metallic nanoparticles.* Phys. Rev. B **65** (2002), 155427.

[79] T. Reiners, C. Ellert, M. Schmidt, and H. Haberland. *Size Dependence of the Optical Response of Spherical Sodium Clusters.* Phys. Rev. Lett. **74** (1995), 1558.

[80] M. Schmidt and H. Haberland. *Optical spectra and their moments for sodium clusters, Na_n^+, with $3 \leq n \leq 64$.* Eur. Phys. J. D **6** (1999), 109.

[81] V. V. Flambaum, G. F. Gribarkin, and F. M. Izrailev. *Correlations within eigenvectors and transition amplitudes in the two-body random interaction model.* Phys. Rev. E **53** (1996), 5729.

[82] P. Jacquod and D. L. Shepelyansky. *Emergence of Quantum Chaos in the Finite Interacting Fermi Systems.* Phys. Rev. Lett. **79** (1997), 1837.

[83] B. Georgeot and D. L. Shepelyansky. *Breit-Wigner Width and Inverse Participation Ratio in Finite Interacting Fermi Systems.* Phys. Rev. Lett. **79** (1997), 4365.

[84] M. J. Frisch, G. W. Trucks, H. B. Schlegel, G. E. Scuseria, M. A. Robb, J. R. Cheeseman, *et al.. Gaussian, Inc., Pittsburgh PA* (1998).

[85] D. Majumdar, D. Dai, and K. Balasubramanian. *Theoretical study of the electronic states of platinum trimer (Pt_3).* J. Chem. Phys. **113** (2000), 7919.

[86] H. Wang and E. A. Carter. *Metal-Metal Bonding in Transition-Metal Clusters with Open d Shells: Pt_3.* J. Phys. Chem. **96** (1992), 1197.

[87] S. Obara and A. Saika. *Efficient recursive computation of molecular integrals over Cartesian Gaussian functions.* J. Chem. Phys. **84** (1986), 3963.

[88] M. Head-Gordon and J. A. Pople. *A method for two-electron Gaussian integral and integral derivative evaluation using recurrence relations.* J. Chem. Phys. **89** (1988), 5777.

[89] P. C. Martin and J. Schwinger. *Theory of Many-Particle Systems. I.* Phys. Rev. **115** (1959), 1342.

Acknowledgements

At the end of this work I would like to express my gratitude to many people.

I am deeply indebted to my scientific supervisor Prof. Wolfgang Hübner for giving me the opportunity to work under this interesting project, for his patience and constant encouragements during the work, for many scientific discussions that showed me a beauty of computational physics, and for his insistence on the clarity during writing of my thesis.

I wish to thank Prof. Jürgen Kirschner for accepting me into his department at the Max-Planck-Institute für Mikrostructurphysik. Excellent working conditions, interesting seminars and communication with people helped me a lot to complete this work.

Among them are colleagues from my group whom I would like to thank: Dr. Torsten Andersen for his numerous advices about computers and computations, Dr. Mikolay Trze-ciecki for his support during my first year of being here. I gain a lot from the scientific discussions with Dr. Xianghong Qian, Dr. Ricardo Gómez-Abal, Dr. Nataliya Dadoenkova, Khompat Satitkovitchai, and Oleksandr Ney.

I am thankful to my friends at the institute for their advices and encouragements, especially to Dr. Fabrizio Porrati, Oleg Kidun, Volker Kulhmann, and Khompat Satitkovitchai.

Finally, I would like to express my heart-felt gratitude to my parents and brother for their love and support.

Summary

Our work was devoted to **ultrafast electron dynamics in metallic clusters**. Our interest in metallic clusters is raised by the recent advances in nanotechnology, fabrication and investigation of quantum dots, improvement of quantum chemical *ab initio* methods as well as of computational facilities, which enable the modelling of hundreds of atoms. On the other hand progress in technology with its steady tendency to the miniaturization is constantly demanding for novel materials. Clusters, that may be considered to form a new phase of materials lying between macroscopic solids and microscopic particles such as atoms and molecules, possess a large number of physical properties making them so attractive for future applications. Among them stands out a large flexibility in changing their qualities by varying their geometry and size. Addition of even a single atom may change the electronic structure of the cluster drastically. Clusters with certain numbers of atoms (magic numbers) are very stable due to the completion of atomic-like electronic shells. Increasing the number of atoms by one then leads to the formation of a new incomplete shell, lowering the stability. Metallic clusters inhere the high density of electronic states from their bulk material counterparts combining it with a seemingly contradictory large band-gap peculiar to insulators and semi-conductors.

Nontrivial (beyond a change of the phase of the wave-function, which is not observable) electron dynamics is a consequence of *electronic correlations* in the system. It manifests itself as a transition of electrons between states or an excitation during the interaction with an external field and, as relaxation or equilibration of the system due, first, to electron-electron collisions and, then, due to electron-phonon interaction. In the present work two approaches are used to study the electron dynamics in metallic clusters:

- the solution of the time-dependent Hartree-Fock (TDHF) equation in order to monitor the time evolution of the system upon ultrashort laser pulse excitation and

- a Green's function technique, namely the GW method to compute the correction to the eigenstates energies and to obtain decay constants for the plasmon excitations and quasiparticles.

In order to make our thesis self-explanatory we first discuss:

- the description of the electron wave-functions in the clusters by means of *linear combination of atomic orbitals*.

- the *stability* of the clusters

- two different electronic states in the electron gas:

- *quasiparticles*

- *plasmons*

We demonstrate that the properties of the first are very similar to that of the usual particles. They can be analyzed considering the one-particle Green function. The plasmon oscillation is a collective effect, that is most easily studied using the dielectric function.

Furthermore, we explain our implementation of the TDHF and GW methods from a unified point of view. In our work these approaches were applied for the first time to localized systems (such as clusters) using Gaussian basis functions. As a starting point we consider diagrammatic expansions within many-body perturbation theory. Based on that we rewrite the equations in the form suitable for numerical calculations. This is achieved by expanding all operators and functions in a certain basis set (Gaussian in our case, although the formulae are valid in general). In order to achieve high numerical performance every operation is rewritten in matrix form. Because of this the form of some equations differs from the usual notations. That is why we spend additional efforts to clarify relations between different representations of the main results.

Although both approximations are known for a long time (TDHF was established by Dirac in the early 1930s and GW originates from the work of Hedin published in 1965) their numerical implementation became possible only with the development of modern computers. On the first stages a lot of additional approximations were used to facilitate computations. Thus we consider our implementations in the light of previous works.

In parallel we consider the computation of the non-linear optical properties of clusters, in particular, *second harmonic generation*. Symmetry properties of the SHG tensor are discussed and numerical results for a Na_4 cluster based on the Hartree-Fock eigenstates are shown.

In last two chapters of the thesis numerical results of apllication of TDHF and GW methods to real systems are presented.

Electron dynamics from TDHF theory. First we apply the TDHF method to the simple, molecule-like systems in order to better understand the time evolution in this approach and to test the numerical precision of our method. We start our investigation with Na_4 – one of the most widely studied cluster in the literature. The small number of atoms made it accessible to almost all known *ab initio* methods including Configuration Interaction (CI), GW, and TDLDA. As an example regimes of low and high frequency excitations are considered and compared with the adiabatic solution. We find that for excitations of an energy considerably lower than the energy of transitions between different states the dynamics of the system obtained from the full time-dependent treatment differs only slightly from that in the adiabatic approach. After the excitation it returns almost to the initial state, preserving only some small oscillations. By contrast, a completely different behavior is found at higher frequencies. Our calculations indicate that, in the case of a Na_4 cluster, for an excitation energy above 0.5 eV the adiabatic approximation ceases to be valid and one has to resort to methods that explicitly account for the time dependence.

On the second step we study properties of the collective excitations by analyzing the power spectrum of the metallic clusters subject to an ultrafast laser pulse.The application of the TDHF method to the Na_9^+ cluster, previously intensively studied theoretically with

different methods, and the Pt_3 cluster already accessible to experimental investigation revealed the following capabilities of our approach:

- The method is able to accurately predict the position of the plasmon peak (2.7 eV) for the Na_9^+ cluster, although its oscillator strength differs considerably from the TDLDA result.

- The calculation on the open-shell transition metal cluster Pt_3 allowed us not only to determine the position of the plasmon resonance (3.7 eV), but also to estimate its life-time by fitting the power spectrum to a set of Lorentzians. Our value for the decay constant ($\tau_{pl} = 24$ fs) supports the experimental evidence in favor of a bulk-like lifetime (< 70 fs) of the electronic excitations in this cluster despite an electronic structure that strongly differs from bulk Pt.

- The calculation on the two-body random interaction model (TBRIM) supports the possibility to determine the life-time of collective excitations from time-dependent mean-field theory.

Numerical results of GW calculation. An algorithm developed by us for the calculation of the electronic structures of clusters within the GW approximation was applied to a variety of metallic clusters. To our main results belongs:

- a partially self-consistent GW calculation on Na_9^+ cluster that enables us to improve HOMO-LUMO gap (4.5 eV – HF, 3.7 eV – G^0W^0, 3.37 eV GW) and to determine the plasmon width and life-time (2 eV and 4.1 fs respectively).

- a fully self-consistent GW calculation on the TBRIM that helps us to understand the importance of the quasiparticle life-time renormalization and to check with high precision the theoretical prediction that the life-time of the quasiparticle states is inversely proportional to the square of the interaction strength.

- the G^0W^0 calculation on a series of sodium clusters (Na_N^+, N=15-25) to improve their electronic structure obtained on the HF level and to estimate quasiparticle life-times.

- the G^0W^0 calculation on the Pt_3 cluster that reveals an extremely short life-time of the HOMO (70 fs) and LUMO (20 fs) states in striking agreement with the experimental observation and shows the capability of the method to treat large systems.

A lot still remains to be done. The first approach, being almost perfect from the computational point of view can now be applied to a larger class of materials and allows for the exploration of a variety of experimental situations, such as four-wave mixing, second harmonic generation, etc. The second approach requires its further development in seeking the best computational scheme, comparing different additional approximations and finding the optimal level of the theory for each particular class of clusters. Only then its routine application for the design of new materials is possible.

Zusammenfassung

Unsere Arbeit wurde der **ultraschnellen Dynamik von Elektronen in metallischen Clustern** gewidmet. Geweckt wurde unser Interesse an metallischen Clustern durch die neuesten Fortschritte der Nanotechnologie, die Herstellung und Untersuchung von Quantenpunkten, die Verbesserung von quanten-chemischen *ab initio* Methoden sowie durch die computertechnischen Möglichkeiten, welche die Modellierung von hunderten von Atomen ermöglichen. Andererseits erfordert der technische Fortschritt mit seiner Neigung zur stetigen Miniaturisierung neue Materialien. Cluster, die man als neue Zustandsform der Materie, zwischen makroskopischen Festkörpern und mikroskopischen Teilchen wie etwa Atomen oder Molekülen gelegen, ansehen kann, verfügen über eine Anzahl von Eigenschaften, die sie besonders attraktiv für zukünftige Anwendungen machen. Herausragend dabei ist die Flexibilität ihrer Eigenschaften bei Veränderung von Größe und Geometrie. Hinzufügen von nur einem Atom kann die elektronische Struktur von Clustern drastisch verändern. Cluster mit einer ganz bestimmten Anzahl von Atomen (sog. magische Zahl) sind sehr stabil aufgrund der Vervollständigung von Schalen, ähnlich den elektronischen Schalen in Atomen. Wird ein weiteres Atom hinzugefügt, entsteht dadurch eine neue aber unvollständige Schale und der Cluster verliert an Stabilität. Die metallischen Cluster haben ihre hohe elektronische Zustandsdichte von ihren massiveren Pendants, den Festkörpern, und verbinden diese mit der scheinbar widersprüchlich großen Bandlücke, wie sie Halbleitern und Isolatoren eigen ist. Die nicht-triviale (nicht nur ein unbeobachtbarer Wechsel der Phase der Wellenfunktion) Elektronendynamik ist eine Konsequenz der *elektronischen Korrelationen* im System. Das zeigt sich als Übergang von Elektronen zwischen Zuständen oder auch an der Anregung während der Wechselwirkung mit externen Feldern sowie an der Relaxierung oder Equilibrierung des Systems aufgrund von Elektron-Elektron Stössen oder Elektron-Phonon Wechselwirkungen. Die vorliegende Arbeit untersucht die Elekronendynamik in metallischen Clustern mit zweierlei Herangehensweisen:

- die zeitabhängige Hartree-Fock Gleichung (time-dependent Hartree-Fock –TDHF) wird gelöst um damit die zeitliche Entwicklung des Systems nach Anregung mit einem ultrakurzen Laserpuls zu beobachten

- die Methode der Greensfunktionen, und zwar die GW Methode, um die Korrektur der Eigenzustände zu berechnen und um die Zerfallskonstanten von Plasmon Anregungen und Quasiteilchen zu erhalten.

Damit diese Arbeit leicht verständlich wird, diskutieren wir als Erstes:

- die Beschreibung der Wellenfunktionen der Elektronen in Clustern mit Hilfe von *Linearkombinationen von atomaren Orbitalen.*

- die *Stabilität* der Cluster.

- zwei unterschiedliche elektronische Zustände im Elektronengas:

  - *Quasiteilchen*
  - *Plasmonen*

Wir zeigen, dass die Eigenschaften der Ersteren denen von normalen Teilchen sehr ähnlich sind. Sie können unter Betrachtung der Einteilchen-Greenfunktion untersucht werden. Die Plasmonenoszillation ist ein kollektiver Effekt, welcher am einfachsten unter Zuhilfenahme der dielektrischen Funktion untersucht wird.

Des weiteren erklären wir unsere praktische Durchführung der TDHF und der GW Methode aus einer vereinheitlichten Perspektive. In unserer Arbeit wurden diese Herangehensweisen unter Benutzung von Gauss'schen Basisfunktionen zum ersten Mal auf lokalisierte Systeme (wie z.B. Cluster) angewendet. Wir fangen an mit einer diagrammatischen Entwicklung der Vielteilchenstörungstheorie. Davon ausgehend schreiben wir die Gleichungen in eine für numerische Berechnungen passende Form um. Das erreichen wir dadurch, dass wir alle Funktionen und Operatoren nach bestimmten Basissätzen entwickeln (wir benutzen Gauss'sche Basisfunktionen, obwohl die Gleichungen allgemein gültig sind). Um hohe numerische Leistungen zu erreichen, sollten alle Operationen in Matrizenform umgeschrieben werden. Deshalb kann sich das Aussehen einiger Gleichungen von ihrer herkömmlichen Schreibweise unterscheiden und wir haben besondere Anstrengungen unternommen um die Beziehungen zwischen verschiedenen Darstellungen der Hauptergebnisse zu verdeutlichen. Obgleich beide Näherungen seit Langem bekannt sind (TDHF wurde von Dirac in den frühen Dreißigern eingeführt während GWA auf die von Hedin 1965 veröffentlichte Arbeit zurückgeht), wurde ihre numerische Umsetzung erst mit der Entwicklung moderner Computer möglich. In den Anfängen wurden eine Vielzahl zusätzlicher Näherungen benutzt, um Berechnungen überhaupt zu ermöglichen, weshalb wir unsere Umsetzung im Lichte der vorhergegangenen Arbeiten betrachten wollen. Parallel dazu betrachten wir Berechnungen der nichtlinearen optischen Eigenschaften von Clustern, insbesondere die *Frequenzverdopplung* (second harmonic generation – SHG). Wir diskutieren Symmetrieeigenschaften des SHG Tensors und zeigen numerische Ergebnisse von Na_4 Clustern, basierend auf den Hartree-Fock Eigenzuständen. In den zwei letzten Kapiteln der Arbeit werden numerische Ergebnisse der an realen Systemen angewandten TDHF und GW Methode präsentiert.

TDHF und Elektronen Dynamik. Zuerst wenden wir TDHF auf ein einfaches, molekülartiges System an, um die zeitliche Entwicklung besser verstehen zu können und um die numerische Genauigkeit unsere Methode zu untersuchen. Wir beginnen unsere Untersuchung an Na_4, einem der am häufigsten in der Literatur untersuchten Cluster. Die nur kleine Anzahl von Atomen macht es fast allen bekannten *ab initio* Methoden zugänglich, darunter Konfigurations-Wechselwirkung (configuration interaction – CI), GW und TDLDA. Als Beispiel werden Bereiche der Hoch und Niederfrequenzanregung untersucht und mit den adiabatischen Lösungen verglichen. Dabei fanden wir heraus, dass sich die Dynamik des Systems bei vollständig zeitabhängiger Behandlung und Anregung mit Energien deutlich unterhalb der Übergangsenergie zwischen Zuständen nur geringfügig vom adiabatischen Ansatz unterscheidet. Nach der Anregung kehrt das System fast wieder in den Ausgangszustand zurück und behält nur einige kleine Oszillationen. Bei hohen Fre-

quenzen wurde hingegen ein vollständig anderes Verhalten beobachtet. Unsere Berechnungen deuten für den Fall von Na$_4$ Clustern und für Anregungsenergien oberhalb 0.5 eV an, dass die adiabatische Näherung ihre Gültigkeit verliert und man auf Methoden angewiesen ist, die die Zeitabhängigkeit explizit beinhalten. In einem zweiten Schritt untersuchen wir die kollektiven Anregungen indem wir die metallischen Cluster ultraschnellen Laserpulsen aussetzen und dann deren Spektraldichte analysieren. Die Anwendung der TDHF Methode auf Na$_9^+$ Cluster, welche zuvor bereits intensiv theoretisch mit anderen Methoden untersucht wurden, und Pt$_3$ Cluster, welche bereits dem Experiment zugänglich sind, offenbaren die folgenden Möglichkeiten unserer Methode:

- sie ermöglicht eine akkurate Vorhersage der Position des Plasmonen-Maximums für Na$_9^+$ Cluster (2.7 eV), obgleich die Stärke ihrer Oszillation erheblich von dem TDLDA Ergebnis abweicht.

- Die Berechnungen an dem offenenschaligen Übergangsmetall Cluster Pt$_3$ erlaubt uns nicht nur die Position der Plasmonen Resonanz zu bestimmen (3.7 eV) sondern lässt uns auch die Lebensdauer abschätzen, indem wir die Spektraldichte an einen Satz von Lorentzfunktionen anfitten. Unser Wert für die Zerfallskonstante ($\tau_{\mathrm{pl}} = 24$ fs) bekräftigt den experimentellen Nachweis zugunsten der Lebenszeit der elektronisch angeregten Zustände innerhalb des Clusters wie sie in Festkörpern zu finden ist (< 70 fs) trotz der elektronischen Struktur, die ja sich stark von Pt im Festkörper unterscheidet.

- Die Berechnungen am zufälligen Zwei-Körper Wechselwirkungsmodell (two-body random interaction model – TBRIM) unterstützen die Möglichkeit, die Lebensdauer der kollektiven Anregungszustände mit der zeitabhängigen Molekularfeld-Theorie bestimmen zu können.

Numerische Ergebnisse der GW Berechnungen. Wir haben den von uns entwickelten Algorithmus zur Berechnung der elektronischen Zustände von Cluster innerhalb der GW Näherung auf eine Vielzahl von metallischen Clustern angewandt. Zu unseren Hauptergebnissen zählen:

- eine teilweise selbst-konsistente GW Berechnung der Na$_9^+$ Cluster, welche es uns erlaubt, die HOMO-LUMO Lücke zu verbessern (4.5 eV – HF, 3.7 eV – G^{0}W^0, 3.37 eV – GW) und die Linienbreite und Lebensdauer der Plasmonen zu bestimmen (2 eV bzw. 4.1 fs).

- eine vollständig selbst-konsistente GW Berechnung der TBRIM, welche uns die Bedeutung der Renormierung der Lebensdauer der Quasiteilchen zu verstehen hilft, und mit Hilfe derer wir die theoretische Vorhersage, dass die Lebensdauer der Quasiteilchenzustände umgekehrt proportional zum Quadrat der Stärke der Wechselwirkung ist, mit grosser Genauigkeit überprüfen können.

- die G^{0}W^0 Berechnungen an einer Reihe von Natrium Clustern (Na$_N^+$, $N = 15 - 25$), um die elektronische Strukturen, wie sie HF Berechnungen ergaben, zu verbessern und um die Lebensdauer der Quasiteilchen abzuschätzen.

- G^0W^0 Berechnungen am Pt_3 Cluster offenbaren eine extrem kurze Lebensdauer der HOMO (70 fs) und LUMO (20 fs) Zustände, welche in bemerkenswerter Übereinstimmung mit der experimentellen Beobachtung stehen und die Leistungsfähigkeit der Methode angewandt auf große Systeme bezeugen.

Es bleibt noch viel zu tun. Der erste Ansatz, vom rechnerischen Gesichtspunkt aus nahezu perfekt, kann jetzt auf eine größere Gruppe von Materialien Anwendung finden und erlaubt die Erforschung einer Vielzahl von experimentellen Situationen, wie zum Beispiel vierwellen-Mischung, Frequenzverdopplung etc. Der zweite Ansatz erfordert eine Weitereentwicklung und Suche nach der besten rechnerischen Vorgehensweise. Hierbei müssen verschiedene zusätzliche Näherungen verglichen werden, um für jede Gruppe von Clustern eine optimale Theorie zu finden. Nur damit wird diese Methode in der Entwicklung neuer Materialien Anwendung finden.

List of publications

- Y. Pavlyukh and W. Hübner. Electron dynamics in Na_9^+ and Pt_3 clusters from time-dependent Hartree-Fock theory, Eur. Phys. J. D **21** (2002), 239.

- K. Satitkovitchai, Y. Pavlyukh and W. Hübner. *Ab initio* embedded cluster study of optical second-harmonic generation below the gap of a NiO (001) surface, *submitted to* Phys. Rev. B

Erklärung

Hiermit erkläre ich, dass ich diese Dissertation selbstständig und ohne fremde Hilfe verfasst habe. Ich habe keine anderen als die angegebenen Quellen und Hilfsmittel benutzt. Die den benutzten Werken wörtlich oder inhaltlich entnommenen Stellen habe ich als solche kenntlich gemacht.

Halle (Saale), den 11. November 2002

Yaroslav Pavlyukh

Curriculum vitae

since 23.01.2000	PhD student at Max-Planck Institute für Mikrostrukturphysik in Halle (Salle), Germany
1999	Diploma work on "Simulation of the topological structure of highly dispersed disordered systems " at L'viv State University, Ukraine
1994-1999	Study of physics at L'viv State University
1992-1994	L'viv Physics and Mathematics Lyceum
1983-1992	School in Drogobych, Ukraine
26.02.1976	Was born in Drogobych

Yaroslav Pavlyukh